Intergenerational transport of double-stranded RNA limits heritable

epigenetic changes

Marré<sup>1</sup>, and Antony M. Jose<sup>1\*</sup>

Authors: Nathan Shugarts<sup>1</sup>, Aishwarya Sathya<sup>1</sup>, Andrew L. Yi<sup>1</sup>, Winnie M. Chan<sup>1</sup>, Julia A.

**Affiliations:** 

<sup>1</sup>Department of Cell Biology and Molecular Genetics, University of Maryland, College Park,

MD 20742, USA.

\*Correspondence to: amjose@umd.edu

**ABSTRACT** 

RNAs in circulation carry sequence-specific regulatory information between cells in plant,

animal, and host-pathogen systems. Such RNA can cross generational boundaries, as evidenced

by somatic double-stranded RNA (dsRNA) in the nematode C. elegans silencing genes of

matching sequence in progeny. Here we dissect the intergenerational path taken by dsRNA from

parental circulation and discover that cytosolic import through the dsRNA importer SID-1 in the

parental germline and/or developing progeny varies with developmental time and dsRNA

substrates. Loss of SID-1 enhances initiation of heritable RNA silencing within the germline and

causes changes in the expression of the sid-1-dependent gene sdg-1 that last for more than 100

generations after restoration of SID-1. The SDG-1 protein is enriched in perinuclear Z granules

required for heritable RNA silencing but is expressed from a retrotransposon targeted by such

silencing. This auto-inhibitory loop reveals how retrotransposons could persist by hosting genes

that regulate their own silencing.

**Key words:** RNAi, transport, heritable silencing, stochastic, germline, gene expression

#### **MAIN TEXT**

RNAs released into circulation can act as intercellular messages that are used for gene regulation in distant cells. Examples include secretion of small RNAs within exosomes in response to pathogenic fungal infection in Arabidopsis<sup>1</sup>, virus-like proteins with their coding mRNAs in developing *Drosophila*<sup>2</sup> and mice<sup>3</sup>, microRNAs from adipose tissue in mice<sup>4</sup> and small RNAs from the epididymis in mice<sup>5,6,7,8</sup>. Such extracellular RNAs have also been detected in humans, but their roles in gene regulation remain unclear despite their use as diagnostic markers for diseases (reviewed in ref.<sup>9</sup>). Furthermore, the recent development of double-stranded RNA (dsRNA)-based drugs (reviewed in ref. 10; refs. 11,12) that can silence genes of matching sequence through RNA interference<sup>13</sup> has heightened interest in understanding the import of dsRNA into cells. A conserved dsRNA-selective importer, SID-1<sup>14,15,16</sup>, is required for the import of extracellular dsRNA into the cytosol of any cell in the nematode C. elegans. This entry into the cytosol is distinct from and can follow the uptake of dsRNA into cells, which can rely on other receptors (e.g., SID-2 for uptake from the intestinal lumen<sup>17,18</sup>). SID-1 has two homologs in mammals – SIDT1 and SIDT2. Although similar cytosolic entry of dsRNA through these mammalian homologs of SID-1 is supported by studies in mice reporting entry of viral dsRNA through SIDT2<sup>19</sup>, enhanced dsRNA uptake when SIDT1 is overexpressed in vitro<sup>20</sup>, and uptake of ingested dsRNA into cells through SIDT1<sup>21</sup>, alternative roles for SIDT1 and/or SIDT2 in the uptake of cholesterol have also been proposed<sup>22</sup>.

Secretion of dsRNA from *C. elegans* tissues expressing dsRNA from transgenes has been inferred based upon the SID-1-dependent silencing of matching genes in other tissues<sup>14,23</sup>.

Secreted dsRNA from neurons can silence genes of matching sequence in most somatic cells<sup>24</sup> and within the germline<sup>25</sup>. Extracellular dsRNA delivered into parental circulation by injection or

ingestion also enters the germline and can cause silencing of matching genes in progeny<sup>13,26,27,28,29</sup>. In every case, the entry of dsRNA into the cytosol dictates when and where the processing of extracellular dsRNA can begin. Such intergenerational transport of RNA is an attractive mechanism for explaining endogenous, gene-specific effects in progeny that could occur in response to changes in somatic tissues of parents. However, which conditions induce transport of dsRNA into the germline, when during development this transport occurs, and what regulatory consequences ensue in progeny upon uptake of extracellular dsRNA from parents are all unknown. Despite this lack of knowledge, the analysis of transgenerational gene silencing triggered by dsRNA has revealed that a class of small RNAs called 22G RNA made using the mRNA targeted by dsRNA and bound by Argonaute proteins in the germline<sup>30,31</sup> is necessary for observing silencing in every generation.

Timed dsRNA injection into animals or timed dsRNA ingestion by animals has been the only way to study mechanisms of dsRNA transport throughout *C elegans* development since no tools to induce dsRNA secretion from cells have been developed. Injection of dsRNA into adult *sid-1(-)* animals demonstrated that extracellular dsRNA can be directly transmitted to progeny without entry into the cytosol<sup>28,29</sup>. This intergenerational transmission of dsRNA in *sid-1(-)* adult animals requires the yolk receptor RME-2<sup>32</sup> and is independent of parental 22G RNA production because dsRNA cannot enter the cytosol in the parent. In further support of the initial intergenerational transport of extracellular dsRNA or dsRNA-derived signals not requiring 22G RNAs, *gfp*-dsRNA from parents that lack *gfp* sequences are transported to progeny (Fig. 1E in ref.<sup>28</sup>). Thus, the silencing signals transported from parent to progeny include the extracellular dsRNA and its derived silencing signals, independent of 22G RNAs. However, 22G RNAs are

required for silencing and they may be used for intergenerational transport in subsequent generations.

All dsRNAs, regardless of length, have been assumed to be equivalent substrates for entry into the cytosol. This assumption is supported by the uptake of a variety of dsRNA substrates when *C. elegans* SID-1 is overexpressed in heterologous *Drosophila* S2 cells<sup>16</sup>. Yet, two key observations suggest that dsRNA can take multiple routes *in vivo* before SID-1-dependent entry into the cytosol. One, even in the presence of SID-1, dsRNA ingested during early adulthood requires RME-2 to cause silencing in progeny<sup>28</sup>. Two, 50-bp fluorescently-labeled dsRNA requires RME-2 for entry from parental circulation into oocytes<sup>28</sup>. Establishing the contexts for the use of different modes of dsRNA transport is crucial for understanding the processes regulated by endogenous extracellular dsRNA.

Here, we dissect the intergenerational transport of extracellular dsRNA and discover a role for this mechanism in modulating RNA regulation within the germline. Extracellular dsRNA is transported with developmental and substrate specificity from parental circulation to progeny, and its release from neurons can be enhanced using light-induced oxidative damage. Blocking dsRNA import into the cytosol of all cells revealed heritable changes in gene expression and led to the identification of *sid-1-dependent gene-1* (*sdg-1*). The *sdg-1* coding sequence is located within a retrotransposon that is targeted by RNA silencing in the germline. Yet, the SDG-1 protein colocalizes with regulators of RNA silencing in perinuclear granules within the germline and dynamically enters the nucleus in proximal oocytes and in cells of developing embryos. Measurements of *sdg-1* expression using native mRNA, a translational reporter, or a transcriptional reporter reveal that expression is easily perturbed in different mutants that impact dsRNA-mediated gene regulation. Expression varies between the two gonad arms of wild-type

animals, and different mutant isolates can show an increase or decrease in expression, indicative of a loss of buffered gene expression within the germline. However, consistent with an overall role for SDG-1 (and potentially other SDGs) in promoting RNA silencing, either loss of SID-1 or overexpression of SDG-1 enhances piRNA-mediated silencing within the germline initiated by mating. Therefore, we propose that the import of extracellular dsRNA into the germline tunes intracellular pathways that cause heritable RNA silencing.

# Requirements for the entry of extracellular dsRNA into the germline change during development

A convenient method for the delivery of extracellular dsRNA into *C. elegans* at various times during larval development is the expression of dsRNA in the bacteria that the animals ingest as food<sup>26</sup>. To determine when ingested dsRNA can enter the germline and cause silencing, we exposed developing animals with a ubiquitously expressed protein (GTBP-1) tagged with GFP to bacteria that express gfp-dsRNA. Silencing was detectable within the germline from the second larval stage (L2) onwards (Fig. 1a and Extended Data Fig. 1a), but either exposure to ingested dsRNA beyond the fourth larval stage (L4) (Fig. 1b) or injection of dsRNA into the 1day old adult germline (Extended Data Fig. 1b) was required to observe silencing in the germline of 3-day old adults. Combined with the need for exposure to dsRNA after the L4 stage<sup>28,29</sup> for silencing in progeny, even for just 24 hours (Extended Data Fig. 1c), these observations suggest that heritable RNA silencing is not effectively initiated during early development of the germline despite detectable silencing within the germline. One possible explanation for this observation could be that both RNAs derived from the imported dsRNA and downstream silencing signals are continually diluted by the proliferation of germ cells. Heritable silencing by dsRNA ingested from the L4 stage to the first day of adulthood likely relies on entry of dsRNA into the proximal

germline because silencing of a somatic gene in progeny after parental ingestion of dsRNA during this period required RME-2 (Extended Data Fig. 1c), which is enriched in the proximal germline (Extended Data Fig. 1d and ref.<sup>32</sup>), and some *gtbp-1::gfp* animals exposed to *gfp*-dsRNA up to the first day of adulthood showed more silencing in the proximal germline (Extended Data Fig. 1e).

Thus, these results reveal three periods of germline development that can be broadly distinguished based on the response to ingested dsRNA: (1) from the first larval to the fourth larval stage when exposure to dsRNA does not result in maximal silencing within the germline in adults (Fig. 1b); (2) from the fourth larval stage to early adulthood when entry of dsRNA primarily occurs in the proximal germline through RME-2 (Extended Data Fig. 1c,e); and (3) later adulthood when germline silencing by ingested dsRNA is maximal (Fig. 1b) and ingested dsRNA can effectively silence progeny independent of RME-2 (Extended Data Fig. 1c and ref.<sup>29</sup>). These differences in the entry of ingested dsRNA into cells and/or subsequent silencing could be driven by a variety of changes during development. These include changes in the uptake of dsRNA into the intestine, distribution of dsRNA to other tissues from the intestine, import of dsRNA into the germline, and availability of RNA silencing factors within the germline.

# Oxidative damage in neurons expressing dsRNA enhances silencing in the germline by neuronal dsRNA

Another approach for delivering extracellular dsRNA into the germline that better mimics dsRNA transport between cells is the secretion of dsRNA from neurons<sup>25</sup>. However, the extent of such secretion throughout development is unpredictable. To modulate the secretion of dsRNA from somatic cells into parental circulation during development, we adapted an optogenetic approach for damaging somatic cells<sup>33</sup>. Specifically, we generated animals that express the mini

singlet oxygen generator (miniSOG) protein in neurons and exposed them to blue light. While animals expressing miniSOG from a single-copy transgene did not show an appreciable defect when compared with wild-type animals, those expressing miniSOG from a multi-copy transgene were paralyzed (Extended Data Fig. 2a,b, top) and had visibly damaged neurons (Extended Data Fig. 2b, bottom). Using this system, we induced oxidative damage in the neurons of animals that expressed dsRNA under the control of a neuronal promoter and evaluated silencing of target genes with matching sequence expressed in other tissues (Fig. 2a). By exposing animals to blue light for 60 minutes at different times during development (Extended Data Fig. 2c), we observed SID-1-dependent enhancement in the silencing of the hypodermal gene bli-1 at the adult stage by neuronal bli-1-dsRNA, with maximal silencing when oxidative damage occurred during mid-tolate larval development (Extended Data Fig. 2d, light exposure every 6 hours from 42 to 66 hours post L4-stage of parent; Extended Data Fig. 2e, ~2-fold increase from 14.9% to 29.1% in a background with enhanced RNA interference (eri-1(-)) and ~6-fold increase from ~1.6% to ~9.8% in a wild-type background). A similar period of maximal SID-1-dependent enhancement of silencing was also observed when neurons expressing gfp-dsRNA were damaged and silencing of a two-gene operon that expresses two fluorescent proteins, mCherry::H2B and GFP::H2B, in the germline was measured (Fig. 2b-d, and Extended Data Fig. 2f – 48 to 60 hours post L4-stage of parent; sid-1(-) allele (jam80[nonsense]) is depicted in Extended Data Fig. 3). While silencing of gfp::h2b was observed throughout the germline, silencing of the other cistron mCherry::h2b was also observed sometimes, albeit restricted to specific regions of the germline. Silencing of *mCherry::h2b* was most frequent in the proximal germline and was not observed in any other region without silencing in the proximal germline (proximal germline – 57%, distal germline – 47%, sperm – 29%, Fig. 2d), likely due to reduction of mCherry::h2b::gfp::h2b premRNA<sup>34</sup> in those regions. Consistently, the silencing of both *gfp::h2b* and *mCherry::h2b* was eliminated in the absence of the nuclear Argonaute HRDE-1 (Extended Data Fig. 2g). The pattern of *mCherry::h2b* silencing is similar to the spatial pattern observed for the RME-2-dependent entry of dsRNA delivered into parental circulation<sup>28</sup> and is consistent with the pattern of target mRNA degradation in the germline by extracellular dsRNA<sup>35</sup>. However, silencing of *gfp::h2b* in the germline by neuronal dsRNA did not show a detectable dependence on RME-2 (Extended Data Fig. 2h - difficulty in obtaining transgenic animals that also lack RME-2 resulted in a low sample size for this experiment).

Thus, by modulating the secretion of dsRNA from somatic cells for the first time, we gained two insights into the intercellular transport of dsRNA: (1) oxidative damage of neurons during particular periods in development increases the amount of dsRNA and/or changes the kinds of dsRNA in circulation either because of specific enhancement of secretion or nonspecific spillage; and (2) there is a preference for silencing by neuronal dsRNA in the proximal germline. However, the temporal and/or spatial preferences observed for silencing by both neuronal and ingested dsRNA could be because of unknown characteristics of the exported neuronal dsRNA or ingested dsRNA expressed from bacteria (e.g., modifications, lengths, structures, etc.) that influence import or subsequent silencing. This hypothesis is supported by the different genetic requirements reported for silencing by neuronal *gfp*-dsRNA compared to other sources of *gfp*-dsRNA<sup>24</sup>. Alternatively, these preferences could reflect universal constraints for silencing using any extracellular dsRNA (e.g. expression patterns of factors that promote the import or processing of dsRNA).

Extracellular dsRNA in parental circulation can be transported through multiple routes to cause silencing in progeny

While the characteristics of extracellular dsRNA imported into the germline from ingested bacteria or from neurons are unknown, delivery of chemically defined dsRNA into the extracellular space in C. elegans can be accomplished using microinjection<sup>13,28</sup>. We examined differences, if any, in the entry of in vitro transcribed dsRNA from the extracellular body cavity into the germline during the L4 and adult stages as evidenced by silencing in the progeny of injected animals. Silencing was comparable regardless of whether wild-type or rme-2(-) parents were injected as L4-staged or adult animals (Fig. 3a and Extended Data Fig. 4a, left; also reported for adults in ref.<sup>29</sup>). However, some dependence on RME-2 for silencing in progeny was discernable when lower concentrations of dsRNA were used (Extended Data Fig. 4a, right). This result and previous results demonstrating proximal germline-specific silencing in contexts where silencing is less robust (Extended Data Fig. 1e and Fig. 2d) are consistent with RME-2dependent uptake of dsRNA being a route for extracellular dsRNA to enter the germline. The difference in parental RME-2 requirement for silencing in progeny observed for dsRNA ingested (Extended Data Fig. 1c) or injected (Extended Data Fig. 4a) at the L4 stage could similarly reflect the accumulation of different amounts of dsRNA in parental circulation (e.g., more upon injection than upon ingestion), and/or different kinds of dsRNA (e.g., because of modifications in bacteria or upon transit through the intestine). However, these possibilities could not be easily distinguished because sensitive northern blotting<sup>36</sup> revealed that both bacterial and in vitro transcribed dsRNA consist of a complex mix of dsRNAs (Extended Data Fig. 4b-d; consistent with refs.<sup>37,38</sup>), hereafter called mixed dsRNA.

In contrast, when synthesized *gfp*-dsRNA of a defined length (50 bp) with a fluorescent label was injected into circulation in adult animals, no entry into the germline was observed in the absence of RME-2<sup>28</sup>. We found that silencing of *unc-22* in progeny by similarly synthesized

but unlabeled 50-bp unc-22-dsRNA with a 5' OH delivered into parental circulation also showed a strong requirement for RME-2, unlike mixed dsRNA (Fig. 3a). Further comparison between the two forms of dsRNA revealed that silencing in progeny by 50-bp dsRNA injected into parental circulation was detectably less efficient in somatic cells (Fig. 3b and Extended Data Fig. 5a,b, *left*), even when ~14X more 50-bp dsRNA was delivered into parental circulation (Extended Data Fig. 5b, right), and was also less efficient in the germline (Fig. 3b and Extended Data Fig. 5a,c). Efficient silencing in response to added dsRNA requires nuclear Argonaute proteins: NRDE-3 in somatic cells<sup>34</sup> and HRDE-1 in the germline<sup>30</sup>. Both 50-bp dsRNA and mixed dsRNA relied on the HRDE-1 for silencing within the germline (Extended Data Fig. 5a,c) and could silence independent of NRDE-3 in somatic cells (Extended Data Fig. 5a,c). Therefore, the observed difference in the extent of silencing cannot be attributed to differential engagement of these Argonautes, but rather could be the result of differences in the ability of each type of dsRNA to bind to upstream factors in the RNA interference pathway (e.g. RDE-4), differences in the stability of each type of dsRNA, and/or differences in the intergenerational transport of each type of dsRNA. In addition to the diversity of RNA lengths observed in mixed dsRNA, another known feature that could distinguish dsRNA transcribed in bacteria or in vitro from synthesized 50-bp dsRNA is the presence of 5' triphosphates on the transcribed dsRNA species instead of the 5' OH present in synthesized 50-bp dsRNA. In support of the impact of 5' phosphates on transport and/or silencing, addition of 5' monophosphates to synthesized 50-bp dsRNA injected into parental circulation reduced the dependence on RME-2 for silencing in progeny (Extended Data Fig. 4e,f), potentially by enhancing the ability of synthesized dsRNA to be imported by other dsRNA importers (e.g. SID-1) in the absence of RME-2. Thus, the requirements for

dsRNA entry into the germline and subsequent silencing vary for different lengths and/or chemical forms of dsRNA (see summary in Extended Data Table 1).

Fluorescently labeled 50-bp dsRNA delivered into parental circulation localized within intestinal cells in progeny (Fig. 3c, top left), as has been observed for vitellogenin proteins<sup>39</sup> and fluorescent dyes<sup>40</sup>. Accumulation of fluorescently labeled dsRNA was also detected at the apical membrane of the intestine, which could reflect exocytosis of dsRNA into the lumen of developing intestinal cells. However, separation of the fluorescent label from dsRNA catalyzed by cellular enzymes cannot be excluded. Therefore, to dissect differences, if any, between the transport of unlabeled short dsRNA (synthesized 50-bp with 5'OH) and mixed dsRNA (mixture transcribed in vitro using ~1 kb DNA template) we injected unc-22-dsRNA into animals with mutations in genes that play roles in the import of dsRNA. We found that maternal SID-1 was required for silencing by short dsRNA in progeny (Fig. 3c, bottom, left bars), suggesting that the SID-1-dependent entry of short dsRNA into the cytosol likely occurs in the injected parent or during early development in progeny. Uptake of dsRNA from the intestinal lumen requires SID-2, a transmembrane protein located in the apical membranes of intestinal cells <sup>17,18</sup>. We found that SID-2 was not required for most silencing in progeny by short or mixed dsRNA injected into parental circulation (Fig. 3c, top right and bottom). Exit of dsRNA from intracellular vesicles requires SID-5, a transmembrane protein located in endolysosomal membranes<sup>41</sup>. Silencing in wild-type animals was comparable to silencing in sid-5(-) animals (Fig. 3c, top right). However, when animals that lacked SID-1 were injected, SID-5 was required in progeny for silencing by mixed dsRNA from parental circulation (Fig. 3c, bottom, right bars; as also reported in ref.<sup>29</sup>). Since dsRNA is expected to be present in vesicles upon entry through RME-2 in the absence of

SID-1<sup>28,29</sup>, this observation suggests that SID-5 is required for the release of mixed dsRNA from inherited vesicles in progeny.

In summary, injected extracellular dsRNA can enter the germline in parents and be transmitted to progeny through two routes with different substrate selectivity. One route is preferentially used by short dsRNA and relies on RME-2-mediated endocytosis of dsRNA into oocytes, where early exit from vesicles is required for silencing in progeny as evidenced by the need for maternal SID-1 (Fig. 3d, blue). The other route appears to exclude short dsRNA but allows mixed dsRNA entry into the cytosol in the parental germline through SID-1 and exit from inherited vesicles in progeny through a process that requires both zygotic SID-1 and SID-5 (Fig. 3d, grey; ref.<sup>29</sup>).

### Expression of SID-1 is consistent with a role in the intergenerational transport of extracellular dsRNA

All routes of dsRNA transport deduced using the experimental addition of dsRNA ultimately require SID-1 for entry into the cytosol. The proposed model (Fig. 3d) for dsRNA transport into the germline and to progeny suggests the expression pattern of SID-1 is likely to include the germline. We used Cas9-mediated genome editing to insert a piRNA-resistant *mCherry* sequence<sup>42,43</sup> into the *sid-1* coding sequence (Fig. 4a) to observe the endogenous expression pattern of SID-1::mCherry. This fusion protein was detectably functional in contrast to other attempts at tagging SID-1 (see *Technical comments* in Methods). Fluorescence from SID-1::mCherry was visible in the proximal and distal regions of the adult germline (Fig. 4b). Expression also progressively increased during development with tissue-specific enrichment in the developing embryo (Fig. 4c, *left*), becoming ubiquitous in hatched L1 larvae (Fig. 4c, *middle*,d). SID-1::mCherry was not easily detectable in the germline during later larval

development (Fig. 4c, *middle* and *right*). In combination with the expression of RME-2 observed in the proximal germline (Extended Data Fig. 1d; ref<sup>32</sup>), this expression pattern of SID-1 is consistent with the entry of most dsRNA from circulation of adult animals into the germline, followed by activity of transport mechanisms in developing embryos and early larvae that inherit parental dsRNA.

To determine if acute, induced expression rather than developmental expression of SID-1 can be sufficient for the import of dsRNA into the germline, we engineered the endogenous sid-1 gene to transcribe a fusion transcript with an aptamer-regulated ribozyme (Extended Data Fig. 6a, *left*) that cleaves itself when not bound to tetracycline (Extended Data Fig. 6a, *right*) (based on ref. 44). Exposing these animals to tetracycline enabled silencing by dsRNA in somatic tissues (hypodermis: Extended Data Fig. 6b, *left*; body-wall muscles: Extended Data Fig. 6b, *right*), indicative of stabilization of sid-1 mRNA, production of SID-1 protein, and subsequent dsRNA import in somatic cells. However, such tetracycline-induced silencing was not detectable in the germline (Extended Data Fig. 6c-f). Yet, similar tagging of the ubiquitously expressed gene gtbp-1::gfp resulted in detectable rescue of expression within the germline by tetracycline (Extended Data Fig. 6g). A possible explanation for the poor rescue of SID-1 activity within the germline is that post-transcriptional mechanisms targeting sid-1 mRNA in the germline but not in somatic cells interfere with tetracycline-dependent stabilization of the sid-1 transcript (e.g., piRNA-based regulation of sid-1 mRNA<sup>45,46</sup>), or that acute stabilization of the sid-1 transcript does not override developmental regulation of SID-1 translation.

Additional attempts to tag the SID-1 protein guided by structure and to modulate *sid-1* transcripts guided by post-transcriptional regulatory interactions could improve control of dsRNA transport between cells. Nevertheless, the developmentally regulated expression

observed for both SID-1 and RME-2 in the germline is consistent with intergenerational or transgenerational effects of endogenous dsRNA from parental circulation after development of the adult germline.

Temporary loss of *sid-1* causes a transgenerational increase in the levels of mRNA from two germline genes

To understand how the dsRNA importer SID-1 might be used in endogenous gene regulation across generations, we searched for sid-1-dependent changes in gene expression that could be heritable (Fig. 5, Extended Data Fig. 3 and Extended Data Fig. 7). To control for genetic background (see *Technical comments* in Methods), we used Cas9-mediated genome editing to delete the entire sid-1 coding sequence or introduce a nonsense mutation in cohorts of the same wild-type animals. By comparing polyA+ RNA from this wild type with that of the newly generated sid-1(jam113[deletion]) (Fig. 5a,b and Extended Data Fig. 7a) or sid-I(jam80[nonsense]) (Fig. 5a-c) animals, we found that 26 genes were significantly (q < 0.05)misregulated in sid-1(jam113[deletion]) (Extended Data Fig. 7b) and 6 in sid-1(jam80[nonsense]) (Fig. 5d, top), both including sid-1 (a list of significantly altered genes is in Extended Data Table 2). The most upregulated gene in sid-1(jam113[deletion]), F14F9.5 (Extended Data Fig. 7b), which is located immediately 3' to sid-1 in the genome, was only misregulated in the deletion mutant and not in the nonsense mutant (Extended Data Fig. 7c, left). Both mutants, however, were equally defective for silencing by ingested dsRNA (Fig. 5b). This observation suggests that while both mutations result in loss of SID-1 protein, the deletion of sid-I also changes local regulatory sequences (potentially explaining upregulation of the neighboring gene F14F9.5) and eliminates sid-1 mRNA, which could participate in RNA-based regulatory interactions within the germline<sup>45,46</sup>. Nevertheless, we could detect two genes that were

upregulated in both sid-1(jam113[deletion]) and sid-1(jam80[nonsense]) animals (red in Fig. 5d, top, and Extended Data Fig. 7b): the identical loci W09B7.2/F07B7.2 (Extended Data Fig. 7c, middle), and Y102A5C.36 (Extended Data Fig. 7c, right). Intriguingly, another gene cls-3 also changed in both mutants (Extended Data Table 2) but in different directions (~3.4-fold decrease in the sid-1(jam80[nonsense]) mutant but a  $\sim$ 5.8-fold increase in the sid-1(jam113[deletion])mutant), suggesting that the direction of change in expression can vary. Conservatively, we began by analyzing only the two genes with mRNA levels that changed in the same direction in both sid-1 mutants. Both W09B7.2/F07B7.2 and Y102A5C.36 have been reported<sup>47</sup> to be expressed within the germline (Extended Data Fig. 7d, *left*) and regulated by endogenous small RNAs (Extended Data Fig. 7d, *middle* and *right*). Spliced mRNA levels measured at a later generation using RT-qPCR demonstrated that both transcripts were upregulated in sid-1(jam80[nonsense]) animals compared to wild-type animals as expected (Fig. 5e), but no upregulation was detectable in sid-1(jam113[deletion]) animals (Extended Data Fig. 7e). This difference between the two sid-1 mutants could reflect increased variation in expression (as was observed for cls-3 using RNAseq) or could reflect complex effects caused by deletion of sid-1 DNA (e.g., F14F9.5 overexpression, loss of sid-1 mRNA, etc.) that could be independent of SID-1 protein function.

To determine if changes in W09B7.2/F07B7.2 and Y102A5C.36 expression were heritable, we reverted the sid-1 nonsense mutation to wild-type sequence using Cas9-mediated genome editing. This immediately restored silencing by ingested dsRNA (Fig. 5b) with concomitant recovery of sid-1 mRNA to wild-type levels (Fig. 5e, top). In contrast, changes in both W09B7.2/F07B7.2 and Y102A5C.36 expression persisted (Fig. 5d, bottom) even after one year of passaging the reverted animals (sid-1(jam86[revertant])) (i.e., after >100 generations,

Fig. 5e, *middle* and *bottom*). Thus, the *sid-1*-dependent accumulation of mRNA from these two germline genes persisted for many generations, likely through mechanisms that maintain heritable epigenetic changes. We hereafter refer to these *sid-1-dependent genes* (*sdg*) that show heritable epigenetic changes in response to temporary loss of SID-1 as *sdg-1* (*W09B7.2/F07B7.2*) and *sdg-2* (*Y102A5C.36*).

# The *sid-1*-dependent gene *sdg-1* is affected by many factors that regulate RNA silencing in the germline

To determine if expression of sdg-1 and sdg-2 is regulated by other proteins that play a role in RNA silencing within the germline, we examined 21 published datasets  $^{30,46,48-58}$  that reported changes that depend on such proteins. For each dataset, we determined if the lists of genes reported as showing significant changes in mutants compared to the respective wild types included sdg-1 and/or sdg-2. This analysis revealed that changes in mRNA and/or antisense small RNAs of sdg-1 were detected in 20 of the 21 datasets while changes in sdg-2 were observed in 9 of 21 (Fig. 5f). When detected, changes in sdg-2 were in the same direction as changes in sdg-1, suggestive of similar regulation of both genes.

RNAs transcribed in the germline can be recognized as they exit the nuclear pores by piRNAs bound to the Argonaute PRG-1, which recruits them for regulation by antisense small RNAs called 22G RNA made by proteins organized within perinuclear germ granules (reviewed in ref.<sup>59</sup>). Interaction with piRNAs was detected for RNA from *sid-1*, *sdg-1*, and *sdg-2*, and the control gene *tbb-2* using crosslinking, ligation, and sequencing of hybrids<sup>53</sup> (Fig. 5f), consistent with their germline expression. Depletion of downstream 22G RNAs targeting both *sid-1* and *sdg-1* was detectable upon loss of the germ granule component MUT-16<sup>51</sup> (Fig. 5f). Both genes were among the top 500 genes targeted by 22G RNAs bound by the secondary Argonaute

HRDE-1/WAGO-9<sup>30</sup> (Fig. 5f), suggesting similar downregulation of both genes using 22G RNAs. Furthermore, multiple datasets support downregulation of *sdg-1* within the germline by HRDE-1/WAGO-9-bound 22G RNAs in the absence of PRG-1. One, loss of HRDE-1/WAGO-9 increased *sdg-1* RNA in whole animals<sup>58</sup> (Fig. 5f) and in dissected gonads<sup>57</sup> (Fig. 5f). Two, loss of PRG-1 decreased *sdg-1* RNA (Fig. 5f) and increased 22G RNAs that are antisense to *sdg-1* (Fig. 5f) in dissected gonads<sup>52</sup>. Three, although animals that lack PRG-1 become progressively sterile, the increase in *sdg-1* 22G RNA persisted in near-sterile animals (Fig. 5f, near-sterile in ref.<sup>52</sup>), and this increase was eliminated upon additional loss of HRDE-1/WAGO-9 (Fig. 5f, near-sterile in ref.<sup>52</sup>).

As expected for *sid-1*-dependent downregulation of *sdg-1*, multiple datasets reveal an inverse relationship between the two genes. In animals lacking PRG-1, *sid-1* RNA levels increased and *sid-1* 22G RNAs decreased<sup>55</sup> (Fig. 5f), but both *sdg-1* RNA and *sdg-2* RNA levels decreased along with an increase in 22G RNAs<sup>51-56</sup> (Fig. 5f). This inverse relationship between *sid-1* and *sdg-1* RNA regulation is also observed when many components of germ granules are mutated as indicated by changes in 22G RNA upon loss of the embryonic P granule components MEG-3/-4<sup>46</sup> (Fig. 5f), the PRG-1 interactor DEPS-1<sup>51</sup> (Fig. 5f), or the Z granule component ZSP-1<sup>50</sup> (Fig. 5f; also known as PID-2<sup>60</sup>).

In addition to the above studies, pioneering studies that used microarrays identified *sdg-1* as upregulated in animals lacking the germ granule component DEPS-1<sup>49</sup> (Fig. 5f) and in animals lacking the dsRNA-binding protein RDE-4 (Fig. 5f; second-most upregulated in ref.<sup>48</sup>), which recruits dsRNA imported through SID-1 and other intracellular dsRNA for processing and eventual gene silencing. Animals that lack RDE-4 show a ~47.5-fold increase in *sdg-1* RNA<sup>48</sup>. A reduction in RDE-4 activity could also contribute to the ~11.6-fold increase in *sdg-1* RNA seen

in *deps-1(-)* animals because these animals also show a ~3.2-fold decrease in *rde-4* RNA<sup>49</sup> (one of 13 downregulated genes). These observations support the idea that appropriate regulation of *sdg-1* RNA requires both piRNA-mediated processes that act via germ granule components such as DEPS-1 and dsRNA-mediated processes that use SID-1 and RDE-4.

In summary, the levels of *sdg-1* RNA are detectably regulated by the dsRNA-selective importer SID-1, the dsRNA-binding protein RDE-4, and the piRNA-binding Argonaute PRG-1. Presence of dsRNA-mediated regulation or loss of piRNA-mediated regulation enhances MUT-16-dependent production of secondary small RNAs that bind the secondary Argonaute HRDE-1/WAGO-9. Consistent with downregulation of these *sid-1*-dependent transcripts by SID-1, disruption of many components of germ granules results in opposite effects on these transcripts and *sid-1* RNA. Intriguingly, a search of protein interaction studies revealed that the SDG-1 protein is among the interactors of two germ granule components: PID-2 by immunoprecipitation<sup>60</sup> (also known as ZSP-1<sup>50</sup>) and DEPS-1 by proximity labeling<sup>61</sup>. Thus, one possibility suggested by these observations is that reduction of *sdg-1* RNA via SID-1 alters the amount of SDG-1 protein, which could interact with components of germ granules to mediate RNA regulation within the germline of wild-type animals.

#### Regulation of sdg-1 RNA is susceptible to epigenetic changes that last for many generations

SDG-1 is encoded by a gene located within a retrotransposon (Extended Data Fig. 8a) that is within a duplicated ~40 kb region and has two recognizable paralogs (Extended Data Fig. 8b). To facilitate analysis of SDG-1 expression, we tagged both loci that encode SDG-1 with *mCherry* coding sequences lacking piRNA-binding sites<sup>42,43</sup> (*mCherry*Δ*pi*) (Extended Data Fig. 8c,d). This tagging resulted in the expression of *sdg-1::mCherry*Δ*pi* mRNA being ~16-fold higher than *sdg-1* mRNA (Extended Data Fig. 8e), potentially because of the reduction in the

overall density of piRNA-binding sites per transcript, the additional introns included in  $mCherry\Delta pi$  (based on refs. 62,63), and/or other unknown factors. Fluorescence from SDG-1::mCherry was observed in the germline of adult animals (Fig. 6a). However, animals showed variation in SDG-1::mCherry expression between their two gonad arms (Fig. 6a, middle shows bright anterior (20% of animals) and *right* shows bright posterior (6% of animals)). A contributing feature for the observed stochasticity could be the location of sdg-1 within a duplicated region (Extended Data Fig. 8a), as suggested by similar stochastic RNA silencing of multi-copy transgenes but not single-copy transgenes<sup>64</sup>. Despite this variation, unbiased passaging of self-progeny for more than 18 generations continuously preserved SDG-1::mCherry expression in an otherwise wild-type background (Fig. 6b). In contrast, mating, which can perturb RNA regulation within the germline in cross progeny<sup>43</sup>, caused dramatic changes in sdg-1 expression that persisted in descendants (Fig. 6c). Mating animals that express SDG-1::mCherry with wild-type animals resulted in heritable changes along lineages that express sdg-1::mCherry\(\Delta\)pi mRNA or that express sdg-1 mRNA (Fig. 6c and Extended Data Fig. 9a). This discovery of mating-induced perturbation in gene expression raises caution in interpreting past studies (summarized in Fig. 5f) where changes in multiple independent isolates were not examined. Nevertheless, when we used genetic crosses to determine the impact of mutations on sdg-1 expression, we observed reduced SDG-1::mCherry fluorescence in mutants predicted to have reduced levels of intracellular dsRNA (Fig. 6d, sid-2(-), sid-5(-)) or reduced processing of intracellular dsRNA (Fig. 6d, eri-1(-)). In contrast, we observed an increase in SDG-1::mCherry fluorescence in animals lacking MUT-16 (Fig. 6d). Finally, animals lacking RME-2, which lack the ability to import many maternal factors (e.g., lipids, proteins, RNAs, etc.), also showed an increase in SDG-1::mCherry fluorescence (Fig. 6d).

To avoid mating-induced perturbations of RNA regulation within the germline, we used Cas9-mediated genome editing to introduce mutations into animals that express SDG-1::mCherry in an otherwise wild-type background. Use of this approach to mutate a control gene with no known roles in RNA regulation within the germline resulted in similar levels of SDG-1::mCherry fluorescence in multiple isolates of animals with and without the mutation (Extended Data Fig. 9b). In contrast, mutating sid-1 using Cas9-mediated genome editing caused a range of expression levels in different isolates when compared with sid-1(+) animals (Fig. 6e - 6 isolates lower, 2 isolates comparable, and 1 isolate higher), which differs from the increase in sdg-1 mRNA observed upon SID-1 loss in the single isolate examined earlier (Fig. 5). One explanation for these observations is that in the absence of SID-1, the levels of SDG-1 vary in different isolates because the sdg-1 gene becomes prone to heritable epigenetic changes, resulting in either high or low expression states being stabilized in different isolates. Alternatively, it is possible that the  $\sim$ 16-fold overexpression of sdg-1::mCherry $\Delta pi$  mRNA perturbs RNA-mediated epigenetic regulation, potentially indicative of a role for the SDG-1 protein in such regulation. Mutating sid-3 also lowered the levels of SDG-1::mCherry in one isolate, but caused no detectable change in another (Fig. 6f). While both isolates with loss of RDE-1 showed lower levels of SDG-1::mCherry, both isolates with loss of the germ granule component DEPS-1 showed higher levels of SDG-1::mCherry (Fig. 6f). These experiments also reveal that in most isolates of animals expected to have reduced levels of intracellular dsRNA (sid-3(-), sid-1(-)) or reduced processing of intracellular dsRNA (*rde-1(-)*), SDG-1::mCherry fluorescence is reduced. In contrast, isolates lacking DEPS-1 showed increased expression of SDG-1::mCherry.

Collectively, the observations on SDG-1 expression using mutants suggest that the uptake and processing of intracellular dsRNA (mediated by SID-1, SID-2, SID-3, SID-5, RDE-1, and

ERI-1) and the function of germ granules (mediated by MUT-16 and DEPS-1) are both necessary to maintain intermediate levels of SDG-1 expression across generations. Once the levels of SDG-1::mCherry were reduced upon loss of SID-1, downregulation persisted across generations even after restoration of wild-type SID-1 (Fig. 6g), just as the upregulation of untagged *sdg-1* mRNA also persisted (Fig. 5). Despite >100 generations of such persistent silencing, the expression of SDG-1::mCherry could be restored by mutating *deps-1* (Fig. 6g), implicating small RNA-based regulation and germ granules in the maintenance of new epigenetic states established upon loss of SID-1.

# SID-1-dependent genes, including SDG-1, could alter RNA-mediated regulation in the germline

Since SDG-1 interacts with regulators of RNA silencing (ZSP-1/PID-2<sup>60</sup> and DEPS-1<sup>61</sup>), loss of SID-1 could both block the entry of extracellular dsRNA into the cytosol and change intracellular RNA regulation through SID-1-dependent genes such as SDG-1. In support of this possibility, intracellular delivery of dsRNA through injection into the syncytial germline of *sid-1(-)* animals showed a weak defect in silencing (Fig. 2D in ref.<sup>28</sup> and Fig. 1 in ref.<sup>29</sup>). To examine if changes in the levels of SDG-1 alone could account for such a defect in silencing by intracellular dsRNA in the germline, we exposed independently-generated *sdg-1* deletion animals and animals that overexpress sdg-1 (i.e., with  $sdg-1::mCherry\Delta pi$ ) to dsRNA matching the germline gene pos-1 for ~16 hours. This short exposure to pos-1-dsRNA caused intermediate levels of silencing in wild-type animals and comparable intermediate silencing in sdg-1 mutant and sdg-1 overexpressing animals (Fig. 7a), suggesting that changes in sdg-1 levels alone are not sufficient to cause a defect in silencing by dsRNA that is detectable using this assay.

Alternatively, the previously described defect in silencing by intracellular dsRNA in sid-1(-)

animals<sup>28,29</sup> could be through the promotion of competing piRNA-mediated gene regulation in the absence of SID-1. This notion that dsRNA-mediated and piRNA-mediated gene regulation compete in the germline is supported by a study that demonstrated that loss of PRG-1 enhances heritable RNA silencing by dsRNA<sup>65</sup>. To test if loss of SID-1 or a *sid-1*-dependent gene enhances piRNA-mediated silencing, we used an experimental system which initiates piRNA-mediated silencing of the two-gene operon described in Fig. 2 through mating, independent of externally provided dsRNA<sup>43</sup>. We found that *sid-1(-)* animals exhibited enhanced mating-induced silencing (Fig. 7b, *top right*: ~50% off in *sid-1(+)* vs 100% off in *sid-1(qt9[nonsense])*), while animals lacking *sdg-1* showed a small reduction in mating-induced silencing that was not statistically significant (Fig. 7b, *bottom right*, ~40% off in *sdg-1(+)* vs ~30% off in *sdg-1(jam232[deletion])*). Taken together, these results support the model that loss of SID-1 weakly inhibits silencing by intracellular dsRNA<sup>28,29</sup> but enhances silencing by piRNAs within the germline, potentially through the action of multiple altered SID-1-dependent genes that collectively promote piRNA-mediated gene regulation.

RNA regulation within the germline using piRNAs relies on phase-separated granules (reviewed in ref.<sup>66</sup>). To determine if the identification of SDG-1 as an interactor of the Z-granule component PID-2<sup>60</sup>/ZSP-1<sup>50</sup> and potentially of the P-granule-adjacent protein DEPS-1<sup>61</sup> could be seen as colocalization with Z-granules *in vivo*, we examined the localization of SDG-1::mCherry within the cytoplasm at high resolution using AiryScan imaging<sup>67</sup>. SDG-1::mCherry was enriched in perinuclear foci in many animals (Fig. 7c, *top*; 7 of 9 animals) and these sites of enrichment colocalized with the Z-granule marker GFP::ZNFX-1<sup>68,69</sup> (Fig. 7c, *bottom*; 100% colocalized in 10 of 12 animals with enrichment). Time-course imaging revealed re-localization of SDG-1::mCherry into the nucleus from the cytoplasm in the -1 oocyte, which will be the first

to be fertilized (Fig. 7d, *left* and Extended Data Movie 1), along with subsequent exclusion from the nucleus before the maternal and paternal pronuclei meet (Fig. 7d, right and Extended Data Movie 2). Such dynamic entry into the nucleus followed by exclusion from the nucleus also occurred during early cell divisions in the developing embryo (Extended Data Movies 3,4). The timing of nuclear entry of SDG-1::mCherry coincides with the nuclear envelope breakdown events that occur during fertilization and early development<sup>70</sup>. The sdg-1 coding sequence was required for regulated nuclear entry because deletion of the sdg-1 open reading frame in sdg- $1::mCherry\Delta pi$  animals resulted in mCherry expression throughout the germline in both the cytoplasm and nuclei (Fig. 7e). Nuclear localization of the SDG-1 protein in the -1 oocyte is like that of the essential Argonaute CSR-1b<sup>71</sup>, thought to play a role in protecting transcripts from silencing. Exposure to ingested dsRNA did not alter the expression of sdg-1p::mCherryΔpi/sdg- $I(\Delta)$ ]::sdg-1 3' UTR (Fig. 7f) but loss of rde-4 perturbed expression such that one isolate showed loss of expression while the other showed enhanced expression (Fig. 7g). These results suggest that while the sdg-1 open reading frame is required for exclusion from germline nuclei, it is not required for the response of the sdg-1 gene to changes in intracellular dsRNA. Together, these observations on the levels and localizations of SDG-1 raise the possibility that this protein is actively regulated by extracellular and intracellular dsRNA with a role in heritable RNA silencing, potentially with Z granules, and additional cell-cycle coupled roles during early development, potentially through nucleocytoplasmic shuttling.

#### **DISCUSSION**

Our analyses suggest a model for the impact of dsRNA from parental circulation on descendants (Fig. 7h). Extracellular dsRNA can accumulate in parental circulation through regulated secretion from neurons (e.g., oxidative damage promotes accumulation) and potentially

other tissues. Uptake into the germline is RME-2-dependent for some forms of dsRNA (blue in Fig. 7h), but RME-2-independent for other forms of dsRNA (grey in Fig. 7h). While all forms of dsRNA require SID-1 for the entry of dsRNA into the cytosol in progeny, RME-2-dependent dsRNA also require SID-5. Such dsRNA from parental circulation along with other intracellular dsRNA are processed with the help of the dsRNA-binding protein RDE-4 in progeny (Fig. 7h, bottom). This processing of dsRNA regulates the SID-1-dependent gene sdg-1 by reducing variation between animals in the levels of sdg-1 mRNA, although the dsRNA sequences likely need not match sdg-1 because no such dsRNA was reported in the published dsRNAome<sup>72</sup> and because this regulation can occur in the absence of the sdg-1 open reading frame. The sdg-1 gene is located within a retrotransposon that is also targeted by heritable RNA silencing, but the SDG-1 protein colocalizes with perinuclear granules called Z granules, which are required for heritable RNA silencing. Consistent with the SDG-1 protein promoting heritable RNA silencing, the sdg- $1::mCherry\Delta pi$  gene is highly susceptible to mating-induced silencing, potentially owing to the ~16-fold higher levels of SDG-1::mCherry compared with that of SDG-1 in wild-type animals. In agreement with this proposal, SID-1 limits heritable RNA silencing because loss of SID-1 enhances mating-induced silencing (Fig. 7b, top). Since the sdg-1 gene is located within a retrotransposon that is targeted by heritable RNA silencing, this mechanism for regulating the regulators of heritable RNA silencing such as SDG-1 (and potentially other SDGs) reveals a strategy for tuning an autoregulatory loop for heritable RNA silencing by using competing dsRNA processing. Intriguingly, SDG-1 becomes enriched within nuclei upon nuclear envelope breakdown during fertilization and during early cell divisions in embryos (Fig. 7h, bottom right) with active exclusion from nuclei after each reformation of the nuclear envelope, suggestive of additional roles for this retrotransposon-encoded protein.

While the physiological conditions that promote secretion of dsRNA are not known, the discovery that oxidative damage of neurons can enhance the secretion of dsRNA suggests that disruption of cell structures by oxidative damage (e.g., membrane integrity) or initiation of cellular processes that repair oxidative damage (e.g., through ejection of damaged macromolecules<sup>73</sup>) also promote the release of dsRNA. Pathologies of the central nervous system in humans, including cancer, stroke, multiple sclerosis, neurodegenerative disease, and brain injury, have been associated with extracellular RNAs detected in circulation (reviewed in ref.<sup>74</sup>), although their origins and regulatory consequences, if any, remain unknown. The gene regulatory effects of neuronal dsRNA released upon oxidative damage of neurons provide convenient readouts that can be analyzed to understand neuronal damage and its consequences in animals.

The trafficking of extracellular dsRNA from parent to progeny has spatial specificity, as evidenced by more silencing within the proximal germline (Fig. 2), temporal specificity, as evidenced by the need for dsRNA beyond the fourth larval stage<sup>28,29</sup> (Fig. 1), and substrate specificity, as evidenced by the differential requirements for 50-bp dsRNA with 5' OH versus a mix of longer dsRNAs with 5' triphosphates (Fig. 3). One possible explanation for these constraints could be that proteins mediating dsRNA transport or subsequent silencing differ in their availability during development and in their affinities for different substrates. For example, SID-1, which was not detected in the developing larval germline but was detected in the adult germline (Fig. 4), has an extracellular domain that binds dsRNA<sup>75</sup> and could prefer dsRNA molecules with 5' phosphates and/or long dsRNA. Although the selectivity uncovered here could apply to all dsRNA delivered into the extracellular space of *C. elegans* from any source (see Extended Data Table 1 for constraints on intergenerational dsRNA transport), the chemistry of

the delivered dsRNA could be modified by yet unidentified enzymes *in vivo* to overcome these requirements. Tracking labeled dsRNA with diverse chemistries from parental circulation to progeny could allow correlation of differences observed in progeny silencing to differences in intergenerational trafficking.

The germline is a major site of dsRNA import in *C. elegans* as evidenced by three key observations: the expression of SID-1 in the germline (Fig. 4), heritable misregulation of germline genes in sid-1(-) animals (Fig. 5 and Fig. 6), and accumulation of fluorescently-labeled dsRNA from the extracellular space in the germline<sup>28,29</sup>. As a result, sid-1(-) animals could have a defect in the germline that is detectable only under conditions that promote dsRNA transport (e.g., oxidative damage). Multiple physiological defects in the germline and soma of sid-1(-) animals have been reported but have not been widely reproduced, have only been characterized within single generations, or have not been attributed to any specific *sid-1*-dependent gene(s). These include defects in animals with some misfolded proteins in the endoplasmic reticulum<sup>76</sup>, in animals exiting the dauer stage<sup>77,78</sup>, in animals exposed to pathogenic *P. aeruginosa*<sup>79,80,81</sup>, in animals exposed to odor<sup>82</sup>, in intestinal cells that develop in the presence of a multi-copy transgene<sup>83</sup>, and in animals that overexpress α-synuclein<sup>84</sup>. RNA-seq experiments in this study and comparisons to those of previous studies suggest that genetic background-dependent changes can obscure genuine sid-1-dependent changes (see Extended Data Fig. 7 and Technical comments in Methods), raising caution in the interpretation of putative sid-1-dependent defects. Comparing multiple sid-1 mutants generated using genome editing with animals in which the mutated sequence has been reverted to wild-type sequence in the same genetic background could provide a firmer basis for the identification of additional *sid-1*-dependent processes.

Genes expressed within the germline are likely regulated by positive feedback loops that are required to continually produce factors for maintaining germline immortality and for preserving form and function across generations<sup>85,86</sup>. Thus, germline genes could be particularly vulnerable to heritable epigenetic changes, where deviations in the expression levels of a gene that is regulated by or is part of such feedback loops has the potential to become permanent in descendants. Our analysis of sdg-1 expression suggests that it is part of a regulatory architecture that is susceptible to heritable epigenetic changes through the perturbation of RNA regulation (Fig. 5, Fig. 6, and Fig. 7). Such architectures within the germline could be exploited by 'selfish' genetic elements such as retrotransposons to persist across evolution if one of these elements also include genes encoding a regulator. In support of a wider use of such a strategy, a paralog of SDG-1, ZK262.8 (Extended Data Fig. 8b), is also encoded by a gene located within a retrotransposon and its loss along with that of the miRNA-associated Argonaute ALG-2 was reported to be synthetic lethal<sup>87</sup>. To buffer against heritable epigenetic changes, levels of gene expression would need to be maintained within a particular range for a certain regulatory context. Given the association of SDG-1 protein with germ granule components ZSP-1/PID-2 and DEPS-1, and the maintenance of heritable changes in  $sdg-1::mCherry\Delta pi$  expression by DEPS-1, buffering against changes in gene expression could involve both RNA- and proteinbased regulation that tunes the function of perinuclear granules. We therefore speculate that one role for extracellular RNAs that enter germ cells in other systems (e.g., tRNA fragments in mammals<sup>5,6,8</sup>) could be to similarly buffer against heritable changes in gene expression.

#### **ACKNOWLEDGEMENTS**

We thank Sindhuja Devanapally for data on silencing by neuronal dsRNA in *hrde-1(-)* animals and mating-induced silencing in *sid-1(-)* animals; Daphne Knudsen for the generation of

mut-16(jam148[nonsense]); Mary Chey, Samiha Tasnim, and Daphne Knudsen for comments on the manuscript; the Caenorhabditis elegans Genetic Stock Center, the Seydoux laboratory (Johns Hopkins University) and the Hunter laboratory (Harvard University) for strains; Quentin Gaudry for help in creating our optogenetics apparatus; the Andrews laboratory for use of their Nikon Eclipse Ti spinning disk confocal microscope; Amy Beaven and the Imaging Core Facility for temporary use of a Leica TCS SP8 DLS microscope with HyVolution and the Zeiss LSM 980 AiryScan 2 Laser Scanning Confocal microscope (supported by grant 1S10OD025223-01A1 from the NIH); Lanelle Edwards, Rex Ledesma, Carlos Machado, and Omega Bioservices for help with RNA sequencing and analysis. Funding: This work was supported by UMD CMNS Dean's Matching Award for "Training Program in Cell and Molecular Biology" T32GM080201 to N.S. and in part by National Institutes of Health Grants R01GM111457 and R01GM124356, and National Science Foundation Grant 2120895 to A.M.J.

#### **Author contributions**

N.S., A.S., and A.M.J designed the research. N.S., A.S., A.L.Y., W.M.C., J.A.M., and A.M.J. performed all experiments, and collected and analyzed data. N.S., A.S., and A.M.J. prepared the manuscript with contributions from all authors.

#### **Data Availability**

Source data are provided with this paper. All data are available in the manuscript, the supplementary materials, or on figshare. RNA-seq data has been deposited to Gene Expression Omnibus (GEO) with the accession number GSE185385.

#### **Code Availability**

All code is available within the manuscript, the supplementary materials, or at AntonyJose-Lab/Shugarts\_et\_al\_2023 on github.

### **Declaration of interests**

The authors declare no competing interests.

#### **METHODS**

Strains and oligonucleotides

All strains (listed in Extended Data Table 3) were cultured on Nematode Growth Medium (NGM) plates seeded with 100 μl of OP50 *E. coli* at 20°C and strains made through mating were generated using standard methods<sup>88</sup>. Oligonucleotides used are in Extended Data Table 4 (for genotyping *sid-1(qt9)*: P1-P2, *ttTi5605*: P3-P5, *eri-1(mg366)*: P6-P7, *sid-1(tm2700)*: P8-P10, *hrde-1(tm1200)*: P11-P13, *nrde-3(tm1116)*: P14-P16, and *rde-4(ne301)*: P156-P157). Strains made through mating existing mutant strains and genotyping using the above primers are listed below.

<u>To create gtbp-1::gfp animals with hrde-1(tm1200) in the background</u>: AMJ577<sup>25</sup> was crossed with JH3197 males to create AMJ1220 and one other independent isolate.

To create *gtbp-1::gfp* animals with *nrde-3(tm1116)* in the background: JH3197 was crossed with WM156 males to create AMJ1383.

*Transgenesis* 

Animals were transformed with plasmids and/or PCR products using microinjection<sup>89</sup> to generate extrachromosomal arrays or single-copy transgenes. All plasmids were purified from bacterial culture using QIAprep Spin Miniprep Kit (Qiagen) and all PCR products were generated with Phusion<sup>®</sup> High-Fidelity DNA Polymerase (New England BioLabs) and purified using NucleoSpin Gel and PCR Clean-up Kit (Macherey-Nagel).

To express *sid-1::DsRed* in the muscle from an integrated array: pAJ53a (*myo-3p::sid-1::DsRed::unc-54 3'UTR*, made by AMJ while in Hunter Lab, Harvard University) was generated by amplifying part of *sid-1* cDNA from pHC355<sup>23</sup> with primers P27 and P18, *DsRed* and *unc-54 3'UTR* from pHC183<sup>14</sup> with primers P17 and P30, fusing the fragments using PCR

with primers P30 and P31, and then cloning the fusion product into the pHC355 vector backbone using the restriction enzymes NruI and EagI. pAJ53a (40 ng/µl) was then injected into HC196 and animals expressing DsRed were isolated. AMJ3 was isolated as a spontaneous integrant.

AMJ3 males were then crossed with AMJ308 hermaphrodites to generate AMJ327.

To express *sid-1::DsRed* in the germline from a single-copy transgene: The *mex-5* promoter was amplified from pJA252 (Addgene #21512) using the primers P19 and P20. The *sid-1* gene was amplified from N2 genomic DNA using the primers P21 and P22. The *DsRed* gene was amplified from pAJ53a (*myo-3p::sid-1(+)::DsRed::unc-54 3'UTR*; made by AMJ and Tessa Kaplan while in Hunter Lab, Harvard University) using the primers P23 and P24. The *sid-1 3'UTR* was amplified using the primers P25 and P26. Using NEBuilder<sup>®</sup> HiFi DNA Assembly (New England BioLabs), these four amplicons were placed into pCFJ151 (Addgene #19330) digested with AfIII (New England BioLabs) and treated with CIP (New England BioLabs) to generate pJM10. pJM10 (50 ng/μl) and the coinjection markers pCFJ601 (50 ng/μl), pMA122 (10 ng/μl), pGH8 (10 ng/μl), pCFJ90 (2.5 ng/μl), and pCFJ104 (5 ng/μl) (plasmids described in ref.<sup>90</sup>) were injected into the germline of adult EG4322 animals. One transgenic line was isolated as described previously<sup>90</sup> and crossed with HC196 males to generate AMJ576. The integration of *mex-5p::sid-1(+)::DsRed::sid-1 3'UTR* in AMJ576 was verified by genotyping with primers P3-P5 and Sanger sequencing of the insertion.

To express *sid-1::gfp* in the muscle from an extrachromosomal array: pTK2 (*myo-3p::sid-1::gfp*, made by AMJ and Tessa Kaplan while in Hunter Lab, Harvard University) was constructed by amplifying part of *sid-1* cDNA from pHC355<sup>23</sup> with primers P27 and P28, *gfp* and *unc-54 3'UTR* from pPD95.75 (Addgene #1494) using primers P29 and P30, and then fusing the fragments using PCR with primers P30 and P31 and cloning the product into the pHC355

vector backbone using the restriction enzymes NruI and EagI. pTK2 (10 ng/μl) was injected into HC196 and animals expressing GFP were isolated as AMJ706.

To express *PH::miniSOG* in neurons from an extrachromosomal array: pNMS03 (*rgef-lp::PH::miniSOG::unc-54 3'UTR*) was generated by amplifying the vector backbone of pHC337 excluding the *gfp*-dsRNA hairpin sequence using primers P35 and P36, and assembling it with *PH::miniSOG(Q103L)* amplified from pCZGY2851 (gift from Andrew Chisholm) with primers P33 and P34 using NEBuilder<sup>®</sup> HiFi DNA Assembly (New England BioLabs). pNMS03 (40 ng/μl) was injected into N2 animals with pHC448<sup>91</sup> (*myo-2p::DsRed2::unc-54 3'UTR*; 40 ng/μl) as a coinjection marker to create AMJ837 and two other isolates.

pNMS03 (40 ng/μl) was also injected into N2 animals with PCR products forming *rgef-lp::DsRed* (40 ng/μl) generated previously<sup>91</sup> as a coinjection marker to create AMJ936 and two other isolates.

To express *PH::miniSOG* in neurons from a single-copy transgene: pNMS05 (*rgef-lp::PH::miniSOG::unc-54 3'UTR* with *ttTi5605* homology arms and *Cbr-unc-119(+)*) was generated by amplifying the transgene *rgef-lp::PH::miniSOG::unc-54 3'UTR* from pNMS03 with primers P37 and P38 containing AvrII restriction sites and cloning the fragment into pCFJ151 after AvrII (New England BioLabs) digestion. pNMS05 (50 ng/μl) and the coinjection markers pCFJ601 (50 ng/μl), pMA122 (10 ng/μl), pGH8 (10 ng/μl), pCFJ90 (2.5 ng/μl), and pCFJ104 (5 ng/μl) (plasmids described in ref.<sup>90</sup>) were injected into the germline of adult EG4322 animals. One transgenic line was isolated as described previously<sup>90</sup> and designated as AMJ1019. The integration of *rgef-lp::PH::miniSOG::unc-54 3'UTR* in AMJ1019 was verified by genotyping with primers P3-P5 and Sanger sequencing of the insertion.

To express *PH::miniSOG* with *bli-1*-dsRNA in neurons from an extrachromosomal array: pNMS03 (40 ng/μl) was injected with *rgef-1p::bli-1-sense* (40 ng/μl) and *rgef-1p::bli-1-antisense* (40 ng/μl) PCR products generated previously<sup>92</sup> into GR1373 animals with pHC448 (*myo-2p::DsRed2::unc-54 3'UTR*) as a coinjection marker (40 ng/μl) to create AMJ1007 and one other independent isolate. AMJ1007 was crossed with HC731 males to create AMJ1108 and two other isolates. AMJ1108 was crossed with HC196 males to create AMJ1114 and one other isolate. AMJ1007 was crossed with N2 males to create AMJ1123 and one other isolate. AMJ1123 males were crossed with 3X outcrossed FX02700 (designated as AMJ1153) to create AMJ1151 and two other isolates. AMJ1151 was crossed with GR1373 males to create AMJ1173 and two other isolates.

To express *PH::miniSOG* with *gfp*-dsRNA in neurons from an extrachromosomal array: pNMS03 (40 ng/μl) and pHC337 (*rgef-1p::gfp-dsRNA::unc-54 3'UTR*; 40 ng/μl) were injected into AMJ819<sup>43</sup> with pHC448 (*myo-2p::DsRed2::unc-54 3'UTR*; 40 ng/μl) as a coinjection marker to create AMJ1009 and one other independent isolate. AMJ1009 was crossed with N2 males to create AMJ1134. AMJ1159 was crossed with AMJ1134 males to create AMJ1312 and two other isolates.

All other transgenes were generated previously ( $ccIs4251^{13}$ ;  $oxSi487^{90}$ ;  $tmIs1005^{93}$ ;  $jamEx140^{25}$ ;  $qtEx136^{24}$ ).

#### Cas9-mediated genome editing

Genome editing was performed by injecting nuclear-localized Cas9 (PNA Bio) preincubated at 37°C for 10 min with either a single-guide RNA (sgRNA) generated by *in vitro* transcription (SP6 RNA Polymerase, New England BioLabs) or hybridized crRNA/tracrRNA

(IDT), as well as an oligonucleotide or PCR-amplified homology repair template, into the *C. elegans* distal gonad. Screening for plates with successfully edited F1 animals was performed using either *dpy-10* co-CRISPR<sup>94,95</sup> or the pRF4 plasmid used as a co-injection marker<sup>96</sup>. All plasmids were purified from bacterial culture using QIAprep Spin Miniprep Kit (Qiagen) and all PCR products were generated with Phusion® High-Fidelity DNA Polymerase (New England BioLabs) and purified using NucleoSpin Gel and PCR Clean-up Kit (Macherey-Nagel). Alleles generated by genome editing are schematized in Fig. 4a (*sid-1*), Fig. 5a (*sid-1*), Extended Data Fig. 1d (*rme-2*), Extended Data Fig. 3 (*deps-1*, *mut-16*, *sid-2*, *rme-2*, *sid-1*, *rde-1*, *sid-5*, and *sid-3*), Extended Data Fig. 6a (*sid-1*), and Extended Data Fig. 8c (*W09B7.2/F07B7.2* (*sdg-1*)), and oligonucleotides used are in Extended Data Table 4.

To delete the *rme-2* coding sequence: Two sgRNAs targeting the start and end of the *rme-2* coding sequence were *in vitro* transcribed from a SP6 transcription template amplified from pDD162 (Addgene #47549) using primers P42 (start sgRNA) or P43 (end sgRNA) as forward primers and P40 as a universal reverse primer. An sgRNA targeting *dpy-10* for co-CRISPR was also *in vitro* transcribed using a similar template amplified from pDD162 with primers P39 and P40. All sgRNAs were purified using organic extraction, were precipitated using ethanol, and resuspended in water prior to injection. Injection into HC196 with all sgRNAs, Cas9 and the homology repair templates for *rme-2* (P44) and *dpy-10* (P41), and screening for edited animals were performed as described above. Genotyping for *rme-2*(*deletion*) was performed using a triplex PCR with primers P45-P47 to isolate AMJ1120 and one other isolate and the *rme-2* deletion was verified using Sanger sequencing. AMJ1120 was crossed with N2 males to isolate AMJ1131. AMJ1131 males were crossed with EG6787 and AMJ471 hermaphrodites to isolate AMJ1146 and AMJ1204 animals, respectively.

To delete the *sid-1* coding sequence: Injection of crRNAs targeting the start (P59) and end (P52) of the *sid-1* coding sequence (IDT), tracrRNA, Cas9, a *sid-1* (*deletion*) homology repair template (P60) and pRF4 into N2 and AMJ1372, and subsequent screening were performed as described above. Genotyping for *sid-1* (*deletion*) was performed using triplex PCR with primers P8, P54 and P55 to isolate AMJ1324 and one other independent isolate from N2 and AMJ1479-AMJ1482 from AMJ1372. The *sid-1* deletion was verified by Sanger sequencing in all isolates. AMJ1324 was crossed with AMJ1131 males to create AMJ1366.

To delete the *sid-2* coding sequence: Injection of crRNAs targeting the start (P71) and end (P72) of the *sid-2* coding sequence (IDT), tracrRNA, Cas9, a *sid-2(deletion)* homology repair template (P73) and pRF4 into N2, and subsequent screening were performed as described above. Genotyping for *sid-2(deletion)* was performed using triplex PCR with primers P74-P76 to isolate AMJ1368 and one other independent isolate. The *sid-2* deletion was verified by Sanger sequencing in both isolates. AMJ1368 was crossed with AMJ1324 males to create AMJ1380.

To delete the *sid-5* coding sequence: Injection of crRNAs targeting the start (P61) and end (P62) of the *sid-5* coding sequence (IDT), tracrRNA, Cas9, a *sid-5(deletion)* homology repair template (P63) and pRF4 into N2, and subsequent screening were performed as described above. Genotyping for *sid-5(deletion)* was performed using duplex PCR with primers P64 and P65 to isolate AMJ1332 and three other independent isolates. The *sid-5* deletion was verified by Sanger sequencing in all four isolates. AMJ1332 was crossed with AMJ1324 males to create AMJ1367.

<u>To introduce a nonsense mutation into sid-1 coding sequence</u>: An sgRNA was designed to introduce into sid-1 a nonsense mutation mimicking the qt9 allele<sup>14</sup>. This sgRNA was in vitro transcribed from a SP6 transcription template amplified from pDD162 (Addgene #47549) using

primers P48 and P40. An sgRNA targeting *dpy-10* for co-CRISPR was also *in vitro* transcribed using a similar template amplified from pDD162 with primers P39 and P40. Both sgRNAs were purified using organic extraction and were precipitated using ethanol prior to injection. Both sgRNAs, Cas9 and the homology repair templates for *sid-1(nonsense)* (P49) that includes a missense mutation (S155P) and nonsense mutation (R156\*) downstream that would prevent recutting of edited DNA by Cas9, and for *dpy-10* (P41) were injected into N2. Screening for edited animals was performed as described above. Genotyping for *sid-1(nonsense)* was performed using a duplex PCR with primers P1 and P2 followed by restriction digestion with HpyCH4V to isolate AMJ1159. The nonsense mutation was confirmed using Sanger sequencing. AMJ1159 males were crossed with AMJ581<sup>25</sup> to create AMJ1504 and two other independent isolates.

Injection of a crRNA with the same target sequence (P88) (IDT) as the sgRNA described above, tracrRNA, Cas9, the same *sid-1(nonsense)* homology repair template (P49) and pRF4 into N2 and AMJ1372 and subsequent screening were performed as described above. Genotyping for *sid-1(nonsense)* was performed using duplex PCR with primers P1 and P2 followed by restriction digestion with HpyCH4V to distinguish AMJ1399 from N2, and AMJ1389 and AMJ1442-AMJ1446 from AMJ1372. The nonsense mutation was verified using Sanger sequencing in all isolates.

To revert the mutation in *sid-1(nonsense)* animals: An sgRNA was designed to revert the nonsense mutation described above back to wild-type *sid-1* sequence. The sgRNA was *in vitro* transcribed from a SP6 transcription template amplified from pDD162 (Addgene #47549) using primers P50 and P40. An sgRNA targeting *dpy-10* for co-CRISPR was also *in vitro* transcribed using a similar template amplified from pDD162 with primers P39 and P40. Both sgRNAs were

purified using organic extraction and were precipitated using ethanol prior to injection. Injection into AMJ1159 with both sgRNAs, Cas9 and the homology repair template for *sid-1(revertant)* (P51), which also reverted the missense mutation (S155P) and nonsense mutation (R156\*) downstream of *sid-1(nonsense)* to wild-type sequence, and *dpy-10* (P41). Screening for edited animals was performed as described above. Genotyping for *sid-1(revertant)* was performed using duplex PCR with primers P1 and P2 followed by restriction digestion with HpyCH4V to isolate AMJ1217 and two other independent isolates. The revertant was verified using Sanger sequencing in all isolates.

Injection of a crRNA with the same target sequence (P93) (IDT) as the sgRNA described above, tracrRNA, Cas9, a *sid-1(revertant)* homology repair template (P51) and pRF4 into AMJ1389 and AMJ1399, and subsequent screening were performed as described above. Genotyping for *sid-1(revertant)* was performed using duplex PCR with primers P1 and P2 followed by restriction digestion with HpyCH4V to distinguish AMJ1412 and AMJ1413 from AMJ1389, and AMJ1405-AMJ1410 from AMJ1399. The revertant was verified using Sanger sequencing in all isolates.

To tag W09B7.2/F07B7.2 with mCherry: Injection of a crRNA with the target sequence listed as P80 (IDT), tracrRNA, Cas9, an mCherry sequence lacking piRNA binding sites amplified using primers P81 and P82 from pSD6<sup>43</sup> as a homology repair template with homology arms to the C-terminus of W09B7.2/F07B7.2, and pRF4 into N2, and subsequent screening were performed as described above. Genotyping for identical tags W09B7.2::mCherryΔpi and F07B7.2::mCherryΔpi in isolate AMJ1372 was performed using triplex PCR with primers P79, P83 and P84. Tagging of both loci is evident in Extended Data Fig. 8d. The mCherryΔpi insertion was verified by Sanger sequencing. AMJ1372 hermaphrodites and males generated by

heatshock were mated with N2 males and hermaphrodites, respectively, to examine expression in cross progeny and in homozygosed wild-type and *W09B7.2/F07B7.2(jam137[mCherryΔpi]*) animals across generations in six independent F1 lineages from each cross. See Fig. 6c and Extended Data Fig. 9a for associated data. YY916 males were crossed with AMJ1372 to generate AMJ1662. The *3xflag::gfp::znfx-1* locus was genotyped using primers P153, P154, and P155.

To introduce a nonsense mutation into *rde-1* coding sequence: Injection of a crRNA with the target sequence listed as P94 (IDT), tracrRNA, Cas9, a *rde-1(nonsense)* homology repair template (P95) mimicking *rde-1(ne300)*<sup>97</sup>, and pRF4 into AMJ1372 and subsequent screening were performed as described above. Genotyping for *rde-1(nonsense)* was performed using duplex PCR with primers P96 and P97 and restriction digestion with NlaIII to isolate AMJ1447 and AMJ1448. The nonsense mutation was verified by Sanger sequencing for all isolates.

To tag *sid-1* with *wrmScarlet* at the 3' end: Injection of a crRNA with the target sequence listed as P52 (IDT), tracrRNA, Cas9, a *sid-1::wrmScarlet13* homology repair template with the beginning (1) and end (3) but not the middle (2) of the coding sequence<sup>98</sup> (P53), and pRF4 into N2 and subsequent screening were performed as described above. Genotyping for *wrmScarlet13* was performed using duplex PCR with primers P54 and P55 to isolate AMJ1280. The *wrmScarlet13* insertion was verified by Sanger sequencing. Subsequent injections were performed into AMJ1280 with a *wrmScarlet13* specific crRNA with the target sequence listed as P56 (IDT), a complete *wrmScarlet* coding sequence amplified from pSEM89 (made in Boulin Lab – gift from Kevin O'Connell) with primers P57 and P58 and the same components as described previously. After similar screening, genotyping for full *wrmScarlet* insertion was performed using duplex PCR with primers P54 and P55 to isolate AMJ1282 and one other

independent isolate. The full *wrmScarlet* insertion was verified by Sanger sequencing. AMJ1282 was crossed with AMJ577 males to create AMJ1365.

To tag *rme-2* with *wrmScarlet* at the 3' end: Injection of a crRNA with the target sequence listed as P67 (IDT), tracrRNA, Cas9, a *rme-2::wrmScarlet13* homology repair template with the beginning (1) and end (3) but not the middle (2) of the coding sequence<sup>98</sup> (P69), and pRF4 into N2 and subsequent screening were performed as described above. Genotyping for *wrmScarlet13* was performed using duplex PCR with primers P70 and P47 to isolate AMJ1281. The *wrmScarlet13* insertion was verified by Sanger sequencing. Subsequent injections were performed into AMJ1281 with a *wrmScarlet13* specific crRNA with the target sequence listed as P77 (IDT), a complete *wrmScarlet* coding sequence amplified from pSEM89 (made in Boulin Lab – gift from Kevin O'Connell) with primers P57 and P58 and the same components as described previously. After similar screening, genotyping for full *wrmScarlet* insertion was performed using duplex PCR with primers P54 and P55 to isolate AMJ1284 and two other independent isolates. The full *wrmScarlet* insertion was verified by Sanger sequencing.

To tag *sid-1* internally with *mCherry*: Injection of a crRNA with the target sequence listed as P110 (IDT), tracrRNA, Cas9, an *mCherry* lacking piRNA binding sites amplified from pSD6<sup>43</sup> as a homology repair template with homology arms to exon 4 of *sid-1* with primers P111 and P112, and pRF4 into N2 and subsequent screening were performed as described above. Genotyping for *mCherry*Δpi was performed using triplex PCR with primers P113, P114 and P79 to isolate AMJ1438 and one other isolate from the same lineage. The *mCherry*Δpi insertion was verified by Sanger sequencing. Subsequent injections were performed into AMJ1438 with a crRNA targeting the 5'-end of *mCherry*Δpi (P115) (IDT), a homology repair template containing a 45-nt linker sequence (P116) and the same components as described previously. After similar

screening, genotyping for the linker insertion was performed using duplex PCR with primers P113 and P79 to isolate AMJ1485 and two other independent isolates. Insertion of the linker was verified by Sanger sequencing in all three isolates.

To introduce a nonsense mutation into *sid-3* coding sequence: Injection of a crRNA with the target sequence listed as P66 (IDT), tracrRNA, Cas9, a *sid-3(nonsense)* homology repair template (P85) mimicking *sid-3(qt31)*<sup>99</sup> and pRF4 into AMJ1372 and subsequent screening were performed as described above. Genotyping for *sid-3(nonsense)* was performed using duplex PCR with primers P86 and P87, and restriction digestion with StyI to isolate AMJ1449 and AMJ1450. The nonsense mutation was verified by Sanger sequencing for both isolates.

To introduce a nonsense mutation into *deps-1* coding sequence: Injection of a crRNA with the target sequence listed as P68 (IDT), tracrRNA, Cas9, a *deps-1(nonsense)* homology repair template (P137) mimicking *deps-1(bn124)*<sup>49</sup> and pRF4 into AMJ1372 and AMJ1412 and subsequent screening were performed as described above. Genotyping for *deps-1(nonsense)* was performed using allele specific PCR with primers P138 and P139 amplifying the wild-type sequence and primers P140 and P141 amplifying the mutant allele to isolate AMJ1451-AMJ1452 from AMJ1372 and AMJ1574-AMJ1575 from AMJ1412. The nonsense mutation was verified by Sanger sequencing for both isolates.

To insert the tetracycline K4 aptazyme into the 3'UTR of sid-1: Injection of a crRNA with the target sequence listed as P52 (IDT), tracrRNA, Cas9, a sid-1::tetracycline-K4-aptazyme homology repair template (P78) and pRF4 into N2 and subsequent screening were performed as described above. Genotyping for insertion of the aptazyme sequence was performed using duplex PCR with primers P54 and P55 to isolate AMJ1323. The aptazyme insertion was verified by Sanger sequencing. AMJ1323 hermaphrodites was crossed with AMJ477<sup>24</sup> males to create

AMJ1330 and with AMJ471<sup>25</sup> males to create AMJ1350. AMJ1323 males were crossed with JH3197 to create AMJ1355.

To insert the tetracycline K4 aptazyme into the 3'UTR of gtbp-1(ax2053[gtbp-1::gfp]): Injection of a crRNA with the target sequence listed as P89 (IDT), tracrRNA, Cas9, a gtbp-1::gfp::tetracycline-K4-aptazyme homology repair template (P90) and pRF4 into JH3197 and subsequent screening were performed as described above. Genotyping for insertion of the aptazyme sequence was performed using duplex PCR with primers P91 and P92 to isolate AMJ1542. The aptazyme insertion was verified by Sanger sequencing.

To introduce a missense mutation into *dpy-10* coding sequence: Injection of crRNA with the target sequence listed as P142 (IDT), tracrRNA, Cas9, and a *dpy-10(mis)* homology repair template (P41) mimicking *dpy-10(cn64)*<sup>100</sup> into AMJ1372 was performed as described above and heterozygous F1 animals were screened for by passaging "rolling" animals. Animals that appeared wild-type and those that appeared Dpy (homozygous *dpy-10(-)*) were isolated from three independently edited F1 animals. See Extended Data Fig. 9b for associated data.

To delete the *W09B7.2/F07B7.2* coding sequence: Injection of crRNAs targeting the start (P143) and end (P144) of the *W09B7.2/F07B7.2* coding sequence (IDT), tracrRNA, Cas9, a *W09B7.2/F07B7.2* (deletion) homology repair template (P145) and pRF4 into N2, and subsequent screening were performed as described above. Genotyping for *W09B7.2/F07B7.2* (deletion) was performed using triplex PCR with primers P146-P148 to isolate AMJ1577, AMJ1612, and AMJ1613. Deletion of both *W09B7.2/F07B7.2* loci was verified by absence of wild-type band by PCR (see Extended Data Fig. 8d) and Sanger sequencing in all three isolates.

<u>To delete the W09B7.2/F07B7.2 coding sequence from W09B7.2/F07B7.2::mCherry $\Delta pi$ :</u> Injection of crRNAs targeting the start (P143) and end (P149) of the W09B7.2/F07B7.2 coding

sequence (IDT), tracrRNA, Cas9, a *W09B7.2/F07B7.2(deletion)* homology repair template (P150) and pRF4 into AMJ1372, and subsequent screening were performed as described above. Genotyping for *W09B7.2/F07B7.2(deletion)* was performed using triplex PCR with primers P148, P151, and P152 to isolate AMJ1615, AMJ1616, and AMJ1617. Deletion of both *W09B7.2/F07B7.2* loci was verified by absence of wild-type band by PCR (see Extended Data Fig. 8d) and Sanger sequencing in all three isolates. AMJ1615 was outcrossed 1X with N2 males to generate AMJ1770. Genotyping was performed using primers P158-P160 and expression was verified by widefield microscopy. AMJ1615 was crossed with WM49 males to generate AMJ1766 and AMJ1767. Many of the AMJ1770 and AMJ1766 animals had defective germline morphology and therefore only animals with apparently normal morphology were selected for quantification of *sdg-1p::mCherryΔpi* expression. Genotyping for *sdg-1p::mCherryΔpi* was performed using the same primers (P158-P160) and initial expression was verified by widefield microscopy.

## Light-induced damage of neurons

Optimizing duration of light exposure: 20-30 animals expressing PH::miniSOG in neurons (multi copy, AMJ837; single copy, AMJ1019) were placed on an unseeded NGM plate and exposed to blue light (470 nm wavelength) at a distance of approximately 7.5 cm from an LED (Cree Xlamp XP-E2 Color High Power LED Star – Single 1 UP, LED supply) producing light at a power of ~2 mW/mm² flashing at a frequency of 2 Hz for different durations of time. Animals were then scored for movement defects immediately after light exposure, OP50 was seeded onto the plate, and animals were scored again 24 h post light exposure (Extended Data Fig. 2a). Wild-type animals were exposed to blue light for the same durations as control.

Representative widefield images of unparalyzed (wild type) and paralyzed (coiled, AMJ837) animals were taken using a Nikon AZ100 microscope and Photometrics Cool SNAP HQ<sup>2</sup> camera (Extended Data Fig. 2b, *top*). Confocal images of animals expressing PH::miniSOG and DsRed in neurons (AMJ936) with and without 30 minutes of blue light exposure were taken using a Leica TCS SP8 DLS microscope with HyVolution using a 40X oil objective lens. DsRed was excited using a 638 nm laser and fluorescence was collected through a 598 nm emission filter (Extended Data Fig. 2b, *bottom*). Images were adjusted for display using Fiji<sup>101</sup> (NIH).

Silencing by *bli-1*-dsRNA: Five L4 animals with an extrachromosomal array expressing PH::miniSOG and *bli-1*-dsRNA in neurons were placed on seeded NGM plates and allowed to lay progeny for 24 h. P0 animals were then removed and F1 progeny were exposed to blue light as described above for 60 min at different time points after initial P0 L4 animals were passaged. 96 h post light exposure F1 progeny with the array were scored for *bli-1* silencing (presence of blisters) in gravid adults (Extended Data Fig. 2c, *top*, d,e).

Silencing by *gfp*-dsRNA: L4 animals with the *mex-5p::mCherry::h2b::gfp::h2b* transgene (*oxSi487*) (Fig. 2b) were mated with L4 male animals with an extrachromosomal array expressing PH::miniSOG and *gfp*-dsRNA in neurons (Fig. 2a). After 36 h of mating and laying progeny, P0 animals were removed from plates and F1 progeny were exposed to blue light as described above for 60 min at different time points after initial P0 L4 animals were mated. 96 h after mating, F1 cross progeny hermaphrodites with the array were imaged as adults (Extended Data Fig. 2c, *bottom*) under a coverslip in 10 μl of 3 mM levamisole on a 2% agar pad using a Nikon AZ100 microscope and Photometrics Cool SNAP HQ<sup>2</sup> camera. A C-HGFI Intensilight Hg Illuminator was used to excite GFP (filter cube: 450 to 490 nm excitation, 495 dichroic, and 500 to 550 nm emission) and mCherry (filter cube: 530 to 560 nm excitation, 570 dichroic, and 590

to 650 nm emission). Animals were scored as bright if fluorescence was easily detectable without adjusting levels, dim if fluorescence could be observed after level was adjusted to saturation, and not detectable if fluorescence was still not observed after level adjustments (Extended Data Fig. 2f). Representative images were adjusted in Adobe Photoshop to identical levels for presentation (Fig. 2b-d).

### Sensitive northern blotting

Double-stranded RNA was in vitro transcribed from a PCR amplicon using T7 RNA Polymerase (New England BioLabs) (Extended Data Fig. 4d) or expressed in HT115 E. coli after IPTG induction during exponential growth (Extended Data Fig. 4b,c) and extracted using TRIzol (Fisher Scientific). RNA was then separated by size using fully denaturing formaldehyde polyacrylamide gel electrophoresis (FDF-PAGE)<sup>102</sup> wherein 10 µg RNA samples were heated with formaldehyde to disrupt dsRNA duplexes and run on a 4% denaturing polyacrylamide gel next to 1-kb and 100-bp DNA ladders for size comparison. After migration, the ladder lanes were stained with ethidium bromide and imaged, and the RNA lanes were transferred to a positively charged nitrocellulose membrane using a Trans-Blot® Turbo<sup>TM</sup> Transfer System (Bio-Rad) and crosslinked using 120 mJ/cm<sup>2</sup> UV radiation. Blots were then exposed to 2.5 pmol of 40-nt HPLC purified DNA oligonucleotides conjugated to digoxigenin (DIG) using the DIG Oligonucleotide Tailing Kit (Roche) hybridized to the nitrocellulose membrane at 60°C overnight (42°C for 2 h for 5S rRNA) in ULTRAhyb<sup>TM</sup> buffer (Invitrogen<sup>TM</sup>) to probe the sense or antisense strands of *unc-22* (Extended Data Fig. 4b,d) or *gfp*-dsRNA (Extended Data Fig. 4c) at different positions (protocol adapted from ref. 36). After hybridization, the membrane was washed and blocked using the DIG Wash and Block Buffer Set (Roche), incubated with AntiDIG-AP, Fab fragments (Roche) and developed with CSPD (Roche) at 37°C for 15 min. Chemiluminescence from the AP/CSPD reaction was imaged using a LAS-3000 (Fujifilm) or iBright<sup>TM</sup> CL1000 (Invitrogen<sup>TM</sup>) imager. Blots were compared to ethidium bromide-stained ladders after imaging to visualize fragment size. Blots were stripped using two washes with 5% SDS (Sigma Aldrich) and two washes with 2X SSC (Sigma Aldrich) and the hybridization, blocking and development procedures were repeated for each probe (5S RNA probe: P118; *unc-22* probes: P119-P124; *gfp* probes: P125-P130).

### Injection of dsRNA

Injection of synthetic dsRNA: RNA oligonucleotides were purchased from IDT and resuspended in IDT Duplex Buffer (*unc-22*: P131 and P132; *gfp*: P133 and P134; fluorescently labeled *gfp*: P135 and P136). 1 μg each of HPLC purified 50-nt sense and antisense oligonucleotide was diluted to 100-350 ng/μl with IDT Duplex Buffer at a final volume of 10 μl. Alternatively, *unc-22* single-stranded RNA was treated with polynucleotide kinase and annealed in equal proportion at a final concentration of ~97 ng/μl of *unc-22*-dsRNA in IDT Duplex Buffer (Extended Data Fig. 4e,f). This mixture was heated to 95°C for 1 min and cooled at a rate of 1°C/min to a final temperature of 25°C. The mix was centrifuged at 16500 x g for 20-30 min and loaded into a microinjection needle. Young adult animals were injected 24 h after the L4 stage in the body cavity just beyond the bend of the posterior gonad arm<sup>28</sup>. Injected animals were recovered with M9 buffer and isolated onto NGM plates and allowed to lay progeny. In cases where animals were mated with N2 males post injection, two adult N2 males were placed on each plate with an injected hermaphrodite.

Injection of *in vitro* transcribed dsRNA: Templates for transcription were amplified from RNAi vectors using one common primer specific to the T7 promoter sequence (P117). PCR products were purified using column purification (Macherey-Nagel, ref. 740609.50) and subsequently used for transcription by T7 RNA Polymerase (New England BioLabs). Many transcription reactions were pooled and purified using one column to produce concentrated RNA samples. Annealing, centrifugation, and injection into the body cavity of animals staged as L4s (injected between pharynx and anterior intestine) or young adults were performed as described for synthetic dsRNA with identical concentrations unless otherwise indicated in figure legends. In cases where animals were mated with N2 males post injection, two adult N2 males were placed on each plate with an injected hermaphrodite.

Scoring of gene silencing: For scoring silencing by *unc-22* dsRNA, 10-30 L4 animals were passaged into 10 μl of 3 mM levamisole and scored for twitching, observed as rapid movement of the head and/or tail (as in ref.<sup>28</sup>), 3-4 days after injection for progeny of *rme-2(+)* parents and 4-5 days after injection for progeny of *rme-2(-)* parents with no appreciable difference between days in which animals were scored post injection. Weak and strong twitching were scored as in Movies S1-S3 of ref.<sup>28</sup>. Numbers of silenced animals and total animals scored were summed across all days of scoring and experimental replicates.

When scoring silencing of *gfp*, animals were either scored by eye in comparison to animals injected with duplex buffer only (i.e. buffer; Extended Data Fig. 1b) or were mounted in 10 µl of 3 mM levamisole on a 2% agar pad and imaged under a coverslip as P0 adults (2 days post injection) or F1 L4s (3 days post P0 injection) using a Nikon AZ100 microscope and Photometrics Cool SNAP HQ<sup>2</sup> camera. A C-HGFI Intensilight Hg Illuminator was used to excite GFP (filter cube: 450 to 490 nm excitation, 495 dichroic, and 500 to 550 nm emission).

Representative images for *gfp* expression in F1 animals after P0 injection were adjusted to identical levels in Adobe Photoshop for presentation (Fig. 3b and Extended Data Fig. 1e). See "Imaging and quantification of reporters using widefield microscopy" for other methods of scoring *gfp* expression after imaging.

Imaging of fluorescently labeled dsRNA: Embryos were imaged 22 hours post P0 injection with labeled dsRNA. Laid embryos were picked off plates and placed into 5 μl of 3 mM levamisole on a coverslip for at least 5 minutes before placing on a 2% agarose pad on a slide. Embryos were imaged using the Eclipse Ti Spinning Disk Confocal (Nikon) with the 60X objective lens. Atto 565 was excited using a 561 nm laser and fluorescence was collected through a 415-475 nm and 580-650 nm emission filter. Images were adjusted for display using Fiji<sup>101</sup> (NIH).

## Feeding RNAi

P0 and F1 feeding: E. coli (HT115) expressing dsRNA was cultured in LB media with 100 μg/μl carbenicillin overnight at 250 rpm. 100 μl of cultured bacteria was then seeded onto RNAi plates and incubated at room temperature for approximately 24 h. L4 animals were passaged onto seeded RNAi plates and progeny were scored for silencing by bacteria expressing dsRNA targeting unc-22 (twitching in levamisole), bli-1 (blisters), pos-1 (dead eggs) or expressing L4440 as an empty vector control.

P0 only feeding: RNAi bacteria were cultured and seeded as described above. L4-stage or young adult-stage (24 h post L4) animals were passaged onto seeded RNAi plates and cultured at 20°C for approximately 24 h. In some cases, fed P0 animals were then scored for silencing as described above and subsequently imaged under widefield microscopy (Fig. 7f). To score unfed

progeny, fed P0 animals were picked into 1 ml of M9 buffer and washed four times to remove any residual bacteria (as in ref.<sup>28</sup>). After washing, animals were resuspended in 200 µl of remaining M9 buffer and placed onto a seeded NGM plate. 1 h later, animals were isolated onto single NGM plates and their progeny were scored for silencing as described above.

Limited P0 only feeding: RNAi bacteria were cultured and seeded as described above. L4-stage animals were passaged onto seeded RNAi plates and cultured at 20°C for approximately 16 h. Animals were then passaged onto NGM plates seeded with *E. coli* (OP50) and cultured for 1.5 h at room temperature. Animals were then again passaged to new OP50 seeded plates (1 animal on each plate) and progeny (only L3 larvae, L4 larvae and adults) were counted after 4 days of being cultured at 20°C (~96 hours after moving to new OP50 plates).

<u>F1 only feeding</u>: L4-staged animals were passaged onto RNAi plates seeded with 10 μl of *E. coli* (OP50). Animals were allowed to develop into adults and lay eggs over 24 h at 20°C and then removed from plates. Plates with eggs were then seeded with RNAi bacteria cultured and seeded as described above and further cultured at 20°C. Hatched progeny were imaged throughout development or as adults 3 days after being staged as L4 animals (day 3 adults).

## Tetracycline-induced expression

For animals cultured with OP50 *E. coli*: 81.6  $\mu$ l of a 500  $\mu$ M solution of tetracycline in water was added to 4 mL NGM plates previously seeded with OP50 *E. coli* (at least two days earlier) to create plates with ~10  $\mu$ M tetracycline (concentration based on ref.<sup>44</sup>). Volumes of 166.7  $\mu$ l and 444.4  $\mu$ l of tetracycline solution were used to create plates with final concentrations of ~20  $\mu$ M or ~50  $\mu$ M, respectively (see Extended Data Fig. 6d). Control plates were also made by adding the same amount of water to seeded NGM plates without tetracycline. Tetracycline

plates and control plates were incubated at room temperature out of direct light overnight to allow any remaining liquid to dry. Animals were passaged to tetracycline or water plates with or without previous injection of 10 μM tetracycline or water into adult gonads. Progeny expressing neuronal *unc-22* or *gfp*-dsRNA were scored for silencing on the first day of adulthood. In the case of silencing of *gtbp-1::gfp* by neuronal *gfp*-dsRNA, animals with the array expressing *gfp*-dsRNA were passaged as L4s onto new tetracycline or water plates to be imaged as day 1 adults. The brood size of animals cultured on OP50 with 10 μM tetracycline or water was scored by staging single L4 animals on NGM plates with 10 μM tetracycline or water and moving animals every 24 h to new 10 μM tetracycline or water plates. Progeny laid on each of the four days were counted after growing to adulthood, continuously cultured under either condition.

For animals cultured on HT115 *E. coli* expressing dsRNA: Bacteria expressing *bli-1*-dsRNA, *gfp*-dsRNA, *pos-1*-dsRNA or L4440 control vector were cultured overnight to a maximum time of 24 hours (for *gfp*-dsRNA and L4440 only) and 100 μl of bacteria was seeded onto RNAi plates. Plates were incubated for 1-2 days at room temperature to allow for growth and drying of bacteria. 10 μM tetracycline or water was added to newly seeded plates as described above. After drying of tetracycline and water, P0 animals were added to plates and F1 animals were scored for silencing by *bli-1*-dsRNA or *gfp*-dsRNA as adults in the next generation. Silencing by *pos-1*-dsRNA was scored by measuring the brood of three L4 animals staged on a single RNAi plate with *pos-1*-dsRNA and 10 μM tetracycline or water. Brood size over four days was measured after moving all P0 animals every 24 h to new 10 μM tetracycline or water plates and scoring adult progeny cultured under either condition.

In all experiments, animals expressing *unc-22*-dsRNA in neurons were exposed to the same tetracycline and water solutions used and scored for *unc-22* silencing as adults as a control for effectiveness of tetracycline (see summary of data in Extended Data Fig. 6b).

*Imaging and quantification of reporters using widefield microscopy* 

All animals and embryos expressing fluorescent reporters were imaged in 10 μl of 3 mM levamisole on a 2% agar pad using a Nikon AZ100 microscope and Photometrics Cool SNAP HQ<sup>2</sup> camera. A C-HGFI Intensilight Hg Illuminator was used to excite mCherry (filter cube: 530 to 560 nm excitation, 570 nm dichroic, and 590 to 650 nm emission), GFP or other autofluorescent molecules in the green channel (filter cube: 450 to 490 nm excitation, 495 nm dichroic, and 500 to 550 nm emission) and autofluorescent molecules in the blue channel (filter cube: 325 to 375 nm excitation, 400 nm dichroic, 435 to 485 nm emission). Intensity of GFP and mCherry were quantified in Fiji<sup>101</sup> (NIH) using the methods described below. Representative images were adjusted in Fiji<sup>101</sup> (NIH) and/or Adobe Photoshop to identical levels for presentation (Fig. 4b,c, Fig. 6a, Fig. 7e, Extended Data Fig. 6c-e,g).

For GTBP-1::GFP quantification post dsRNA injection: Somatic gfp expression was quantified between the pharynx and anterior gonad arm by drawing a circle or ventral to dorsal line within the boundaries of the animal (Extended Data Fig. 5a) on a brightfield image, creating a mask, imposing that mask onto the GFP channel image and measuring average intensity or intensity along the line, respectively. To measure background fluorescence, the same circle or a new circle was used to measure average intensity outside of the animal. Germline GFP expression was quantified by freely selecting part of the distal or proximal region of the anterior or posterior gonad arm (Extended Data Fig. 5a) excluding the intestine to avoid intestinal

autofluorescence. Selection was performed using a brightfield image, a mask was created and imposed onto the GFP channel image and average intensity was measured. To measure background fluorescence, the same selection boundary was moved outside of the animal and average background intensity was measured. To plot average GFP intensity measured by a circle or free selection, average background intensity was subtracted from GFP intensity for each image and plotted with a box plot (Extended Data Fig. 5c). To plot GFP intensity along the ventral to dorsal axis in the anterior soma, the average intensity in each tenth of the axis was calculated for each animal and plotted with a shaded region representing 95% confidence intervals (Extended Data Fig. 5b, *top*). To calculate differences in intensity between the interior and exterior of animals, the average intensity of the 0.4-0.6 region of the axis was divided by the average intensity of the 0.1 and 0.9 points of the axis. These values were calculated and shown for each animal as a box plot (Extended Data Fig. 5b, *bottom*). All plotting was done using custom R scripts.

For GTBP-1::GFP quantification after exposure to dsRNA via feeding or neuronal expression: Animals fed L4440 or *gfp*-dsRNA for different durations of the P0 and/or F1 generation were scored for silencing in the germline and soma at different stages during the F1 generation (Fig. 1 and Extended Data Fig. 1a). Somatic GFP intensity (a.u.) was quantified in the tail region by drawing a ventral to dorsal line within the boundaries of the animal (Extended Data Fig. 6c,e) on a brightfield image, creating a mask, imposing that mask onto the GFP channel image and measuring average intensity or intensity along the line. To measure background fluorescence, a circle was used to measure average intensity outside of the animal. Germline GFP intensity (a.u.) was measured by free selection of germ cells but avoiding intestinal cells at each stage, selecting a region around the primordial vulva in L2 animals, in one of two extending

gonad arms in L3 and L4 animals, in the proximal or distal gonad in young adults, and of eggs *in utero* in gravid adults. To measure background fluorescence, the same selection or a new selection was used to measure average intensity outside of the animal. To plot average GFP intensity measured by free selection, average background intensity was subtracted from GFP intensity for each image and shown as a box plot (Fig. 1, Extended Data Fig. 1a and Extended Data Fig. 6c,e). All plotting was done using custom R scripts.

Adjustment of fluorescence images of  $sid-1::mCherry\Delta pi$  animals for comparison to images of wild-type animals: Representative images of  $sid-1(jam195[linker::mCherry\Delta pi])$  and wild type animals at different stages were adjusted to the same maximum and minimum displayed values of intensity using Fiji<sup>101</sup> (NIH) to highlight each region of interest below saturation (Fig. 4b,c).

For quantification of SDG-1::mCherry and mCherry expressed under the *sdg-1* promoter: Germline mCherry intensity was quantified by freely selecting part of the distal (for Fig. 7f,g) or proximal region of the anterior or posterior gonad arm excluding the intestine to avoid quantifying intestinal autofluorescence. Selection was performed using a brightfield image, a mask was created and imposed onto the mCherry channel image and average intensity was measured. To measure background fluorescence, the same selection boundary was moved outside of the measured gonad arm and average background intensity was measured. To plot average mCherry intensity, average background intensity was subtracted from mCherry intensity for each gonad arm and shown as a box plot using custom R scripts (Fig. 6b-g, Fig. 7f,g, and Extended Data Fig. 9). In Fig. 6c, SDG-1::mCherry intensity measurements, adjusted by subtracting background intensity and intensity measurements made in a wild-type animal lacking mCherry, were normalized to RT-qPCR measurements by multiplying each median intensity

value by a conversion factor. This conversion factor was calculated by dividing the median SDG-1::mCherry intensity in AMJ1372 animals by the median relative *sdg-1* mRNA level in AMJ1372 RNA samples. All estimated relative *sdg-1* expression values were then normalized to those of wild-type animals by dividing all values by the wild-type value.

Imaging and quantification of reporters using confocal microscopy.

For the endogenous gene tag *sid-1::mCherryΔpi*: SID-1::mCherry fluorescence from an L1-staged animal was imaged using LSM 980 Airyscan 2 Laser Scanning Confocal (Zeiss) with a 63X oil objective lens after paralyzing the worm as above. mCherry was excited using a 561 nm laser and fluorescence was collected through a 422-477 nm and 573-627 nm emission filter. For Fig. 4d, after removing noise using a 3D gaussian blur with 2.0 sigma in X, Y, and Z, depth-coded maximum intensity projections of Z-stacks were stitched together for display as described earlier<sup>24</sup>.

For the endogenous gene tag *W09B7.2/F07B7.2::mCherryΔpi*: Adult animals were placed in 10 μl of 3 mM levamisole and imaged using the Eclipse Ti Spinning Disk Confocal (Nikon) with a 60X objective lens or the LSM 980 Airyscan 2 Laser Scanning Confocal (Zeiss) with a 63X oil objective lens. GFP was excited using a 488 nm laser and fluorescence was collected through a 499-557 nm and 659-735 nm emission filter, and mCherry fluorescence was excited and collected as described above. Images and movies were adjusted in Fiji<sup>101</sup> (NIH) and Adobe Photoshop to identical levels for presentation (Fig. 7c,d and Extended Data Movies 1-4).

RNA sequencing, principal component analysis and differential expression analysis

For analysis of previously generated sid-1(-) alleles: Mixed-stage animals were washed from 10 plates in biological duplicate 5 days after passaging L4-staged animals. Total RNA was extracted from pellets using TRIzol (Fisher Scientific). PolyA+ RNAs were purified and converted to DNA libraries by the University of Maryland Genomics Core using the Illumina TruSeq Library Preparation Kit. FASTO files were processed<sup>103</sup> using the command "cutadapt -j 0 -a AGATCGGAAGAGCACACGTCTGAACTCCAGTCA -m 20 -q 20 o cutread.gz fasta1.gz". Reads were assigned transcript IDs and counted 104 using the command "salmon quant -i celegans.index -l A -r cutread.gz -p 8 validateMappings -o quant file". For conversion of transcript IDs to gene IDs, a table of matching transcript and gene IDs was generated from a GTF file using the command "grep "^[^#]" Caenorhabditis elegans.Wbcel235.101.gtf | awk '{if(\$3 == "transcript"){print}}' | awk '{print \$12,\$14}' | tr d '";' > transcript id gene id.tsv". Conversion was then made using this table with tximport<sup>105</sup> in R, whereafter only genes with more than 0.1 counts per million for at least 2 samples were used in subsequent analyses with pairs of sample types (sid-1(qt9[nonsense]) vs. wild type and sid-1(tm2700[deletion]); tmIs1005[sid-1(+) vs. sid-1(tm2700[deletion])). After normalizing samples using the trimmed mean of M-values method<sup>106</sup>, principal component analysis was performed in R by comparing samples based on the 500 genes with the largest standard deviations in their log<sub>2</sub>-fold change between each set of samples (see *Technical* comments). Differential expression analysis was performed using limma(voom)<sup>107</sup> in R (example available at AntonyJose-Lab/Shugarts et al 2023 on github). Volcano plots of differential expression for all genes compared were plotted using custom R scripts with genes having an

adjusted p-value threshold (q-value) less than 0.05 in black and those greater than 0.05 in grey (see *Technical comments*).

For analysis of newly generated sid-1(-) alleles: Total RNA >200 nt was extracted using RNAzol (Sigma-Aldrich) from 200 µl pellets of mixed-stage animals collected from 6 nonstarved but crowded plates in biological triplicate for each strain. PolyA+ RNAs were purified and converted to DNA libraries using the Illumina TruSeq Stranded mRNA Library Preparation Kit. Library quality was assayed using TapeStation (Agilent) and libraries were sequenced using a HiSeq X10 (Illumina) by Omega Bioservices. FASTQ files were processed using the command "cutadapt -j 0 -a AGATCGGAAGAGCACACGTCTGAACTCCAGTCA -A AGATCGGAAGAGCGTCGTGTAGGGAAAGAGTGT -m 20 -q 20 -o cutread1.gz -p cutread2.gz read1.gz read2.gz". Reads were assigned transcript IDs and counted 104 using the command "salmon quant -i celegans.index -l A -1 cutread1.gz -2 cutread2.gz -p 8 -validateMappings -o quant files". For conversion of transcript IDs to gene IDs, a table of matching transcript and gene IDs was generated as described above. Conversion was then made using this table with tximport<sup>105</sup> in R, whereafter only genes with more than 0.1 counts per million for at least 3 samples were used in subsequent analyses. Normalization, principal component analysis (Fig. 5c and Extended Data Fig. 7a) and differential expression analysis were performed as described above. Volcano plots of differential expression were plotted as described above (Fig. 5d and Extended Data Fig. 7b). Genes that were similarly misregulated in Fig. 5d and Extended Data Fig. 7b are in red.

For analysis of data from Reed et al., 2020: FASTQ files were processed using the command "cutadapt -j 0 -a AGATCGGAAGAGCACACGTCTGAACTCCAGTCA -m 20 -g 20 -o cutread.gz fastal.gz". Reads were assigned transcript IDs and counted 104

using the command "salmon quant -i celegans.index -l A -r cutread.gz -p 8 -validateMappings -o quant\_file". For conversion of transcript IDs to gene IDs, a table of matching transcript and gene IDs was generated as described above. Conversion was then made using this table with tximport<sup>105</sup> in R. Normalization and differential expression analysis were performed as described above. Volcano plots of differential expression were plotted as described above with *sid-1*, *sdg-1* (*W09B7.2/F07B7.2*) and *sdg-2* (*Y102A5C.36*) in red and all other genes in grey (Extended Data Fig. 7d).

Genome mapping and visualization of sequencing reads for sid-1-dependent genes

After RNA sequencing samples were processed as described above, reads were mapped to the *C. elegans* genome<sup>108</sup> using the command "hisat2 -p 8 -x Celegans98index -1 cutread1.gz -2 cutread2.gz -S sam1". The SAM file outputs were then converted to BAM files<sup>109</sup> using the command "samtools view -b sam1 | samtools sort -> bam1.bam" and BAM index files were created for visualization using "samtools index bam1.bam". Reads for the *sid-1* and *F14F9.5* locus, *W09B7.2/F07B7.2* locus, and *Y102A5C.36* locus were plotted using custom R scripts and axes were normalized for each sample based on its total mapped reads, calculated using the command "samtools view -c -F 4 bam1.bam" (Extended Data Fig. 7c).

### Comparisons with published datasets

Datasets in 21 published studies were collected and compared based on the gene names to identify changes in *sid-1*, *sdg-1*, *sdg-2* and *tbb-2* (control), if reported (Fig. 5f). After standardizing the names across all datasets, the fold-changes reported, if available, were used to

plot a heatmap. Cases where fold-changes were not available were set conservatively as log2(fold change) = 2. The R script used is available at AntonyJose-Lab/Shugarts\_et\_al\_2023 on github.

# Reverse transcription and quantitative PCR

Total RNA was extracted using TRIzol (Fisher Scientific) from 200 µl pellets of mixedstage animals collected from 3-6 non-starved but crowded plates in biological triplicate for each strain. The aqueous phase was then washed with an equal amount of chloroform and precipitated overnight on ice with 100 μl of 3 M sodium acetate, 1 ml of 100% ethanol and 10 μg glycogen (Invitrogen). RNA pellets were washed twice with 70% ethanol and resuspended in 22 µl nuclease free water. RNA samples were then Dnase-treated in Dnase buffer (10 mM Tris-HCl pH 8.5, 2.5 mM MgCl<sub>2</sub>, 0.5 mM CaCl<sub>2</sub>) with 0.5 U Dnase I (New England BioLabs) at 37°C for 60 minutes followed by heat inactivation at 75°C for 10 minutes. RNA concentration was measured and 1 µg of total RNA was used as input for reverse transcription using 50 U SuperScript III Reverse Transcriptase (Invitrogen) (+RT) or no reverse transcriptase as a negative control (-RT) (RT primers: tbb-2 (P98), sid-1 (P101), W09B7.2/F07B7.2 (P104), Y102A5C.36 (P107)). For qPCR, each +RT biological replicate was assayed in technical triplicate for each gene target, along with a single -RT sample for each corresponding biological replicate using 2 µl cDNA and a no template control (NTC) with the LightCycler® 480 SYBR Green I Master kit (Roche). Ct values were measured with the Bio-Rad C1000 CFX96 Real-Time System and Bio-Rad CFX Software (qPCR primers: tbb-2 (P99 and P100), sid-1 (P102 and P103), W09B7.2/F07B7.2 (P105 and P106), Y102A5C.36 (P108 and P109)). To calculate relative change in mRNA abundance compared to wild type, we calculated log<sub>2</sub>(2<sup>(-(gene Ct - tbb-2 Ct))</sup>) using the median of technical replicates for the biological triplicates of each genotype. Ct values were

only used if they were lower than corresponding -RT and NTC Ct values. The median value of wild-type biological replicates was then subtracted from the value for each sample to plot calculated values with respect to wild-type levels (Fig. 5e, Extended Data Fig. 7e, Extended Data Fig. 8e and Extended Data Fig. 9a).

BLAST searches and protein alignment

BLAST (NCBI) searches were performed using the W09B7.2/F07B7.2 (SDG-1) amino acid sequence with default parameters and any homologs identified were aligned to SDG-1 using Clustal Omega<sup>110</sup> with default parameters. Alignments produced are shown in Extended Data Fig. 8b with residues shared by two proteins (grey highlight) or all three proteins (black highlight) indicated.

Annotation of the Cer9 retrotransposon containing W09B7.2/F07B7.2

The *Cer9* retrotransposon containing *W09B7.2/F07B7.2* (*sdg-1*) was annotated using sequence features from UCSC Genome Browser and amino acid sequences obtained from ref.<sup>111</sup>. The 5' and 3' LTR sequences were identified using RepeatMasker and were confirmed to have TC and GA dinucleotides at the beginning and end of each sequence, respectively<sup>111</sup>. Amino acid sequences from ref.<sup>111</sup> corresponding to *gag* and *pol* (PR: protease, RT: reverse transcriptase, RH: RNaseH, IN: integrase) elements of *Cer9* were used in tblastn (NCBI) searches to determine their positions in the *Cer9* retrotransposon sequence that also contains *sdg-1*.

*Mating-induced silencing* 

Mating-induced silencing was assayed by crossing males with the transgene labeled *T* (*oxSi487*) encoding *mex-5p::mCherry::h2b::gfp::h2b* to hermaphrodites lacking the transgene, both in otherwise wild-type backgrounds or indicated mutant backgrounds. Reciprocal control crosses were performed in parallel where hermaphrodites with *T* were crossed to males lacking *T*. Animals were imaged and scored as described for this transgene in the "Light-induced damage of neurons" section.

### Technical comments

Making a *sid-1* translational reporter: Previous attempts at observing SID-1 localization relied on multi-copy transgenes<sup>14</sup>, which can become silenced within the germline<sup>112</sup> and could produce a variety of tagged and untagged proteins<sup>64</sup>. When using multi-copy transgenes to express a SID-1 fusion protein tagged at the C-terminus with DsRed or GFP (Extended Data Fig. 10a) under the control of a promoter that drives expression within body-wall muscles, we observed intracellular localization of SID-1::DsRed or SID-1::GFP (Extended Data Fig. 10b) along with rescue of gene silencing by ingested dsRNA in body-wall muscles by both arrays (for SID-1::DsRed – silencing in wild type = 100% (n = 10), sid-1(qt9) = 0% (n = 11), sid-1(qt9); jamIs2[myo-3p::sid-1(+)::DsRed] = 100% (n = 6); for SID-1::GFP – silencing in wild type = 100% (n = 50), sid-1(qt9); jamEx193[mvo-3p::sid-1(+)::gfp] = 100% (n = 60)). However, similar tagging to express SID-1 fusion proteins from either a single-copy transgene expressed in the germline (SID-1::DsRed) or the endogenous locus (SID-1::wrmScarlet) did not enable gene silencing by ingested dsRNA (for evaluating function of mex-5p::sid-1(+)::DsRed::sid-1 3' UTR (jamSi12): silencing of pos-1 in wild-type = 100% (n = 7), sid-1(qt9) = 0% (n = 7), jamSi12; sid-I(qt9) = 0% (n = 15); for evaluating function of sid-1::wrmScarlet(jam117): silencing of pos-1

in wild-type = 100% (n = 8), sid-1(jam80) = 0% (n = 8), sid-1(jam117) = 0% (n = 8)), suggesting that the C-terminal fusions of SID-1 were likely non-functional and that apparent function when using multi-copy transgenes reflects production of untagged variants. In support of our rationale, a recent prediction of SID-1 structure<sup>113,114</sup> suggests that the C-terminus is sequestered (Extended Data Fig. 10c), a feature that may be disrupted by the addition of C-terminal fluorophores, potentially leading to misfolded proteins that are degraded. Consistently, we found that internal tagging of the sid-1 gene using Cas9-mediated genome editing to express SID-1::mCherry (Fig. 4) resulted in a fusion protein with detectable function (percent unc-22 silencing - wild type = 100% (n = 59),  $sid-1(jam195[sid-1::mCherry\Delta pi]) = ~98\%$  (n = 52); percent bli-1 silencing - wild type = 100% (n = 833),  $sid-1(jam195[sid-1::mCherry\Delta pi]) = ~0.01\%$  (n = 634)).

RNA sequencing analysis of existing sid-1 mutants: We initially analyzed polyA+ RNAs extracted from wild-type animals, two available sid-1 loss-of-function mutants<sup>14,93</sup> (sid-1(-)) and one available rescue strain where sid-1(-) was rescued with a transgene that overexpresses  $sid-1(+)^{93}$ , but found that pairwise comparisons between wild-type and mutant samples with otherwise similar genetic backgrounds did not yield any significantly misregulated genes present in both comparisons (Extended Data Fig. 10d). Strains with similar genotypes (sid-1(+) or sid-1(-)) did not cluster together when using principal component analysis (Extended Data Fig. 10e), suggesting that other differences (e.g., genetic background) obscure or misrepresent differences between sid-1(+) and sid-1(-) animals.

# Rationale for inferences

<u>Prior models and assumptions</u>: All dsRNA is trafficked similarly. Entry of dsRNA into the germline can initiate transgenerational RNA silencing of some but not all genes. No SID-1-

dependent germline genes are known, suggesting that SID-1 could be used solely in response to viral infection by analogy with roles of other members of RNA interference pathways.

Evidence supporting key conclusions: Temporal selectivity of dsRNA transport was probed using three approaches for delivery of dsRNA (damage-induced release from neurons, ingestion, and injection). Spatial selectivity of dsRNA import and/or subsequent silencing was inferred based on differences in the frequency of patterns of silencing within the germline. Substrate selectivity of dsRNA transport pathways was probed using genetic mutants and dsRNA of different lengths and 5' chemistry. Diversity of dsRNAs made in bacteria and upon in vitro transcription was visualized using Northern blotting. Analysis of sid-1 mutants generated from the same wild-type cohort and a revertant was used for better control of genetic background, aiding in the identification of sid-1-dependent genes (sdg). Separate measurement of sdg-1 expression in descendants of independently edited isolates, along different lineages after perturbations, and in different gonads within single animals demonstrated stochasticity in gene expression and revealed establishment of different heritable epigenetic states. Co-localization of SDG-1::mCherry in perinuclear foci with the Z-granule marker GFP::ZNFX-1, its reported association with the Z-granule component ZSP-1/PID-2 and DEPS-1, changes in its levels in response to loss of SID-1 or the dsRNA-binding protein RDE-4 and its dynamic nuclear localization similar to CSR-1b was used to propose that SDG-1 plays a role in small RNA regulation while also being modulated by the activity of SID-1 and RDE-4.

## REFERENCES

- 1. Cai, Q. et al. Plants send small RNAs in extracellular vesicles to fungal pathogen to silence virulence genes. *Science* **360**, 1126-1129 (2018).
- 2. Ashley, J. et al. Retrovirus-like Gag protein Arc1 binds RNA and traffics across synaptic boutons. *Cell* **172**, 262-274.e11 (2018).
- 3. Pastuzyn, E. D. et al. The neuronal gene *Arc* encodes a repurposed retrotransposon Gag protein that mediates intercellular RNA transfer. *Cell* **172**, 275-288.e18 (2018).
- 4. Thomou, T. et al. Adipose-derived circulating miRNAs regulate gene expression in other tissues. *Nature* **542**, 450-455 (2017).
- 5. Sharma, U. et al. Biogenesis and function of tRNA fragments during sperm maturation and fertilization in mammals. *Science* **351**, 391-396 (2016).
- 6. Chen, Q. et al. Sperm tsRNAs contribute to intergenerational inheritance of an acquired metabolic disorder. *Science* **351**, 397-400 (2016).
- 7. Conine, C. C., Sun, F., Song, L., Rivera-Pérez, J. A. & Rando, O. J. Small RNAs gained during epididymal transit of sperm are essential for embryonic development in mice. *Dev. Cell* **46**, 470-480.e3 (2018).
- 8. Sharma, U. et al. Small RNAs are trafficked from the epididymis to developing mammalian sperm. *Dev. Cell* **46**, 481-494.e6 (2018).
- 9. Das, S. et al. The Extracellular RNA Communication Consortium: establishing foundational knowledge and technologies for extracellular RNA research. *Cell* **177**, 231-242 (2019).
- 10. Setten, R. L., Rossi, J. J. & Han, S. P. The current state and future directions of RNAi-based therapeutics. *Nat. Rev. Drug Discov.* **18**, 421-446 (2019).
- 11. Hu, B. et al. Therapeutic siRNA: state of the art. *Signal Transduct. Target Ther.* **5**, 101 (2020).
- 12. Mullard, A. FDA approves fifth RNAi drug Alnylam's next-gen hATTR treatment. *Nat. Rev. Drug. Discov.* **21**, 548-549 (2022).
- 13. Fire, A. et al. Potent and specific genetic interference by double-stranded RNA in *Caenorhabditis elegans*. *Nature* **391**, 806-811 (1998).
- 14. Winston, W. M., Molodowitch, C. & Hunter, C. P. Systemic RNAi in *C. elegans* requires the putative transmembrane protein SID-1. *Science* **295**, 2456-2459 (2002).

- 15. Feinberg, E. H. & Hunter, C. P. Transport of dsRNA into cells by the transmembrane protein SID-1. *Science* **301**, 1545-1547 (2003).
- 16. Shih, J. D., Fitzgerald, M. C., Sutherlin, M. & Hunter, C. P. The SID-1 double-stranded RNA transporter is not selective for dsRNA length. *RNA* **15**, 384-390 (2009).
- 17. Winston, W. M., Sutherlin, M., Wright, A. J., Feinberg, E. H. & Hunter, C. P. *Caenorhabditis elegans* SID-2 is required for environmental RNA interference. *Proc. Natl. Acad. Sci. USA* **104**, 10565-10570 (2007).
- 18. McEwan, D. L., Weisman, A. S. & Hunter, C. P. Uptake of extracellular double-stranded RNA by SID-2. *Mol. Cell* **47**, 746-754 (2012).
- 19. Nguyen, T. A. et al. SIDT2 transports extracellular dsRNA into the cytoplasm for innate immune recognition. *Immunity* **47**, 498-509.e6 (2017).
- 20. Nguyen, T. A. et al. SIDT1 Localizes to Endolysosomes and Mediates Double-Stranded RNA Transport into the Cytoplasm. *J Immunol.* **202**, 3483-3492 (2019).
- 21. Chen, Q. et al. SIDT1-dependent absorption in the stomach mediates host update of dietary and orally administered microRNAs. *Cell Res.* **31**, 247-258 (2021).
- 22. Méndez-Acevedo, K. M., Valdes, V. J., Asanov, A. & Vaca, L. A novel family of mammalian transmembrane proteins involved in cholesterol transport. *Sci. Rep.* 7, 7450 (2017).
- 23. Jose, A. M., Smith, J. J. & Hunter, C. P. Export of RNA silencing from *C. elegans* tissues does not require the RNA channel SID-1. *Proc. Natl. Acad. Sci. USA* **106**, 2283-2288 (2009).
- 24. Ravikumar, S., Devanapally, S. & Jose, A. M. Gene silencing by double-stranded RNA from *C. elegans* neurons reveals functional mosaicism of RNA interference. *Nucleic Acids Res.* **47**, 10059-10071 (2019).
- 25. Devanapally, S., Ravikumar, S. & Jose, A. M. Double-stranded RNA made in *C. elegans* neurons can enter the germline and cause transgenerational gene silencing. *Proc. Natl. Acad. Sci. USA* **112**, 2133-2138 (2015).
- 26. Timmons, L. & Fire, A. Specific interference by ingested dsRNA. *Nature* **395**, 854 (1998).
- 27. Grishok, A., Tabara, H. & Mello, C. C. Genetic requirements for inheritance of RNAi in *C. elegans. Science* **287**, 2494-2497 (2000).
- 28. Marré, J., Traver, E. C. & Jose, A. M. Extracellular RNA is transported from one generation to the next in *Caenorhabditis elegans*. *Proc. Natl. Acad. Sci. USA* **113**, 12496-12501 (2016).
- 29. Wang, E. & Hunter, C. P. SID-1 functions in multiple roles to support parental RNAi in *Caenorhabditis elegans. Genetics* **207**, 547-557 (2017).

- 30. Buckley, B. A. et al. A nuclear Argonaute promotes multigenerational epigenetic inheritance and germline immortality. *Nature* **489**, 447-451 (2012).
- 31. Xu, F. et al. A cytoplasmic Argonaute protein promotes the inheritance of RNAi. *Cell Rep.* **23**, 2483-2494 (2018).
- 32. Grant, B. & Hirsh, D. Receptor-mediated endocytosis in the *Caenorhabditis elegans* oocyte. *Mol. Biol. Cell* **10**, 4311-4326 (1999).
- 33. Xu, S. & Chisholm, A. D. Highly efficient optogenetic cell ablation in *C. elegans* using membrane-targeted miniSOG. *Sci. Rep.* **6**, 21271 (2016).
- 34. Guang, S. et al. An Argonaute transports siRNAs from the cytoplasm to the nucleus. *Science* **321**, 537-541 (2008).
- 35. Ouyang, J. P. T., Zhang, W. & Seydoux, G. The conserved helicase ZNFX-1 memorializes silenced RNAs in perinuclear condensates. *Nat. Cell Biol.* **24**, 1129-1140 (2022).
- 36. Choi, Y. S., Edwards, L. O., DiBello, A. & Jose, A. M. Removing bias against short sequences enables northern blotting to better complement RNA-seq for the study of small RNAs. *Nucleic Acids Res.* **45**, e87 (2017).
- 37. Tabara, H., Yigit, E., Siomi, H. & Mello, C. C. The dsRNA binding protein RDE-4 interacts with RDE-1, DCR-1, and a DexH-box helicase to direct RNAi in *C. elegans. Cell* **109**, 861-871 (2002).
- 38. Jain, N. et al. Transcription polymerase-catalyzed emergence of novel RNA replicons. *Science* **368**, eaay0688 (2020).
- 39. Sharrock, W. J. Yolk proteins of Caenorhabditis elegans. Dev. Biol. 96, 182-188 (1983).
- 40. Bossinger, O. & Schierenberg, E. The use of fluorescent marker dyes for studying intercellular communication in nematode embryos. *Int. J. Dev. Biol.* **40**, 431-439 (1996).
- 41. Hinas, A., Wright, A. J. & Hunter, C. P. SID-5 is an endosome-associated protein required for efficient systemic RNAi in *C. elegans. Curr. Biol.* **22**, 1938-1943 (2012).
- 42. Zhang, D. et al. The piRNA targeting rules and the resistance to piRNA silencing in endogenous genes. *Science* **359**, 587-592 (2018).
- 43. Devanapally, S. et al. Mating can initiate stable RNA silencing that overcomes epigenetic recovery. *Nat. Commun.* **12**, 4239 (2021).

- 44. Wurmthaler, L. A., Sack, M., Gense, K., Hartig, J. S. & Gamerdinger, M. A tetracycline-dependent ribozyme switch allows conditional induction of gene expression in *Caenorhabditis elegans*. *Nat. Commun.* **10**, 491 (2019).
- 45. Ouyang, J. P. T. et al. P granules protect RNA interference genes from silencing by piRNAs. *Dev. Cell* **50**, 716-728.e6 (2019).
- 46. Dodson, A. E. & Kennedy, S. Germ granules coordinate RNA-based epigenetic inheritance pathways. *Dev. Cell* **50**, 704-715.e4 (2019).
- 47. Reed, K. J. et al. Widespread roles for piRNAs and WAGO-class siRNAs in shaping the germline transcriptome of *Caenorhabditis elegans*. *Nucleic Acids Res.* **48**, 1811-1827 (2020).
- 48. Welker, N. C., Habig, J. W. & Bass, B. L. Genes misregulated in *C. elegans* deficient in Dicer, RDE-4, or RDE-1 are enriched for innate immunity genes. *RNA* **13**, 1090-1102 (2007).
- 49. Spike, C. A., Bader, J., Reinke, V. & Strome, S. DEPS-1 promotes P-granule assembly and RNA interference in *C. elegans* germ cells. *Development* **135**, 983-993 (2008).
- 50. Wan, G. et al. ZSP-1 is a Z granule surface protein required for Z granule fluidity and germline immortality in *Caenorhabditis elegans*. *EMBO J.* **40**, e105612 (2021).
- 51. Suen, K. M. et al. DEPS-1 is required for piRNA-dependent silencing and PIWI condensate organisation in *Caenorhabditis elegans*. *Nat. Commun.* **11**, 4242 (2020).
- 52. Wahba, L., Hansen, L. & Fire, A. Z. An essential role for the piRNA pathway in regulating the ribosomal RNA pool in *C. elegans. Dev. Cell* **56**, 2295-2312.e6 (2021).
- 53. Shen, E. et al. Identification of piRNA binding sites reveals the Argonaute regulatory landscape of the *C. elegans* germline. *Cell* **172**, 937-951.e18 (2018).
- 54. Goh, W. S. et al. A genome-wide RNAi screen identifies factors required for distinct stages of *C. elegans* piRNA biogenesis. *Genes Dev.* **28**, 797-807 (2014).
- 55. Lee, H. et al. *C. elegans* piRNAs mediate the genome-wide surveillance of germline transcripts. *Cell* **150**, 78-87 (2012).
- 56. Batista, P. J. et al. PRG-1 and 21U-RNAs interact to form the piRNA complex required for fertility in *C. elegans. Mol. Cell* **31**, 67-78 (2008).
- 57. Kim, H. et al. HDAC1 SUMOylation promotes Argonaute-directed transcriptional silencing in *C. elegans. eLife* **10**, e63299 (2021).
- 58. Ni, J. Z. et al. A transgenerational role of the germline nuclear RNAi pathway in repressing heat stress-induced transcriptional activation in *C. elegans. Epigenetics Chromatin* **9**, 3 (2016).

- 59. Sundby, A. E., Molnar, R. I. & Claycomb, J. M. Connecting the dots: linking Caenorhabditis elegans small RNA pathways and germ granules. *Trends Cell Biol.* **31**, 387-401 (2021).
- 60. Placentino, M. et al. Intrinsically disordered protein PID-2 modulates Z granules and is required for heritable piRNA-induced silencing in the *Caenorhabditis elegans* embryo. *EMBO J.* **40**, e105280 (2021).
- 61. Price, I. F., Hertz, H. L., Pastore, B., Wagner, J. & Tang, W. Proximity labeling identifies LOTUS domain proteins that promote the formation of perinuclear germ granules in *C. elegans*. *eLife* **10**, e72276 (2021).
- 62. Okkema, P. G., Harrison, S. W., Plunger, V., Aryana, A. & Fire, A. Sequence requirements for myosin gene expression and regulation in *Caenorhabditis elegans*. *Genetics* **135**, 385-404 (1993).
- 63. Crane, M. M. et al. *In vivo* measurements reveal a single 5'-intron is sufficient to increase protein expression level in *Caenorhabditis elegans*. *Sci. Rep.* **9**, 9192 (2019).
- 64. Le, H. H., Looney, M., Strauss, B., Bloodgood, M. & Jose, A. M. Tissue homogeneity requires inhibition of unequal gene silencing during development. *J. Cell Biol.* **14**, 319-331 (2016).
- 65. Shukla, A., Perales, R. & Kennedy, S. piRNAs coordinate poly(UG) tailing to prevent aberrant and perpetual gene silencing. *Curr. Biol.* **31**, 4473-4485 (2021).
- 66. Dodson, A. E. & Kennedy, S. Phase separation in germ cells and development. *Dev. Cell* 55, 4-17 (2020).
- 67. Huff, J. et al. The new 2D Superresolution mode for ZEISS Airyscan. *Nat. Methods* **14**, 1223 (2017).
- 68. Ishidate, T. et al. ZNFX-1 functions within perinuclear nuage to balance epigenetic signals. *Mol. Cell* **70**, 639-649.e6 (2018).
- 69. Wan, G. et al. Spatiotemporal regulation of liquid-like condensates in epigenetic inheritance. *Nature* **557**, 679-683 (2018).
- 70. Huelgas-Morales, G. & Greenstein, D. Control of oocyte meiotic maturation in *C. elegans*. *Semin. Cell Dev. Biol.* **84**, 90-99 (2018).
- 71. Charlesworth, A. G. et al. Two isoforms of the essential *C. elegans* Argonaute CSR-1 differentially regulate sperm and oocyte fertility. *Nucleic Acids Res.* **49**, 8836-8865 (2021).
- 72. Whipple, J. M. et al. Genome-wide profiling of the *C. elegans* dsRNAome. *RNA* **21**, 786-800 (2015).

- 73. Melentijevic, I. et al. *C. elegans* neurons jettison protein aggregates and mitochondria under neurotoxic stress. *Nature* **542**, 367-371 (2017).
- 74. Tielking, K., Fischer, S., Preissner, K. T., Vajkoczy, P. & Xu, R. Extracellular RNA in central nervous system pathologies. *Front. Mol. Neurosci.* **12**, 254 (2019).
- 75. Li, W., Koutmou, K. S., Leahy, D. J. & Li, M. Systemic RNA interference deficiency-1 (SID-1) extracellular domain selectively binds long double-stranded RNA and is required for RNA transport by SID-1. *J. Biol. Chem.* **290**, 18904-18913 (2015).
- 76. Long, O. S. et al. A *C. elegans* model of human α1-antitrypsin deficiency links components of the RNAi pathway to misfolded protein turnover. *Hum. Mol. Genet.* **23**, 5109-5122 (2014).
- 77. Ow, M. C., Borziak, K., Nichitean, A. M., Dorus, S. & Hall, S. E. Early experiences mediate distinct adult gene expression and reproductive programs in *Caenorhabditis elegans*. *PloS Genet*. **14**, e1007219 (2018).
- 78. Kadekar, P. & Roy, R. AMPK regulates germline stem cell quiescence and integrity through an endogenous small RNA pathway. *PloS Biol.* **17**, e3000309 (2019).
- 79. Palominos, M. F. et al. Transgenerational diapause as an avoidance strategy against bacterial pathogens in *Caenorhabditis elegans*. *mBio* **8**, e01234-17 (2017).
- 80. Moore, R. S., Kaletsky, R. & Murphy, C. T. Piwi/PRG-1 Argonaute and TGF-β mediate transgenerational learned pathogenic avoidance. *Cell* **177**, 1827-1841.e12 (2019).
- 81. Kaletsky, R. et al. *C. elegans* interprets bacterial non-coding RNAs to learn pathogenic avoidance. *Nature* **586**, 445-451 (2020).
- 82. Posner, R. et al. Neuronal small RNAs control behavior transgenerationally. *Cell* 177, 1814-1826.e15 (2019).
- 83. Ohno, H. & Bao, Z. Small RNAs couple embryonic developmental programs to gut microbes. *Sci. Adv.* **8**, eabl7663 (2022).
- 84. Gaeta, A. L. et al. Systemic RNA Interference Defective (SID) genes modulate dopaminergic neurodegeneration in C. elegans. *PloS genetics*, **18**, e1010115 (2022).
- 85. Jose, A. M. Heritable epigenetic changes alter transgenerational waveforms maintained by cycling stores of information. *Bioessays* **42**, e1900254 (2020).
- 86. Chey, M. & Jose, A. M. Heritable epigenetic changes at single genes: challenges and opportunities in *Caenorhabditis elegans*. *Trends Genet*. **S0168-9525**, 00253-00257 (2021).

- 87. Tops, B. B., Plasterk, R. H. & Ketting, R. F. The *Caenorhabditis elegans* Argonautes ALG-1 and ALG-2: almost identical yet different. *Cold Spring Harb. Symp. Quant. Biol.* **71**, 189-194 (2006).
- 88. Brenner, S. The genetics of Caenorhabditis elegans. Genetics 77, 71-94 (1974).
- 89. Mello, C. C., Kramer, J. M., Stinchcomb, D. & Ambros, V. Efficient gene transfer in *C. elegans*: extrachromosomal maintenance and integration of transforming sequences. *EMBO J.* **10**, 3959-3970 (1991).
- 90. Frøkjær-Jensen, C., Davis, M. W., Ailion, M. & Jorgensen, E. M. Improved Mos1-mediated transgenesis in *C. elegans. Nat. Methods* **9**, 117-118 (2012).
- 91. Jose, A. M., Garcia, G. A. & Hunter, C. P. Two classes of silencing RNAs move between *C. elegans* tissues. *Nat. Struct. Mol. Biol.* **18**, 1184-1188 (2011).
- 92. Raman, P., Zaghab, S. M., Traver, E. C. & Jose, A. M. The double-stranded RNA binding protein RDE-4 can act cell autonomously during feeding RNAi in *C. elegans. Nucleic Acids Res.* **45**, 8463-8473 (2017).
- 93. Kage-Nakadai, E. et al. A conditional knockout toolkit for *Caenorhabditis elegans* based on the Cre/loxP recombination. *PloS One* **9**, e114680 (2014).
- 94. Arribere, J. A. et al. Efficient marker-free recovery of custom genetic modifications with CRISPR/Cas9 in *Caenorhabditis elegans*. *Genetics* **198**, 837-846 (2014).
- 95. Paix, A., Folkmann, A., Rasoloson, D. & Seydoux, G. High efficiency, homology-directed genome editing in *Caenorhabditis elegans* using CRISPR-Cas9 ribonucleoprotein complexes. *Genetics* **201**, 47-54 (2015).
- 96. Dokshin, G. A., Ghanta, K. S., Piscopo, K. M. & Mello, C. C. Robust genome editing with short single-stranded and long, partially single-stranded DNA donors in *Caenorhabditis elegans*. *Genetics* **210**, 781-787 (2018).
- 97. Tabara, H. et al. The *rde-1* gene, RNA interference, and transposon silencing in *C. elegans*. *Cell* **99**, 123-132 (1999).
- 98. Vicencio, J., Martínez-Fernández, C., Serrat, X. & Cerón, J. Efficient generation of endogenous fluorescent reporters by nested CRISPR in *Caenorhabditis elegans*. *Genetics* **211**, 1143-1154 (2019).
- 99. Jose, A. M., Kim, Y. A., Leal-Ekman, S. & Hunter, C. P. Conserved tyrosine kinase promotes the import of silencing RNA into *Caenorhabditis elegans* cells. *Proc. Natl. Acad. Sci. USA* **109**, 14520-14525 (2012).

- 100. Levy, A. D., Yang, J., Kramer, J. M. Molecular and genetic analyses of the *Caenorhabditis elegans dpy-2* and *dpy-10* collagen genes: a variety of molecular alterations affect organismal morphology. *Mol. Biol. Cell* **4**, 803-817 (1993).
- 101. Schindelin, J. et al. Fiji: an open-source platform for biological-image analysis. *Nat. Methods* **9**, 676-682 (2012).
- 102. Harris, C. J., Molnar, A., Müller, S. Y., Baulcombe, D. C. FDF-PAGE: a powerful technique revealing previously undetected small RNAs sequestered by complementary transcripts. *Nucleic Acids Res.* **43**, 7590-7599 (2015).
- 103. Martin, M. Cutadapt removes adapter sequences from high-throughput sequencing reads. *EMBnet.journal* **17**, 10-12 (2011).
- 104. Patro, R., Duggal, G., Love, M. I., Irizarry, R. A., Kingsford, C. Salmon provides fast and bias-aware quantification of transcript expression. *Nat. Methods* **14**, 417-419 (2017).
- 105. Soneson, C., Love, M. I. & Robinson, M. D. Differential analyses for RNA-seq: transcript-level estimates improve gene-level inferences. *F1000Res.* **4**, 1521 (2015).
- 106. Robinson, M. D. & Oshlack, A. A scaling normalization method for differential expression analysis of RNA-seq data. *Genome Biol.* **11**, R25 (2010).
- 107. Law, C. W., Chen, Y., Shi, W., Smyth, G. K. voom: precision weights unlock linear model analysis tools for RNA-seq read counts. *Genome Biol.* **15**, R29 (2014).
- 108. Kim, D., Paggi, J. M., Park, C., Bennett, C., Salzberg, S. L. Graph-based genome alignment and genotyping with HISAT2 and HISAT-genotype. *Nat. Biotechnol.* **37**, 907-915 (2019).
- 109. Li, H. et al. 1000 Genome Project Data Processing Subgroup, The Sequence Alignment/Map format and SAMtools. *Bioinformatics* **25**, 2078-2079 (2009).
- 110. Madeira, F. et al. The EMBL-EBI search and sequence analysis tools APIs in 2019. *Nucleic Acids Res.* **47**, W636-W641 (2019).
- 111. Bowen, N. J. & McDonald, J. F. Genomic analysis of *Caenorhabditis elegans* reveals ancient families of retroviral-like elements. *Genome Res.* **9**, 924-935 (1999).
- 112. Kelly, W. G., Xu, S., Montgomery, M. K. & Fire, A. Distinct requirements for somatic and germline expression of a generally expressed *Caenorhabditis elegans* gene. *Genetics* **146**, 227-238 (1997).
- 113. Jumper, J. et al. Highly accurate protein structure prediction with AlphaFold. *Nature* **596**, 583-589 (2021).

114. Varadi, M. et al. AlphaFold Protein Structure Database: massively expanding the structural coverage of protein-sequence space with high-accuracy models. *Nucleic Acids Res.* **50**, D439-D444 (2022).

### FIGURES AND LEGENDS

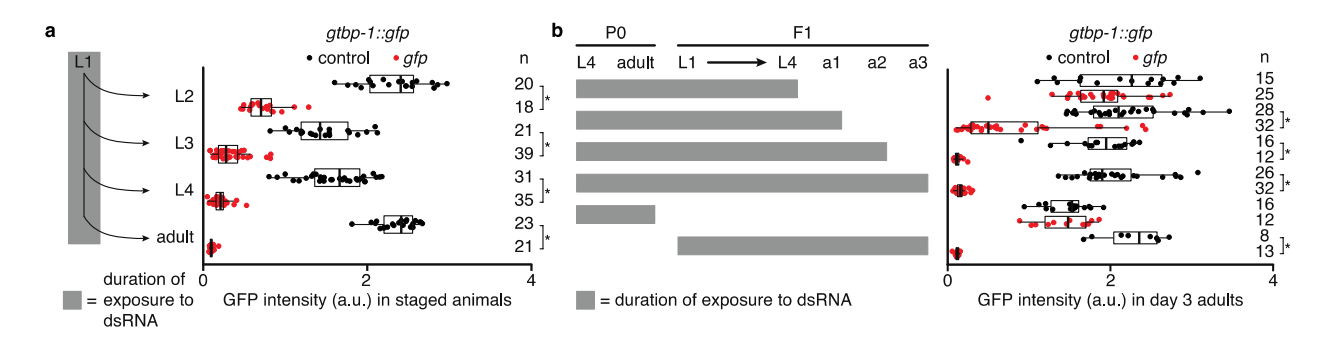


Fig. 1. Gene silencing by ingested dsRNA during larval development does not persist into adulthood. Silencing in the germline was measured after exposure of gtbp-1::gfp animals to bacteria expressing dsRNA by imaging separate cohorts at indicated stages (a) or day 3 of adulthood (b). a and b, left, Schematics depicting stages and durations of exposure to dsRNA. a and b, right, GFP intensity (a.u.) in gtbp-1::gfp animals quantified in germ cells (larvae) or eggs  $in\ utero$  (adults) (a) or in day 3 adult (a3) animals (b) after exposure to control dsRNA (black) or gfp-dsRNA (red). The numbers of animals scored at each stage (n) are indicated. Asterisks indicate P < 0.05 with Bonferroni correction using Mann-Whitney U test for two-sided comparisons between animals exposed to control or gfp-dsRNA. Also see Extended Data Fig. 1.

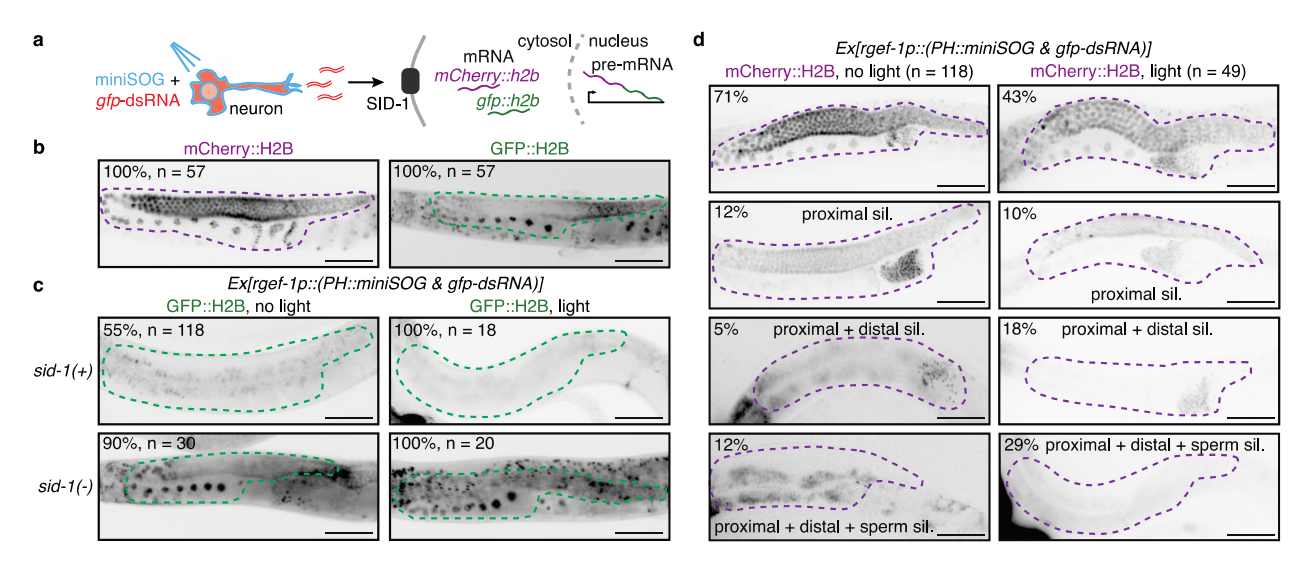


Fig. 2. Oxidative damage of neurons enhances gene silencing by neuronal dsRNA in the adult germline. a, Schematic illustrating exposure to blue light of animals expressing a singlet oxygen generator (miniSOG) and gfp-dsRNA in neurons, and subsequent release of dsRNA. Such extracellular dsRNA is expected to enter the cytosol of the germline through the dsRNA importer SID-1 and silence gfp::h2b mRNA from a two-gene operon that expresses mCherry::h2b and gfp::h2b as part of a single pre-mRNA. b-d, Images of single gonad arms in adult animals with the two-gene operon (mex-5p::mCherry::h2b::gfp::h2b) showing fluorescence (black) of mCherry::H2B (magenta outline) or of GFP::H2B (green outline). Punctate autofluorescence from the intestine can also be seen. Numbers of animals assayed (n) and percentages of adult animals with the depicted expression patterns are indicated. Scale bars, 50 μm. **b**, mCherry::H2B fluorescence is seen throughout the germline (*left*) and GFP::H2B fluorescence is seen in the oocytes and in the distal gonad (right). c, GFP::H2B fluorescence in sid-1(+) and sid-1(-) animals expressing membrane-localized miniSOG (PH::miniSOG) and gfpdsRNA driven by a neuronal promoter (rgef-1p) from a multi-copy transgene (Ex, jamEx214) without (left) or with (right) exposure to blue light at 48 hours post L4-stage of parent. d, mCherry::H2B fluorescence in sid-1(+) animals with the transgene Ex. Silencing of mCherry is

enhanced in the distal gonad (third row) and sperm (fourth row) after exposing animals to blue light at 48 hours and 54 hours post L4-stage of parent. By region, silencing after exposure to light (right) in the proximal germline (57% = 10 + 18 + 29) > distal germline (47% = 18 + 29) > sperm (29%). Also see Extended Data Fig. 2 and Extended Data Fig. 3.

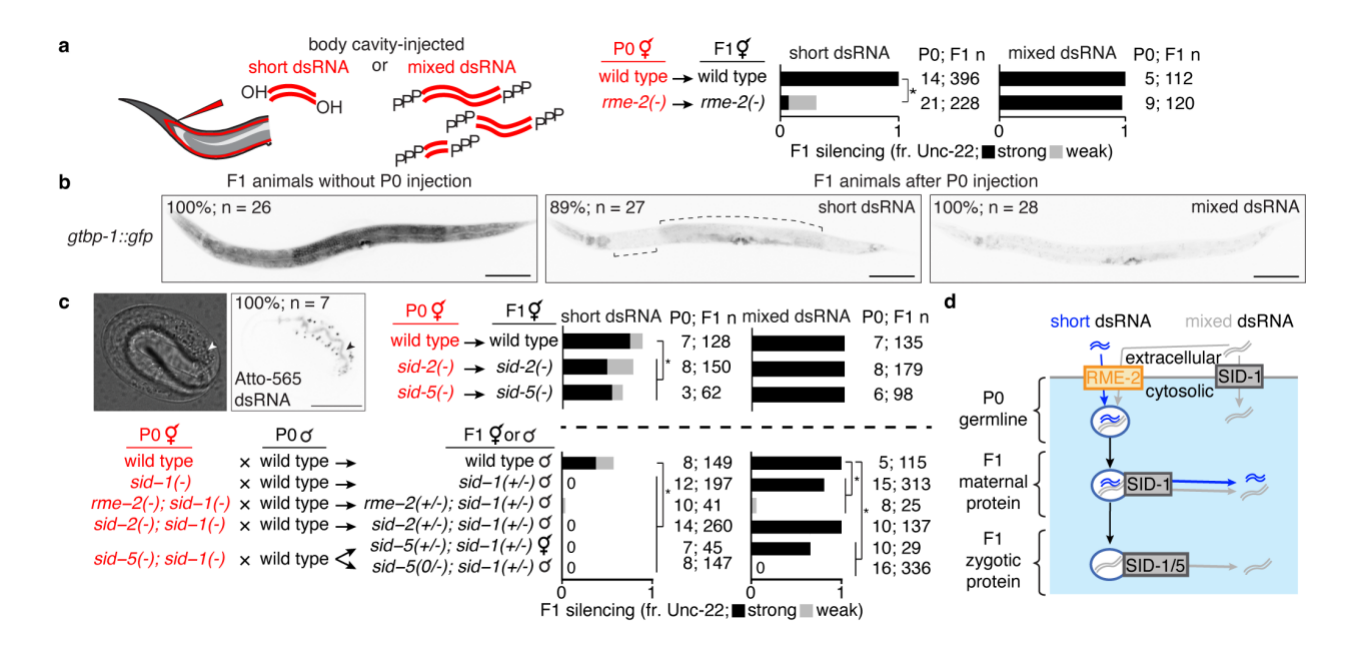


Fig. 3. Transport of dsRNA from parental circulation to progeny occurs through two routes with distinct substrate selectivity. a, Hermaphrodite animals of indicated genotypes (in red) were injected in the body cavity with 50-bp unc-22-dsRNA synthesized with a 5'-OH (short dsRNA, left bars) or unc-22-dsRNA with a 5' triphosphate transcribed from a ~1.1 kb template (mixed dsRNA, right bars). Hermaphrodite self-progeny of injected animals were scored for unc-22 silencing (fr. Unc-22: strong, black; weak, grey). Numbers of injected parents and scored progeny (P0; F1 n) are indicated. Also see Extended Data Fig. 3 and Extended Data Fig. 4. b, Fluorescence images of progeny from animals with a gfp tag of the ubiquitously expressed gene gtbp-1 (gtbp-1::gfp) that were not injected (left), injected with 50-bp gfp-dsRNA (short dsRNA injection, *middle*), or injected with dsRNA transcribed from a ~730-bp template (mixed dsRNA injection, right). Complete silencing is not observed in neurons or in the developing vulva; brackets indicate additional regions with dim GFP fluorescence. Numbers of animals assayed (n) and percentages of L4-staged animals with the depicted expression patterns are indicated. Scale bar, 100 µm. Also see Extended Data Fig. 5. c, Requirements for intergenerational transport of extracellular dsRNA. (top left) Differential Interference Contrast (DIC) and fluorescence images

of a developing embryo from an animal injected in the body cavity with 50-bp dsRNA of the same sequence as in **b** and labeled at the 5' end of the antisense strand with Atto-565. Accumulation within the intestinal lumen (arrowhead), number of embryos imaged (n), and percentage of embryos with depicted pattern of fluorescence are indicated. Scale bar, 20  $\mu$ m. (top right and bottom) Hermaphrodite animals of the indicated genotypes were injected with short dsRNA (left bars) or mixed dsRNA (right bars) and self-progeny (top right) or cross progeny after mating with wild-type males (bottom) were analyzed as in **a**. Cases of no observable silencing are indicated with '0'. **d**, Schematic summarizing requirements for transport of dsRNA from parental circulation to developing progeny. See text for details. Asterisks in **a** and **c** indicate P < 0.05 with Bonferroni correction using  $\chi^2$  test.

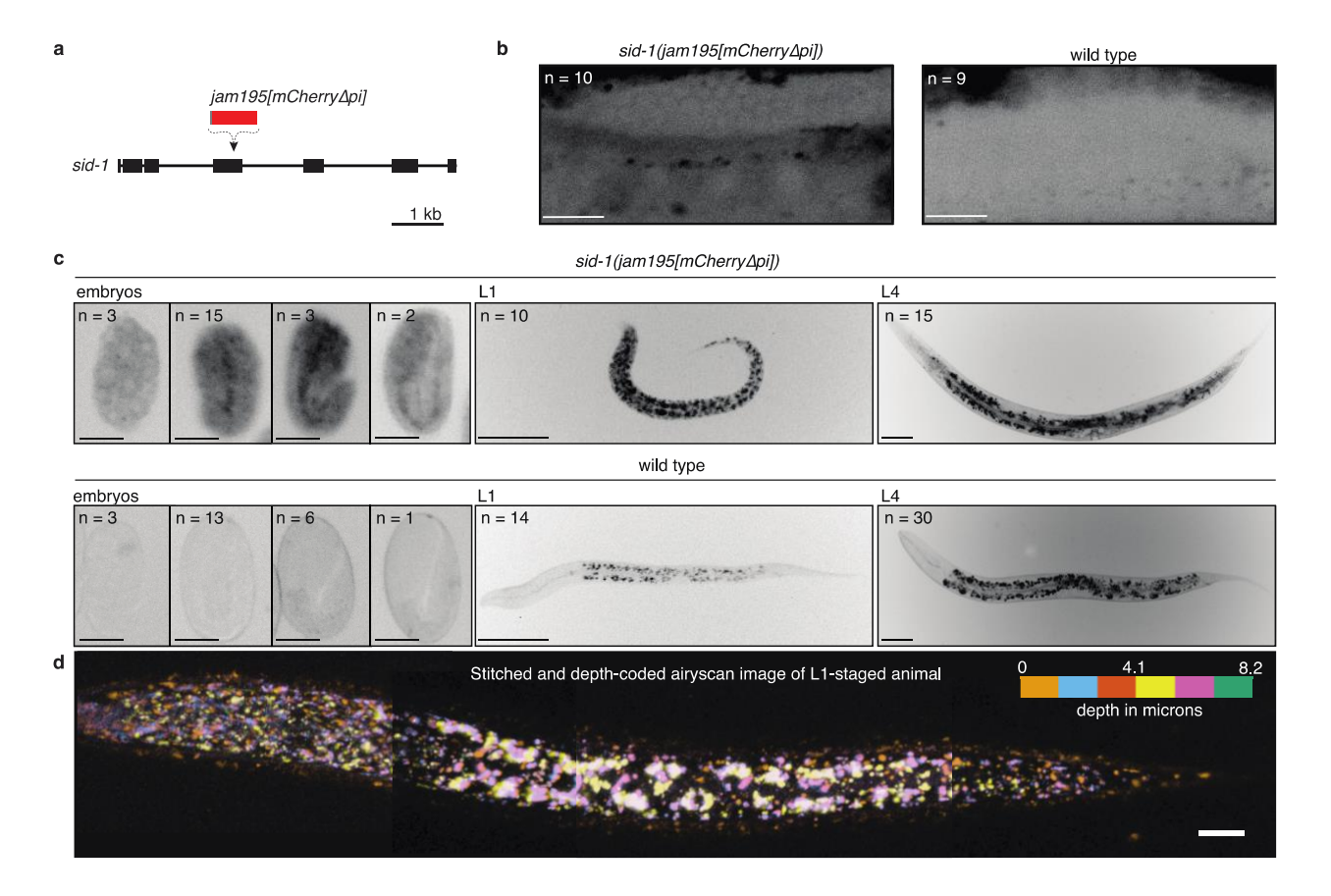


Fig. 4. The expression pattern of SID-1 varies during development. a, Schematic depicting insertion of *mCherry* sequence that lacks piRNA binding sites<sup>42,43</sup> (*jam195[mCherryΔpi]*) into the *sid-1* gene using Cas9-mediated genome editing. b and c, Representative images showing fluorescence from SID-1::mCherry (black) in (b) the adult gonad arm, (c, *left*) developing embryos, (c, *middle*) L1-stage animals, or (c, *right*) L4-stage animals with *sid-1(jam195[mCherryΔpi])* compared to autofluorescence in wild-type animals of the same stages. Numbers (n) of each stage imaged are indicated (100% of animals exhibited the depicted expression patterns). For animals imaged in b, the distal germline was obstructed by the intestine in 1/10 *sid-1(jam195[mCherryΔpi])* and 5/9 wild-type animals. d, Airyscan image of an L1-staged animal assembled by stitching four different Z-stacks after depth-coding and taking maximum projections, illustrating the expression of SID-1::mCherry throughout the animal. Scale bar for adult gonad arms in b and embryos in c, 20 μm; scale bar for larvae in c, 50 μm and

in  ${\bf d}$ , 10  ${\bf \mu}m$ . Also see *Technical comments* on "Making a *sid-1* translational reporter" in Methods.

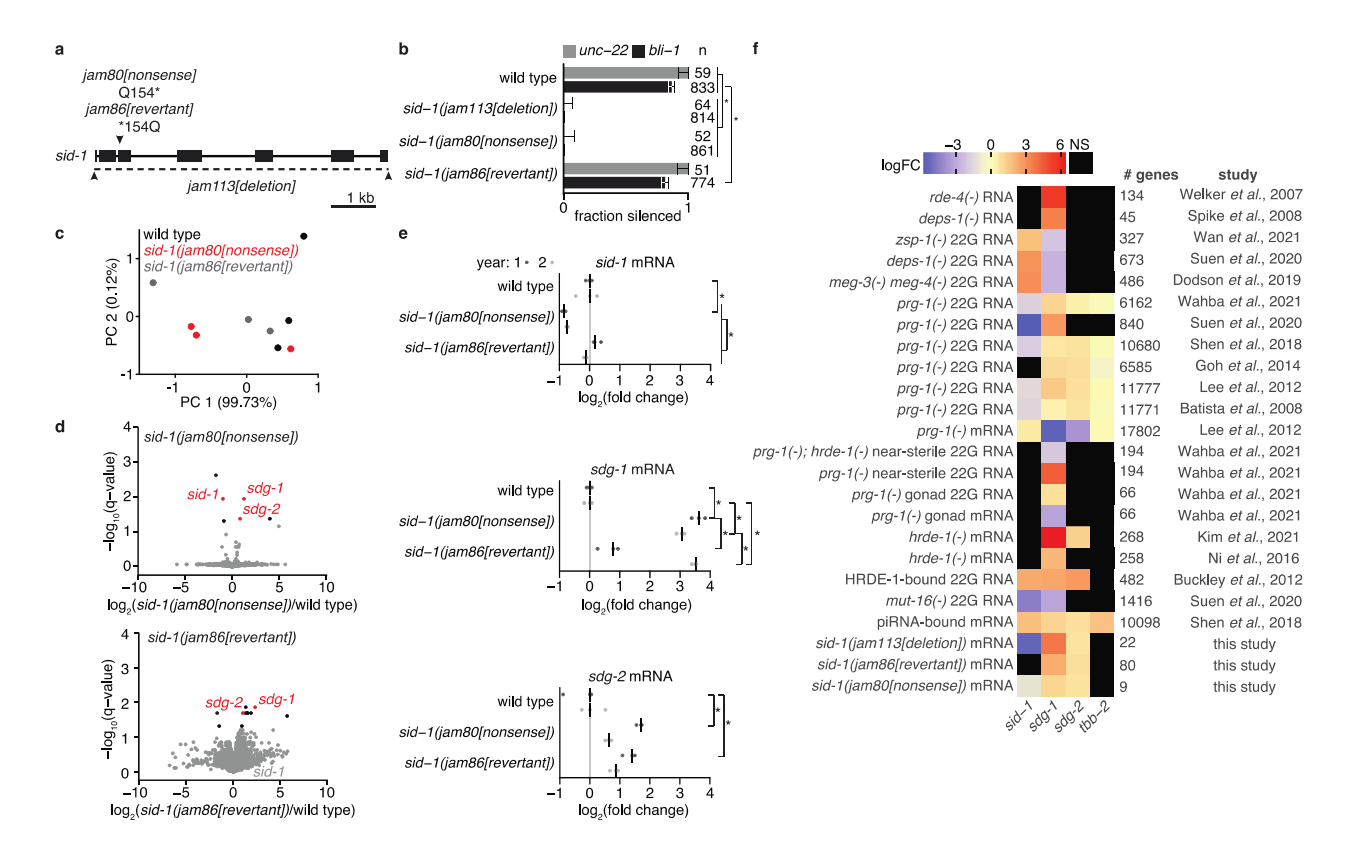
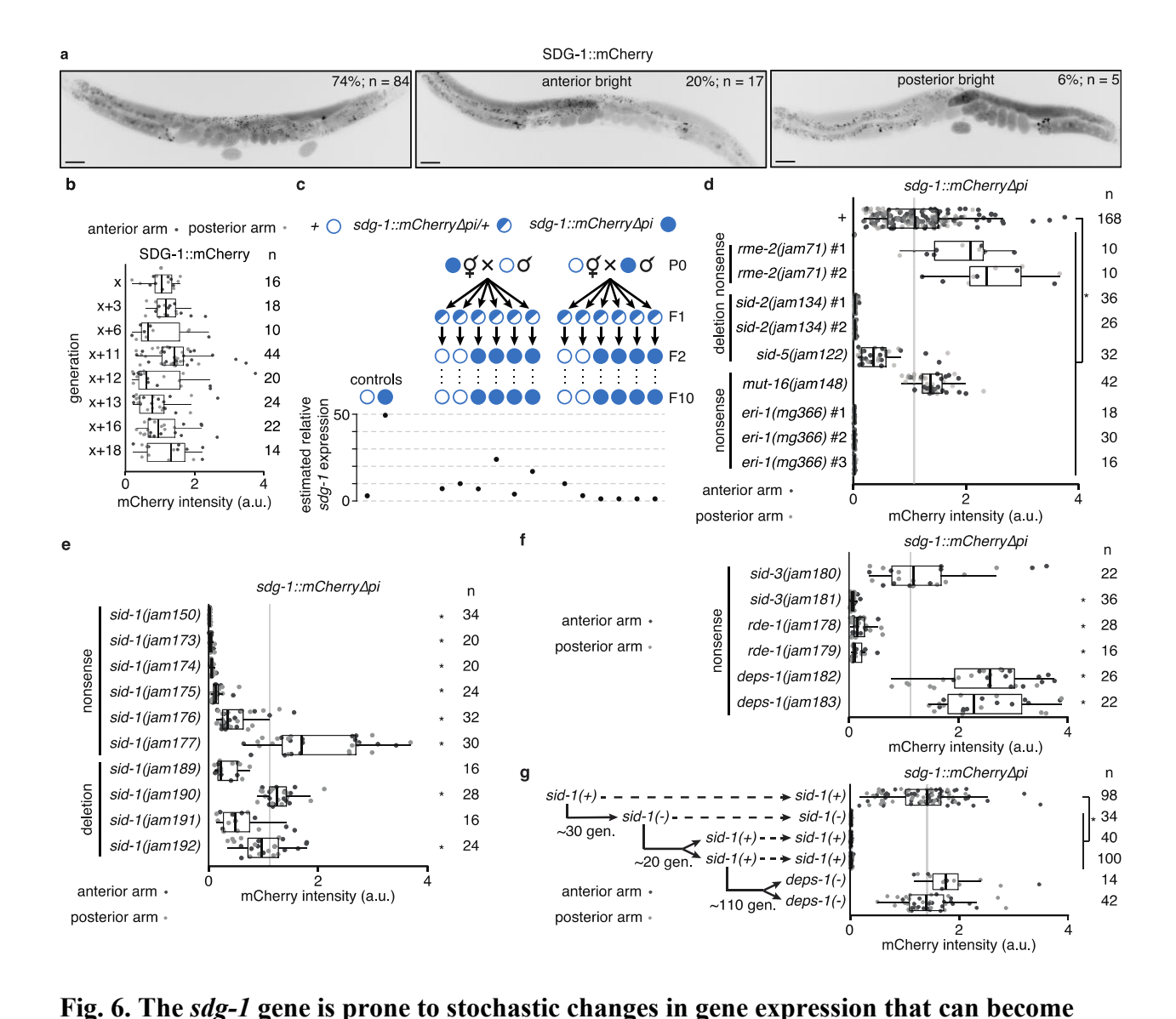


Fig. 5. Ancestral loss of SID-1 causes transgenerational changes in the mRNA levels of two germline genes that are subject to RNA regulation. a, Schematic of modifications at the sid-1 gene generated using Cas9-mediated genome editing. Deletion of the entire coding sequence (jam113[deletion]), a nonsense mutation (jam80[nonsense]), and its reversion to wild-type sequence (jam86[revertant]) are depicted. b, Fractions of animals with the indicated genotypes that show silencing in response to unc-22-dsRNA (grey) or bli-1-dsRNA (black). Numbers of animals scored (n), significant differences using two-tailed test with Wilson's estimates for single proportions (asterisks, P < 0.05 with Bonferroni correction) and 95% CI (error bars) are indicated. c, Principal components explaining the variance between wild type (black), sid-1(jam80[nonsense]) (red), and sid-1(jam86[revertant]) (grey) polyA+ RNA samples. Almost all of the variance between samples is explained by PC 1. d, Volcano plots of changes in the abundance of polyA+ RNA in sid-1(jam80[nonsense]) (top) and sid-1(jam86[revertant])

(bottom) animals compared with wild-type animals (black, q < 0.05; red, both q < 0.05 and change in the same direction in sid-1(jam80[nonsense]) and sid-1(jam113[deletion]); see Extended Data Fig. 7). While sid-1 transcript levels in sid-1(jam86[revertant]) are comparable to that in wild type (grey), sdg-1 (W09B7.2/F07B7.2) and sdg-2 (Y102A5C.36) transcript levels remain elevated in sid-1(jam86[revertant]) (red). e, Levels of spliced sid-1 (top), sdg-1 (middle) and sdg-2 (bottom) transcripts measured using RT-qPCR. The median of three technical replicates is plotted for each of three biological replicates (bar indicates median) assayed before and after 1 year of passaging animals (year 1, dark grey; year 2, light grey). Asterisks indicate P < 0.05 with Bonferroni correction using two-tailed Student's t-test. f, Heatmap showing changes in the levels of transcripts (total RNA or mRNA) or antisense small RNAs (22G RNA) from sid-1, sdg-1, sdg-2, and tbb-2 (abundant germline transcript for comparison). Fold changes (expressed as LogFC, indicating log2 for (m)RNA, log10 for piRNA binding, and log10 for 22G RNA) were deduced by integrating reports (study) of 21 experiments that identify subsets of genes as being subject to RNA-mediated regulation within the germline (# genes). These prior studies include comparisons of RNA or 22G RNA from wild-type animals with that from mutant animals (e.g., mut-16(-) 22G RNA), biochemical detection of piRNA binding to transcripts (piRNA-bound mRNA), and biochemical detection of 22G RNA binding to an Argonaute (HRDE-1-bound 22G RNA). 'NS' indicates cases where changes, if any, were not significant based on the criteria used in the study. A conservative value of 2-fold is assigned to all genes reported as changing >2-fold in ref.<sup>58</sup>.



heritable. a, Representative images showing fluorescence of SDG-1::mCherry (black) in a wild-type background. While most animals showed symmetric expression in the germline (*left*), animals with >2-fold difference in fluorescence between both gonad arms (bright anterior, *middle* and bright posterior, *right*) were also observed. Punctate fluorescence in the intestine likely represents autofluorescence. Scale bar, 50 μm. b, Quantification of SDG-1::mCherry fluorescence intensity (arbitrary units, a.u.) in adult gonad arms (anterior arm, dark grey;

posterior arm, light grey) of  $sdg-1(jam137[mCherry\Delta pi])$  animals starting in one generation (x)

and continuing in successive generations as indicated. Numbers of gonad arms quantified (n) is indicated. Expression in one generation was not significantly different when compared to that in the previous tested generation using Mann-Whitney U test for two-sided comparisons and Bonferroni correction. c, Lineages and estimated relative sdg-1 expression 10 generations after mating wild-type (open circle) males with  $sdg-1::mCherry\Delta pi$  (filled circle) hermaphrodites and vice versa, and isolating sdg-1(+) or sdg-1::mCherry animals from F1 heterozygotes (half-filled circle). Expression of sdg-1 in the F10 generation was measured by RT-qPCR of sdg-1 mRNA purified from pooled wild-type animals of mixed stages or by quantification of SDG-1::mCherry fluorescence in gonad arms of adult  $sdg-1::mCherry\Delta pi$  animals. Relative levels of sdg-1 mRNA and SDG-1::mCherry fluorescence intensity were converted to units of estimated relative sdg-1 expression (see Methods) for comparison. See Extended Data Fig. 9a for raw data. d-f, Fluorescence intensity measurements (quantified as in b) in adult animals with sdg- $1::mCherry\Delta pi$  (+) and additionally with mutations in genes introduced through genetic crosses (in regulators of dsRNA import rme-2, sid-2 or sid-5, or in regulators of RNA silencing mut-16 or eri-1) or through genome editing (in regulators of dsRNA import sid-1 or sid-3, or in regulators of RNA silencing rde-1 or deps-1). Asterisks indicate P < 0.05 with Bonferroni correction using Mann-Whitney U test for two-sided comparisons between animals with sdg- $1::mCherry\Delta pi$  (+) and animals with additional mutations. Nonsense mutations (nonsense) or deletions (deletion) introduced through genetic crosses (isolate numbers #1, #2, etc. in d) or genome editing (different alleles in e and f) and numbers of gonad arms (n) quantified for each isolate are indicated. Mutations in genes required for dsRNA import or subsequent silencing resulted in fewer animals with asymmetric fluorescence between gonad arms (a combined proportion of 21/197 for sid-1, sid-3, rde-1 and deps-1 mutants versus 22/84 for wild type, P =

0.0009 using two-tailed test with Wilson's estimates for single proportions). Animals with at least one gonad arm brighter than the dimmest wild-type gonad arm in **a** and with asymmetric gonad arms were found in different genotypes (anterior bright: sid-1(-) - 5/122, sid-3(-) - 1/29, rde-1(-) - 2/22, deps-1(-) - 4/24, and posterior bright: sid-1(-) - 6/122, rde-1(-) - 2/22, deps-1(-) - 1/24). **g**, Fluorescence intensity measurements as in **b** of animals with  $sdg-1::mCherry\Delta pi$  that show loss of fluorescence when a nonsense mutation is introduced in sid-1 using genome editing  $\sim$ 30 generations (gen.) later remain changed despite reversion of sid-1 nonsense mutation to wild-type sequence after  $\sim$ 20 additional generations. Subsequent mutation of deps-1 after another  $\sim$ 110 generations restored SDG-1::mCherry fluorescence to wild-type levels. Also see Extended Data Fig. 8 and Extended Data Fig. 9.

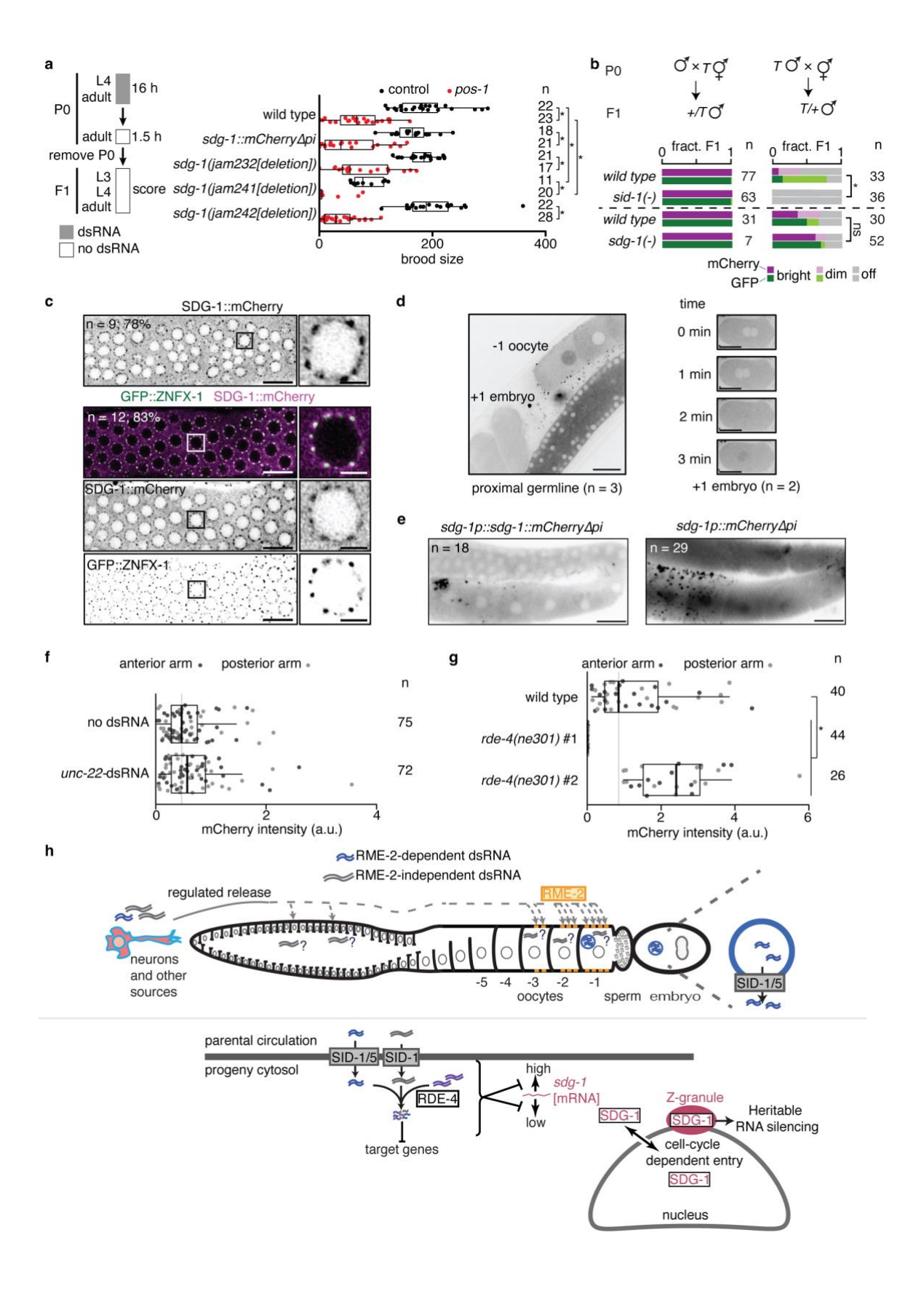


Fig. 7. SID-1 modifies RNA regulation within the germline, potentially through sdg-1 and other sid-1-dependent genes. a, (left) Schematic of assay for sensitive detection of pos-1 silencing by ingested dsRNA. (right) Numbers of developed progeny (> 3<sup>rd</sup> larval stage) laid by wild-type animals, animals with a deletion ( $\Delta$ ) in sdg-1 (jam232, jam241, jam242) or animals with overexpression ( $sdg-1::mCherry\Delta pi$ ) of sdg-1 exposed to pos-1 dsRNA (red) or control dsRNA (black) for 16 hours are plotted. Asterisks indicate P < 0.05 using Mann-Whitney U test for two-sided comparisons with Bonferroni correction. b, Cross progeny males that inherited the mex-5p::mCherry::h2b::gfp::h2b transgene (T)<sup>43</sup> (also used in Fig. 2) from maternal (left) or paternal (right) parents, both of wild-type, sid-1(-), or sdg-1(-) background, were scored for expression of mCherry and GFP (bright, dim, off). Wild-type data for top set (n = 77 and n = 33)are replotted from ref.<sup>43</sup> for comparison. Dashed line separates independent experiments. Asterisk indicates P < 0.05 with Bonferroni correction using  $\chi^2$  test; n.s. indicates not significant. c, Representative AiryScan images of the distal germline (*left*; scale bar, 10 µm) or single germline nuclei (right; scale bar, 2 µm) showing SDG-1::mCherry alone (top) or with GFP::ZNFX-1 (bottom, merge and single channel images). The number of animals imaged (n) and the percentage that show enrichment of SDG-1::mCherry in perinuclear foci are indicated. Sites of SDG-1::mCherry enrichment coincide with GFP::ZNFX-1 localization. Boxes in left mark the nuclei shown in right. d, Representative images showing entry of SDG-1::mCherry into the nucleus in -1 oocytes (*left*) and upon pronuclear fusion in early embryos during the time course indicated (right). Numbers of germlines and embryos imaged are indicated. Scale bars, 20 μm. Also see Extended Data Movies 1-4. e, Representative image of the hermaphrodite germline in animals with a translational (*left*) or transcriptional (*right*) reporter of *sdg-1*. Scale bars, 20 μm. Apparent extracellular punctae of SDG-1::mCherry and mCherry surrounding the proximal

germline requires further study, but could be non-specific because similar localization is observed in animals with other promoters driving mCherry expression, but not GFP expression, in the germline (data not shown). The numbers of animals with the depicted fluorescence pattern are indicated. **f** and **g**, Response of the transcriptional sdg-1 reporter ( $sdg-1p::mCherry\Delta pi[sdg-1(\Delta)]::sdg-1 3' UTR$ ) to the addition of unc-22-dsRNA (**f**) or loss of rde-4 (**g**). Quantification and asterisk are as in Fig. 6. **h**, Models for dsRNA import into the germline (top) and subsequent RNA-mediated regulation of sdg-1 (bottom). See text for details.

#### SUPPLEMENTAL MATERIAL

# Intergenerational transport of double-stranded RNA limits heritable epigenetic changes

**Authors:** Nathan Shugarts<sup>1</sup>, Aishwarya Sathya<sup>1</sup>, Andrew L. Yi<sup>1</sup>, Winnie M. Chan<sup>1</sup>, Julia A. Marré<sup>1</sup>, and Antony M. Jose<sup>1\*</sup>

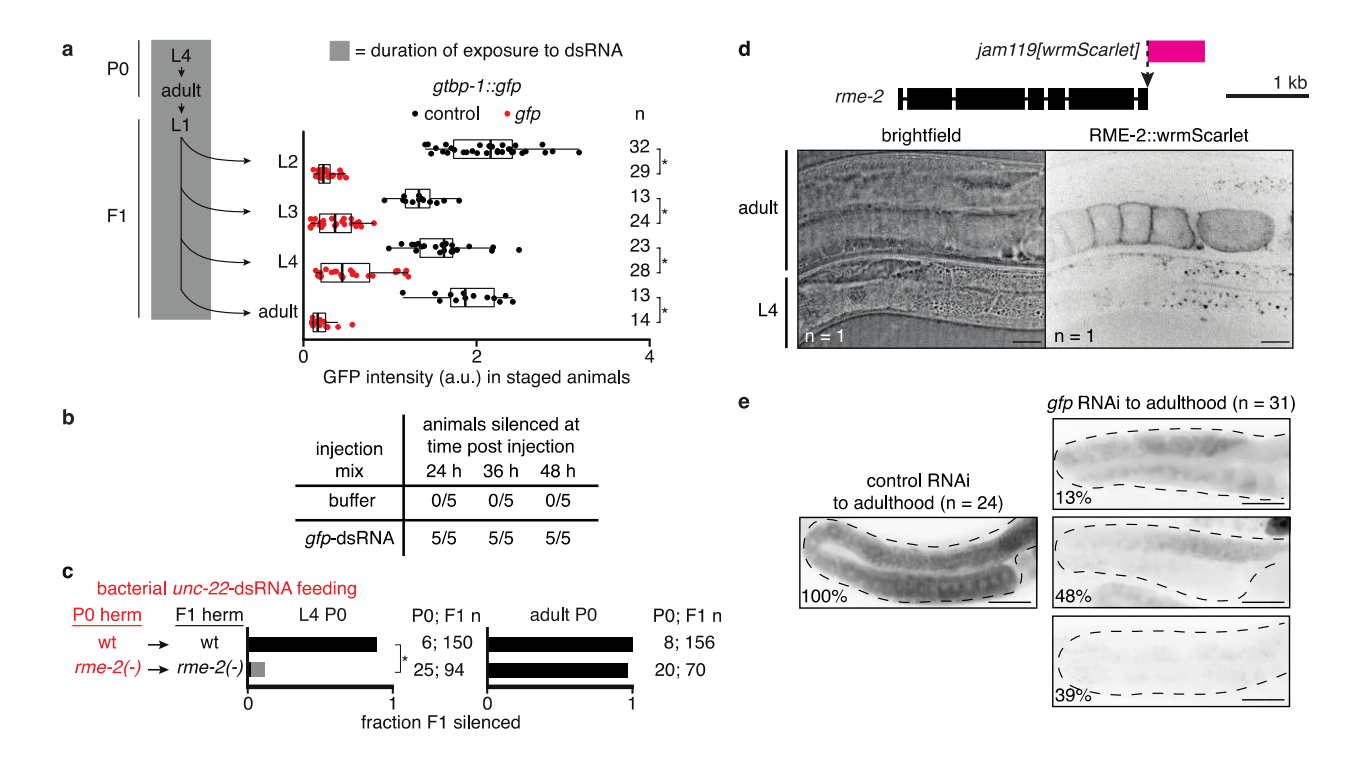
### **Affiliations:**

<sup>1</sup>Department of Cell Biology and Molecular Genetics, University of Maryland, College Park, MD 20742, USA.

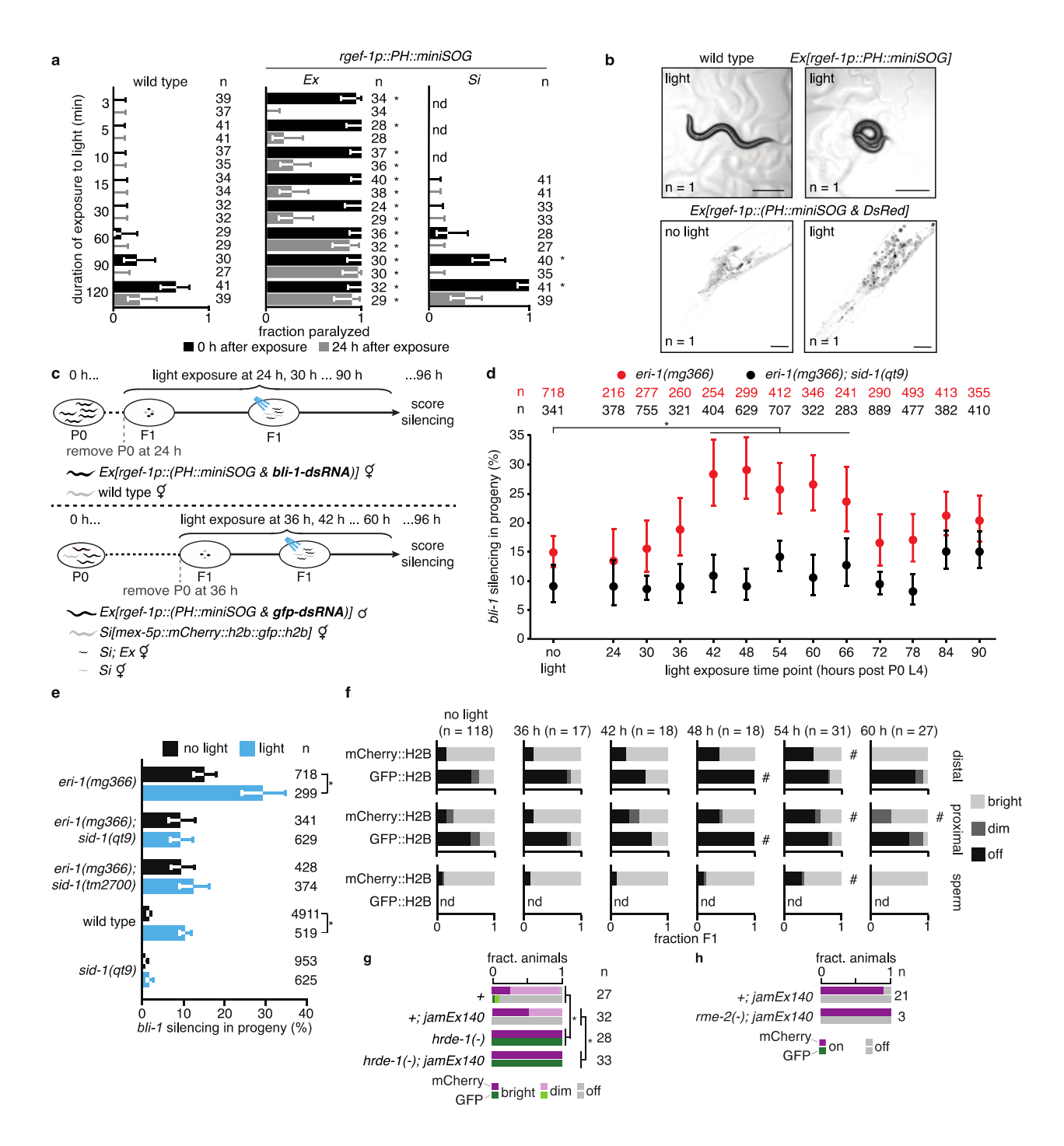
\*Correspondence to: amjose@umd.edu

### Contents:

- 10 Extended Data Figures and Figure Legends
- 4 Extended Data Movie Legends
- 4 Extended Data Tables

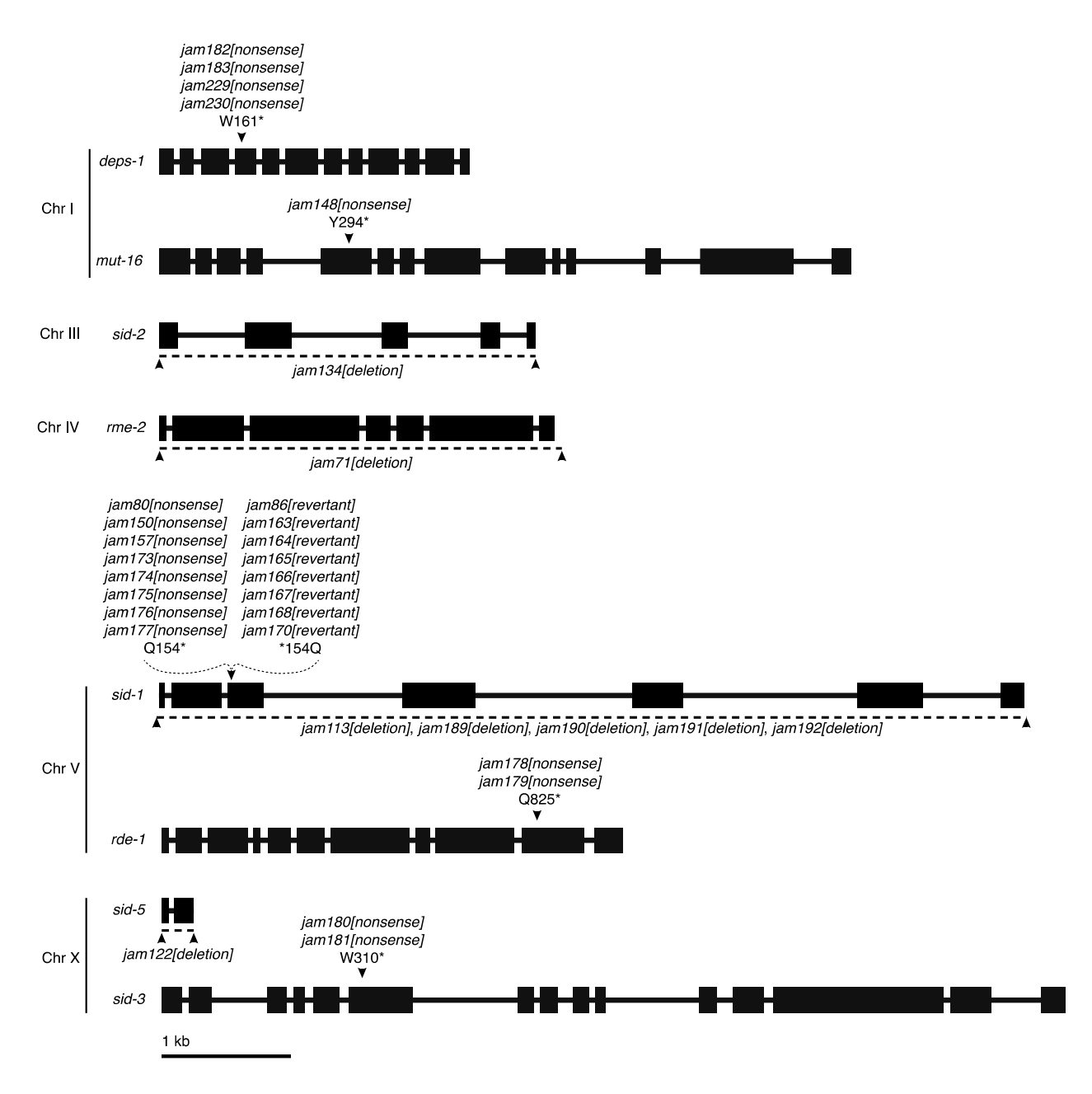


Extended Data Fig. 1. Uptake of dsRNA into the proximal germline by RME-2 is required for silencing during early adulthood. a, (left) Schematic depicting continuous exposure of gtbp-1::gfp P0 animals, starting at the L4 stage, and their F1 progeny to bacteria expressing dsRNA, followed by imaging of animals at the indicated stages. (right) Quantification of GTBP-1::GFP intensity (arbitrary units, a.u.) in representative germ cells (larvae) or embryos in utero (adults) of F1 animals at indicated stages after P0 and F1 exposure to control (dark grey) or gfpdsRNA (red). Numbers of animals scored at each stage (n) are indicated. Asterisks indicate *P* < 0.05 with Bonferroni correction using Mann-Whitney U test for two-sided comparisons between animals exposed to L4440 or gfp-dsRNA. b, Silencing of gtbp-1::gfp in germlines injected with duplex buffer (buffer) or in vitro transcribed gfp-dsRNA in duplex buffer during the first day of adulthood and scored for silencing 24, 36 and 48 h post injection. The numbers of animals out of 5 injected with each injection mix that exhibited silencing of both gonad arms are indicated for each time point. Animals injected with buffer never exhibited silencing in either gonad arm. c, Hermaphrodite animals of the L4 stage (left) or young adult stage (24 hour post L4, right) of the indicated genotypes were fed *unc-22*-dsRNA expressed in bacteria for 24 hours (red). Hermaphrodite self-progeny of fed animals were scored for *unc-22* silencing (strong, black; weak, grey). Numbers of fed P0 parents and scored F1 progeny (P0; F1 n) are as indicated. Asterisk indicates P < 0.05 with Bonferroni correction using  $\chi^2$  test. Previously generated rme-2(-) animals were used in this assay (DH1390). d, Expression of RME-2. (top) Schematic showing insertion of wrmScarlet (rme-2(jam119/wrmScarlet])) at the rme-2 locus. Scale bar, 1 kb. (bottom) Brightfield and fluorescence images of a rme-2(jam119[wrmScarlet]) L4-stage and adult animal (n = 1 confocal plane). Scale bars, 20 µm. e, Representative fluorescence images of GTBP-1::GFP (black) in the germlines (dashed outline) of day 3 gtbp-1::gfp adult animals after P0 and F1 ingestion of control dsRNA (*left*) or *gfp*-dsRNA (*right*) up to the first day of adulthood. Numbers of animals imaged (n) and the percentages of animals exhibiting the depicted expression patterns are shown. Scale bars, 50 µm.

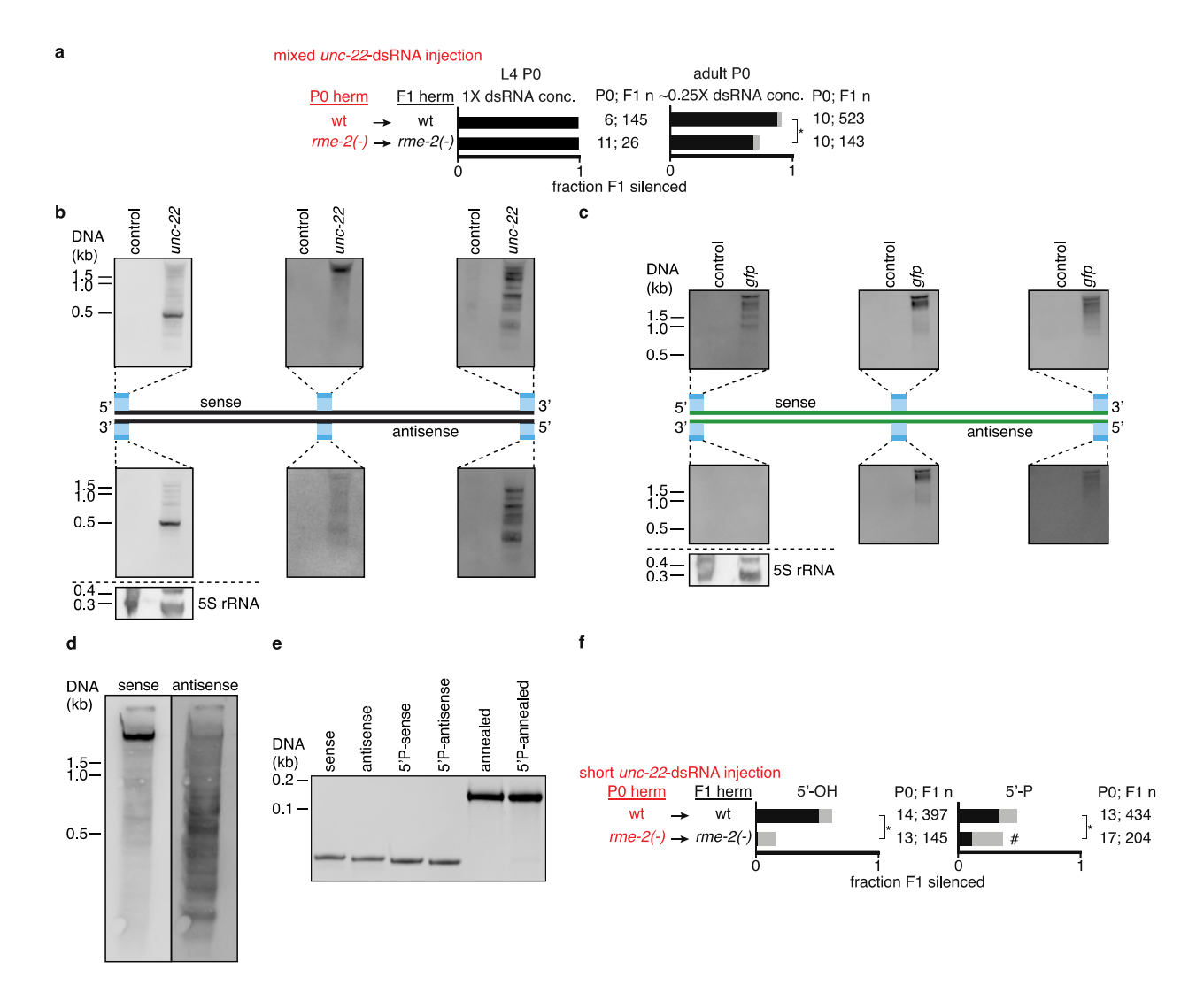


Extended Data Fig. 2. Timed release of neuronal dsRNA by oxidative damage in neurons reveals period of enhanced gene silencing in the soma and germline. a, Wild-type animals (left) and animals expressing membrane-tethered mini singlet oxygen generator protein (PH::miniSOG) from an extrachromosomal array (Ex, middle) or a single-copy transgene (Si, right) under a pan-neuronal promoter (rgef-1p) were exposed to blue light for different durations (minutes) and animals were scored for paralysis immediately after exposure (0 h, black) and 24 hours later (24 h, grey). b, Functional and anatomical evidence for oxidative damage in neurons. (top) Widefield images of animals without (left) and with (right) Ex[rgef-1p::PH::miniSOG]

after 5 minutes of blue light exposure. Animals paralyzed in a often appear coiled (right), likely indicative of a defect in neuronal signaling. Scale bar, 100 µm. (bottom) Confocal fluorescence images of neurons in the head region of animals with Ex[rgef-1p::(PH::miniSOG & DsRed)] without (*left*) and with (*right*) 30 minutes of blue light exposure showing light-induced changes (black, DsRed fluorescence). Scale bar, 20 μm. c, Schematic of assay for measuring the impact of oxidative damage in neurons at different times during development on silencing by neuronal dsRNA. For measuring silencing in the hypodermis (top) or germline (bottom), cohorts of animals with Ex[rgef-1p::(PH::miniSOG & bli-1-dsRNA)] (top), or Ex[rgef-1p::(PH::miniSOG & gfp-dsRNA)] obtained by mating males with the array and hermaphrodites with Si[mex-5p::mCherry::h2b::gfp::h2b] (bottom) were exposed to blue light as indicated and scored for bli-*I* silencing (top) or imaged (bottom) as stage-matched adults (at ~96 hours after the fourth larval stage of parent animals). d, Percentages of eri-1(mg366) (red) or eri-1(mg366); sid-1(qt9) (black) animals silenced when assayed as described in c, top. Silencing in the absence of exposure to blue light (no light) was also measured for comparison. e, Percentages of stagematched animals of the indicated genetic backgrounds with Ex/rgef-1p::(PH::miniSOG & bli-1dsRNA)] that show bli-1 silencing without (black) or with (blue) a 1-hour exposure to blue light 48 hours after the fourth larval stage of parent animals. The 48 hr time point from d is replotted to facilitate comparison. f, Fractions of animals exhibiting bright (light grey), dim (dark grey) or not detectable (black) mCherry::H2B or GFP::H2B fluorescence in the distal gonad (top), proximal gonad (middle) or sperm (bottom) when assayed as described in c, bottom. Silencing in the absence of exposure to blue light (no light) was used as the reference. Numbers of animals scored (n), measurements that were not done (nd), significant differences using two-tailed Wilson's estimates for single proportion compared to wild type (asterisks in a) or no light condition (asterisks in **d** and **e**) or  $\chi^2$  test compared to no light condition (hashes in **f**; P < 0.05with Bonferroni correction), and error bars (95% CI) are indicated. g and h, Animals homozygous (g) or hemizygous (h) for the mex-5p::mCherry::h2b::gfp::h2b transgene (Fig. 2) with or without neuronal gfp-dsRNA (jamEx140) were scored for expression of mCherry and GFP (bright, dim, off) in otherwise wild-type (+), hrde-1(-) (g) or rme-2(-) (h) backgrounds. Animals in g also have a dpy-2(e8) mutation linked to the mex-5p::mCherry::h2b::gfp::h2b transgene. Fraction silenced in wild type animals (+) in  $\mathbf{g}$  were calculated with n = 31 for GFP and n = 27 for mCherry. Asterisks indicates P < 0.05 using  $\chi^2$  test with Bonferroni correction.



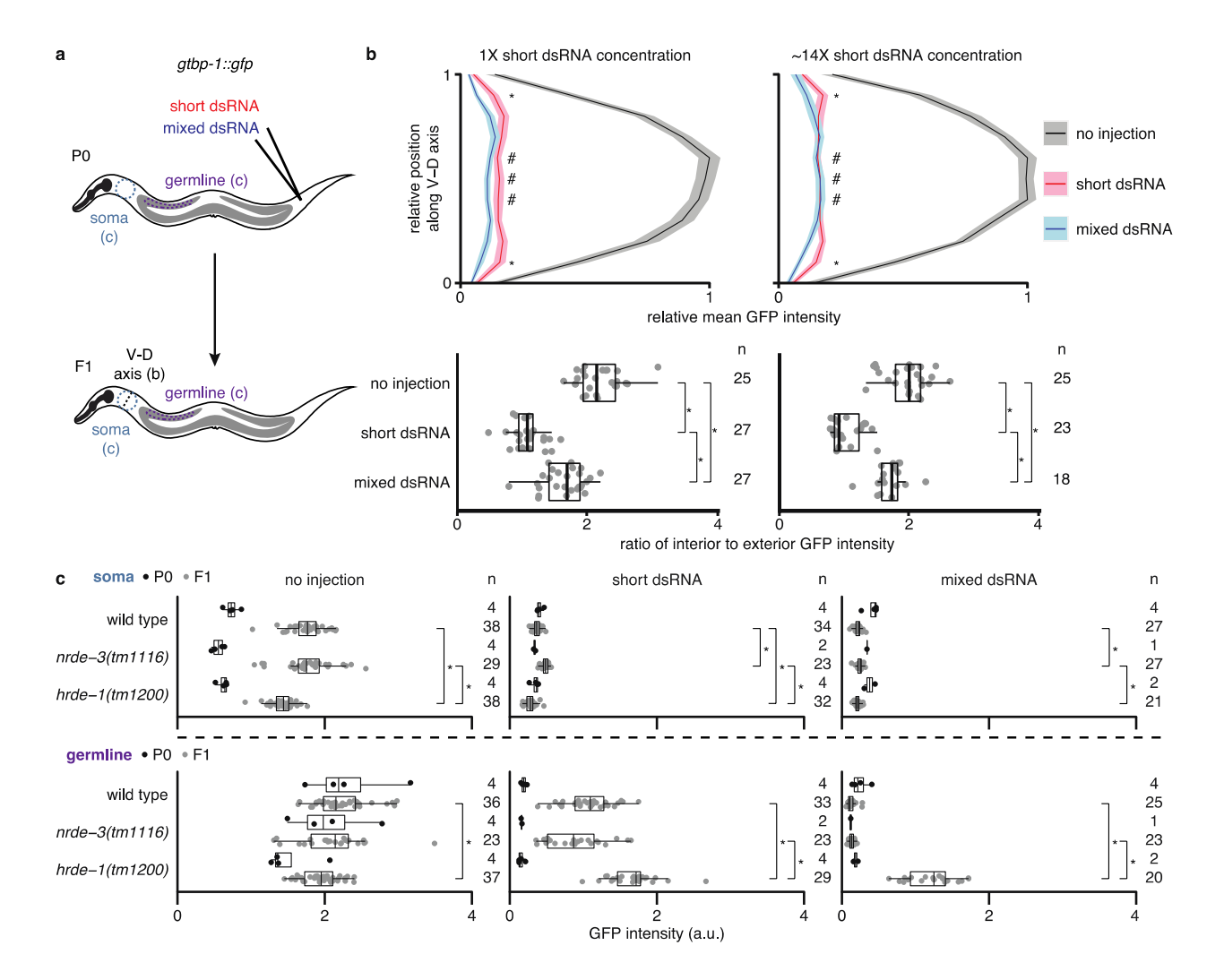
Extended Data Fig. 3. Schematics depicting mutations generated in this study. Structures (boxes, exons; lines, introns) and chromosomal locations of genes with mutations generated using Cas9-mediated genome editing. Nonsense mutations (e.g., jam182[nonsense]) with associated amino acid changes (e.g., W161\* for tryptophan at position 161 to stop) are indicated with black arrowheads and deletions of coding regions (e.g., jam134[deletion]) are indicated with a dashed line (deleted region) and flanking black arrowheads. Scale bar, 1 kb.



## Extended Data Fig. 4. Requirement of RME-2 for silencing in progeny by dsRNA injected into parents depends on concentration, length, and 5' modification of dsRNA. a,

Hermaphrodite animals of indicated genotypes were injected in the body cavity with *unc-22*-dsRNA (red font) and uninjected F1 progeny were scored for *unc-22* silencing (strong, black; weak, grey). Numbers of injected P0 parents and scored F1 progeny (P0; F1 n) are as indicated.. (*left*) L4-staged hermaphrodites were injected with transcribed *unc-22*-dsRNA at the same concentration as in Fig. 3a (1X). (*right*) Young adult-staged hermaphrodites were injected with transcribed *unc-22*-dsRNA at ~0.25X of concentration in Fig. 3a. **b** and **c**, Northern blots of bacterial *unc-22*-dsRNA (*unc-22*, **b**) or *gfp*-dsRNA (*gfp*, **c**) separated alongside empty vector control RNA using fully-denaturing formaldehyde polyacrylamide gel electrophoresis (FDF-PAGE)<sup>102</sup>. 40-nt digoxigenin (DIG)-labeled oligonucleotides (in blue) were used to probe the 5' end, middle and 3' end of the sense (*top*) and antisense (*bottom*) strands of the *unc-22* (**b**) and *gfp* (**c**) sequences present in the bacterial vectors. A 1-kb DNA ladder was used as a size reference and 5S rRNA was probed as a control for equal loading of total RNA. **d**, Northern blot of *unc-22*-dsRNA transcribed from a ~1.1-kb template, separated using FDF-PAGE as in **b** and **c**, and probed using 40-nt DIG-labeled oligonucleotides complementary to the sense (*left*) or antisense (*right*) strands of the *unc-22* gene. **e**, Polyacrylamide gel stained with ethidium

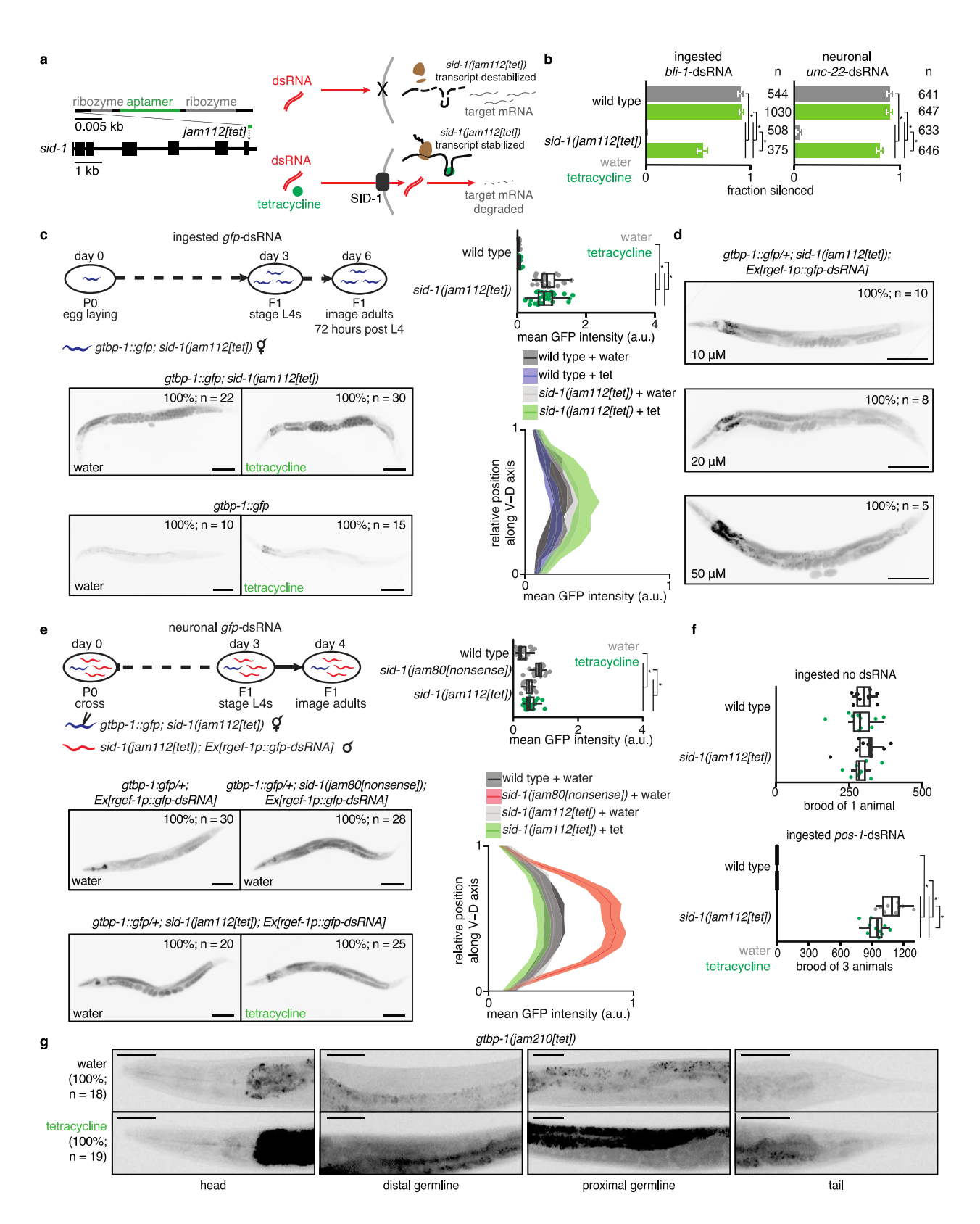
bromide showing 50-nt single-stranded (sense, antisense, 5'P-sense, 5'P-antisense) and 50-bp double-stranded unc-22-RNA (annealed, 5'P-annealed). A 100-bp DNA ladder was run alongside for rough size estimation. 5'-phosphate (5'P) was added using a polynucleotide kinase.  $\mathbf{f}$ , Young adult-staged hermaphrodites were injected in the body cavity with short unc-22-dsRNA with 5'-OH (left) or with 5'-phosphate added using a polynucleotide kinase (right) and self-progeny were scored as in  $\mathbf{a}$ . Newly generated rme-2(-) animals (AMJ1131) were used in  $\mathbf{a}$  and  $\mathbf{f}$ . Comparisons with P < 0.05 after Bonferroni correction using  $\chi^2$  test between genotypes within conditions (asterisks in  $\mathbf{a}$  and  $\mathbf{f}$ ) or between conditions in rme-2(-) animals (hash in  $\mathbf{f}$ ) are indicated.



Extended Data Fig. 5. Extent of silencing in progeny by short or mixed dsRNA injected into parental circulation varies between tissues, but has similar nuclear Argonaute

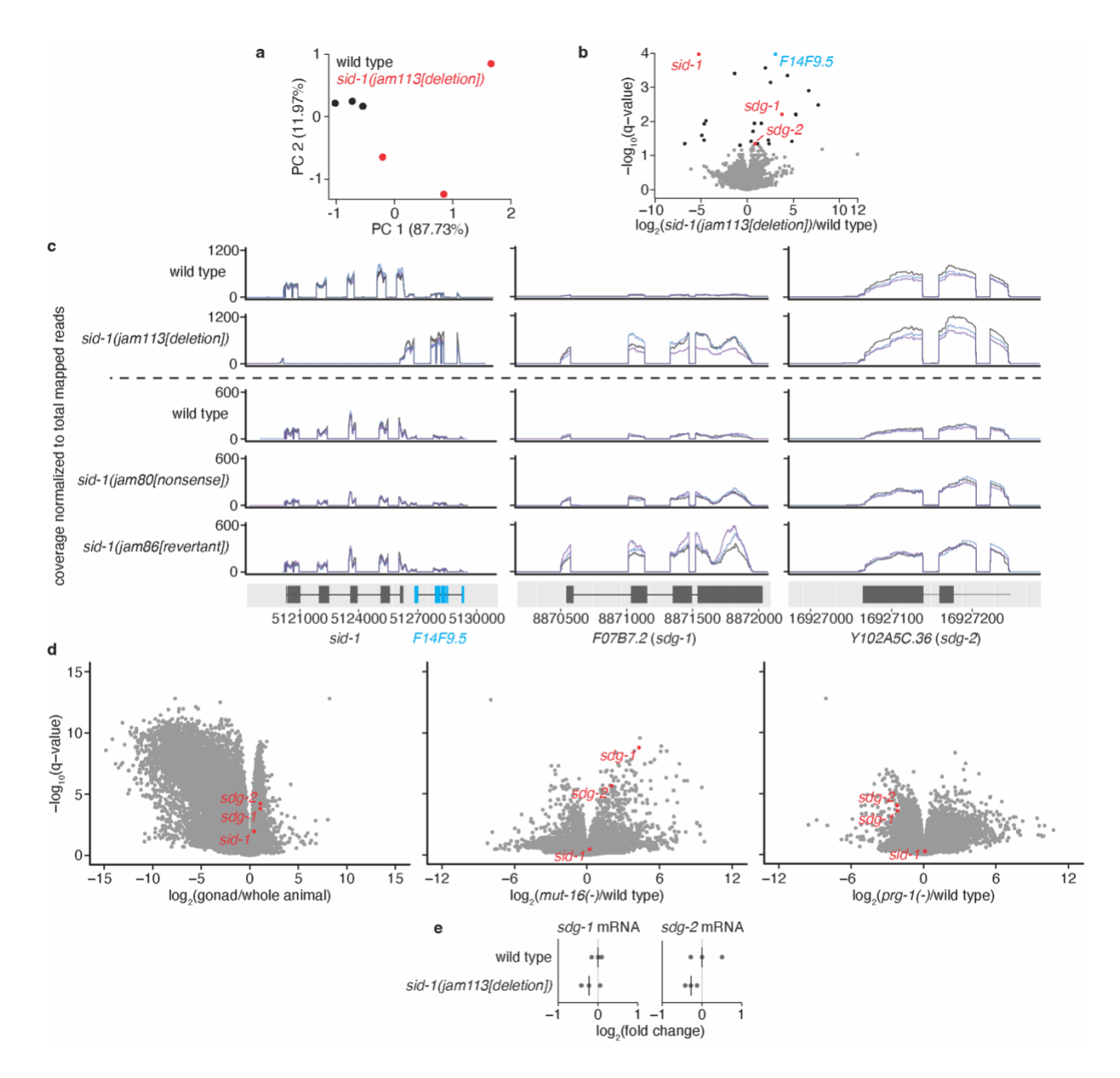
requirements. a to c, GTBP-1::GFP fluorescence from the ubiquitously expressed gene gtbp-1::gfp in the F1 progeny of uninjected P0 animals (no injection) or of P0 animals injected into the body cavity with synthetic 50-bp gfp-dsRNA (short dsRNA) or gfp-dsRNA transcribed from a ~730-bp DNA template (mixed dsRNA) was analyzed. The expression of gtbp-1::gfp is dimmer in P0 animals (imaged as adults) than in F1 animals (imaged as L4s) because of developmental variation in the expression – therefore comparisons are only appropriate during the same generation and not across generations. a, Schematic illustrating injection site and scoring scheme. For the soma, a region between the pharynx and anterior gonad arm within a circle (blue, data in c) or along a ventral to dorsal (V-D) axis (black, data in b) was quantified. For the germline, a gonadal region that excluded the intestine (purple, data in c) was quantified. b, Quantification of F1 progeny after injection of two different concentrations of short dsRNA (1X, 350 ng/µl, left; ~14X, 4977 ng/µl, right) into the body cavity of P0 animals. (top) The relative mean intensity profile of fluorescence along the V-D axis for progeny of uninjected animals (black), animals injected with short dsRNA (red), or animals injected with mixed dsRNA (blue). Shaded bands indicate 95% CI. (bottom) Ratios of mean intensities within interior points (hashes in top) to those of the exterior points (asterisks in top) are depicted for each

imaged animal. **c**, Quantification of P0 (black) and F1 (grey) wild-type, nrde-3(tm1116) or hrde-1(tm1200) animals. Regions within the soma and the germline were quantified as indicated in **a**. The numbers of P0 and F1 animals quantified (P0; F1 n) are indicated. For each genotype, F1 progeny after no injection, short dsRNA injection, or mixed dsRNA injection into P0 animals showed significantly different fluorescence values from each other (P < 0.05 after Bonferroni correction using Mann-Whitney U test for two-sided comparisons). Similarly significant differences between treatments across genotypes are indicated (asterisks).



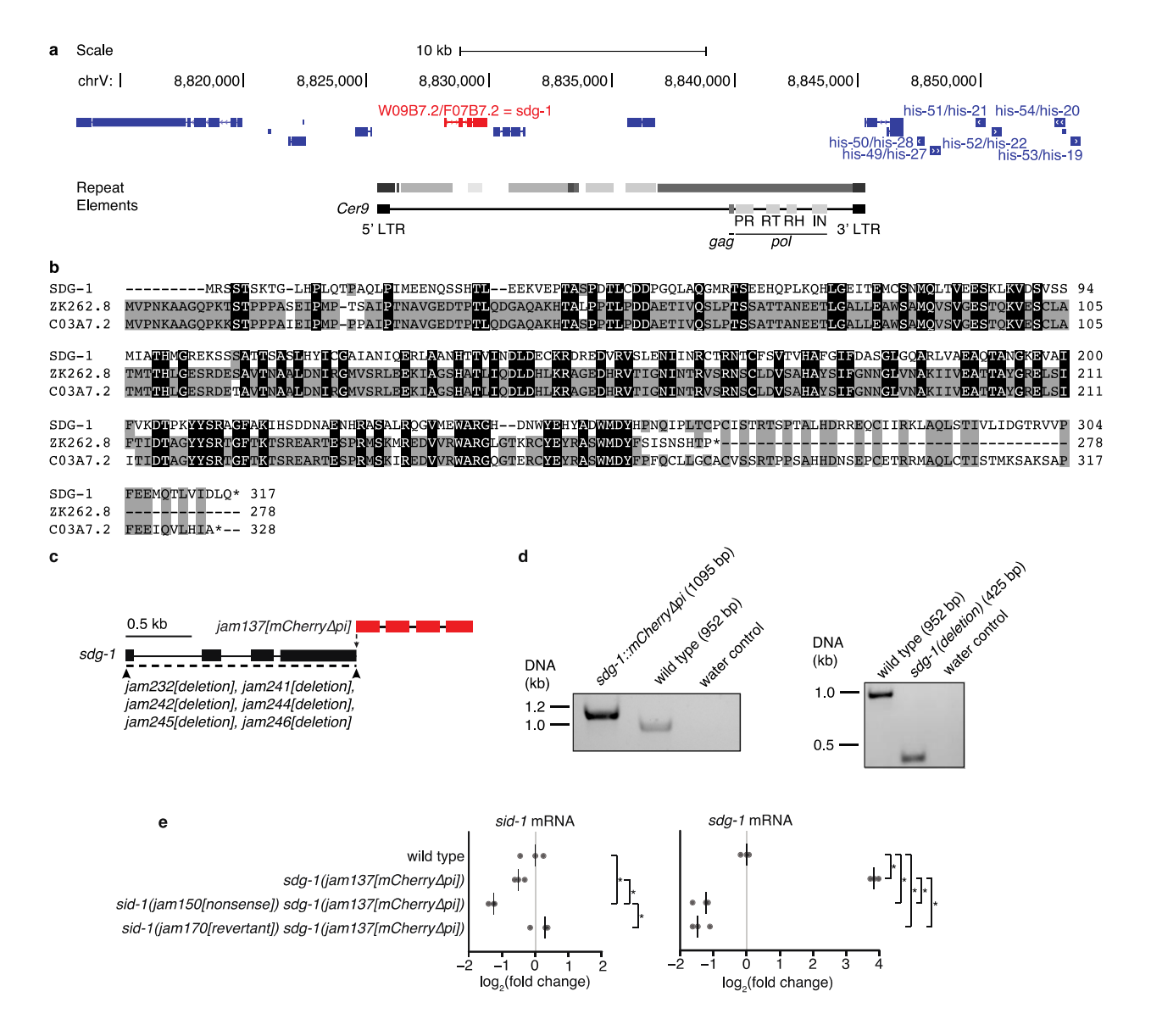
Extended Data Fig. 6. Tetracycline-induced functional rescue of *sid-1* expression is evident in somatic tissues but not within the germline. a, Schematic illustrating a cell expressing *sid-1* 

transcript with a tetracycline aptazyme<sup>44</sup> inserted into the *sid-1* 3'UTR (*left*) in the presence (bottom right) or absence (top right) of tetracycline. Tetracycline stabilizes sid-1 transcripts by inhibiting ribozyme-based cleavage in the 3'UTR and thereby allows for the expression of SID-1 protein and dsRNA import. **b**, Fraction of wild-type or *sid-1(jam112[tet])* animals silenced after ingestion of bli-1-dsRNA (left) or expression of neuronal unc-22-dsRNA (right) in the presence of water (grey bars) or 10 µM tetracycline (green bars). Numbers of animals scored for silencing (n) are depicted. c, The extent of gfp silencing in gtbp-1::gfp; sid-1(jam112[tet]) day 3 adult animals after ingestion of gfp-dsRNA in the presence of water or 10 µM tetracycline. A schematic illustrating the experimental design (top left), representative images of animals from each condition with numbers of animals imaged (n) and percentages of animals represented (bottom left), and quantification of representative germline (top right) and somatic (bottom right) GTBP-1::GFP intensity (a.u.) are depicted. Mean germline GFP intensity was measured in representative regions of the posterior germline and somatic GFP intensity was measured along a dorsal to ventral axis in the tail region (shaded region represents 95% CI) to avoid increased autofluorescence in the intestines of animals exposed to tetracycline. Scale bars, 100 µm. d, Representative images of gtbp-1::gfp; sid-1[jam112[tet]) F1 day 1 adult animals after P0 and F1 ingestion of gfp-dsRNA until day 1 of F1 adulthood in the presence of different concentrations of tetracycline (10 µM, 20 µM, 50 µM). Higher concentrations of tetracycline did not enhance silencing in gtbp-1::gfp; sid-1(jam112[tet]) animals. Scale bars, 100 μm. e, The extent of gfp silencing in cross progeny of gtbp-1::gfp; sid-1(jam112[tet]) hermaphrodites injected with water or 10 μM tetracycline and sid-1(jam112[tet]); Ex[rgef-1p::gfp-dsRNA] males in the presence of water or 10 µM tetracycline. A schematic illustrating the experimental design including injection of gtbp-1::gfp; sid-1(jam112[tet]) hermaphrodites with water or 10 µM tetracycline (top left), representative images of animals with the Ex[rgef-1p::gfp-dsRNA] array from each condition with numbers of animals imaged (n) and percentages of animals represented (bottom left), and quantification of representative germline (top right) and somatic (bottom right) GFP intensity (a.u.) as in c are depicted. Scale bars, 100 μm. f, Total brood of wild-type or sid-1(jam112[tet]) animals after culturing on OP50 E. coli or pos-1-dsRNA bacteria in the presence of water or 10 μM tetracycline. Silencing by pos-1-dsRNA typically results in inviable embryos (wild type, bottom), but culturing sid-1(jam112[tet]) with 10 µM tetracycline and pos-1-dsRNA only resulted in a minor decrease in brood size (sid-1(jam112[tet]), bottom). This decrease was not observed when sid-1(jam112[tet]) animals were cultured on 10 μM tetracycline plates in the absence of pos-1-dsRNA (top, broad of 1 animal; bottom, broad of 3 animals). g, Representative fluorescence images of GTBP-1::GFP (black) in the heads, distal germlines, proximal germlines, and tails of gtbp-1::gfp animals with a tetracycline-aptazyme sequence inserted into the gtbp-1::gfp 3'UTR (gtbp-1(jam210[tet])) after culturing with water or 10 µM tetracycline. The numbers of animals imaged (n) and the percentages of animals with the represented expression patterns are depicted. An increase in GTBP-1::GFP intensity was observed in the soma and germline, but increased fluorescence in the intestine cannot be distinguished from increased autofluorescence caused by culturing with 10 µM tetracycline. Scale bars, 50 µm.



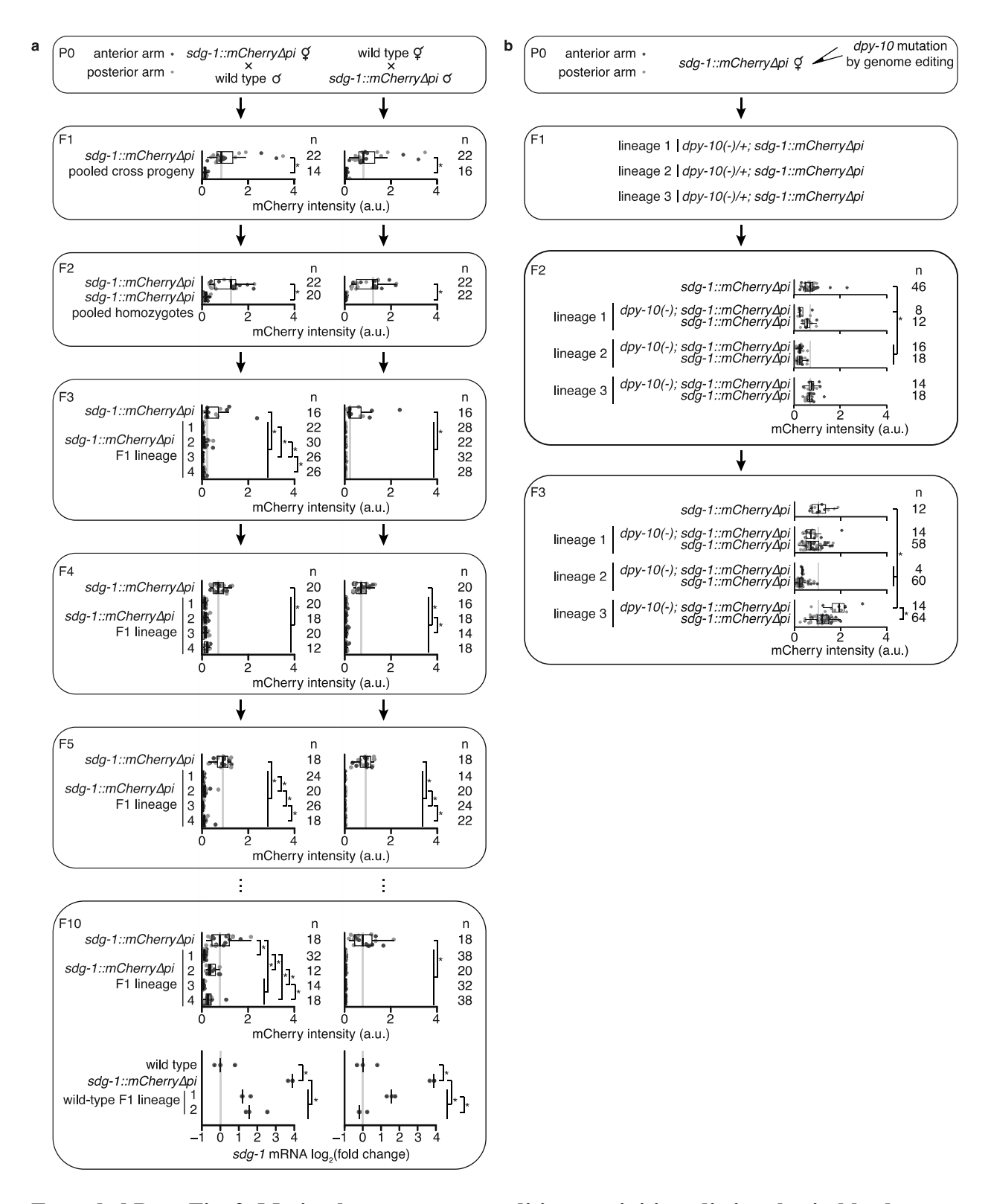
Extended Data Fig. 7. Selective disruption of *sid-1* followed by restoration to wild type reveals two *sid-1*-dependent transcripts expressed in the germline that show heritable change. a, Principal components explaining the variance between wild type (black) and *sid-1(jam113[deletion])* (red) animals. b, Volcano plots of changes in the abundance of polyA+RNA in *sid-1(jam113[deletion])* animals compared with wild-type animals (black, *q* < 0.05; red, *q* < 0.05 and with change in the same direction in *sid-1(jam80[nonsense])*; see Fig. 5d, *top*). c, Read coverage in biological triplicate (black, blue and purple) at *sid-1* and *F14F9.5* (*left*), *W09B7.2/F07B7.2* (*sdg-1*) (represented by *F07B7.2* locus, *middle*) and *Y102A5C.36* (*sdg-2*) (*right*) of polyA+RNA in wild-type and *sid-1(jam113[deletion])* animals (*top*), and in wild-type, *sid-1(jam80[nonsense])*, and *sid-1(jam86[revertant])* animals (*bottom*) normalized to total mapped reads per sample. Deletion of *sid-1* coding sequence caused accumulation of transcripts from *F14F9.5* (blue), requiring point mutation (*jam80[nonsense]*) for selective disruption of *sid-1* (see Fig. 5). d, Volcano plots of changes in the abundance of RNA in wild-type gonads vs.

whole animals (*left*), mut-16(-) vs. wild-type animals (middle), and prg-1(-) vs. wild-type animals (right) using data from ref.<sup>47</sup>. sdg-1, sdg-2 and sid-1 transcripts are highlighted (red). **e**, Levels of spliced sdg-1 and sdg-2 transcripts in animals of the indicated genotypes measured using RT-qPCR. The median (line) of three technical replicates is plotted for each of three biological replicates. P > 0.05 with Bonferroni correction using two-tailed Student's t-test for wild type to mutant comparisons. Levels of sid-1 transcripts were not detectable in sid-1 (jam113[deletion]) animals due to absence of sid-1 coding sequence (data not shown).



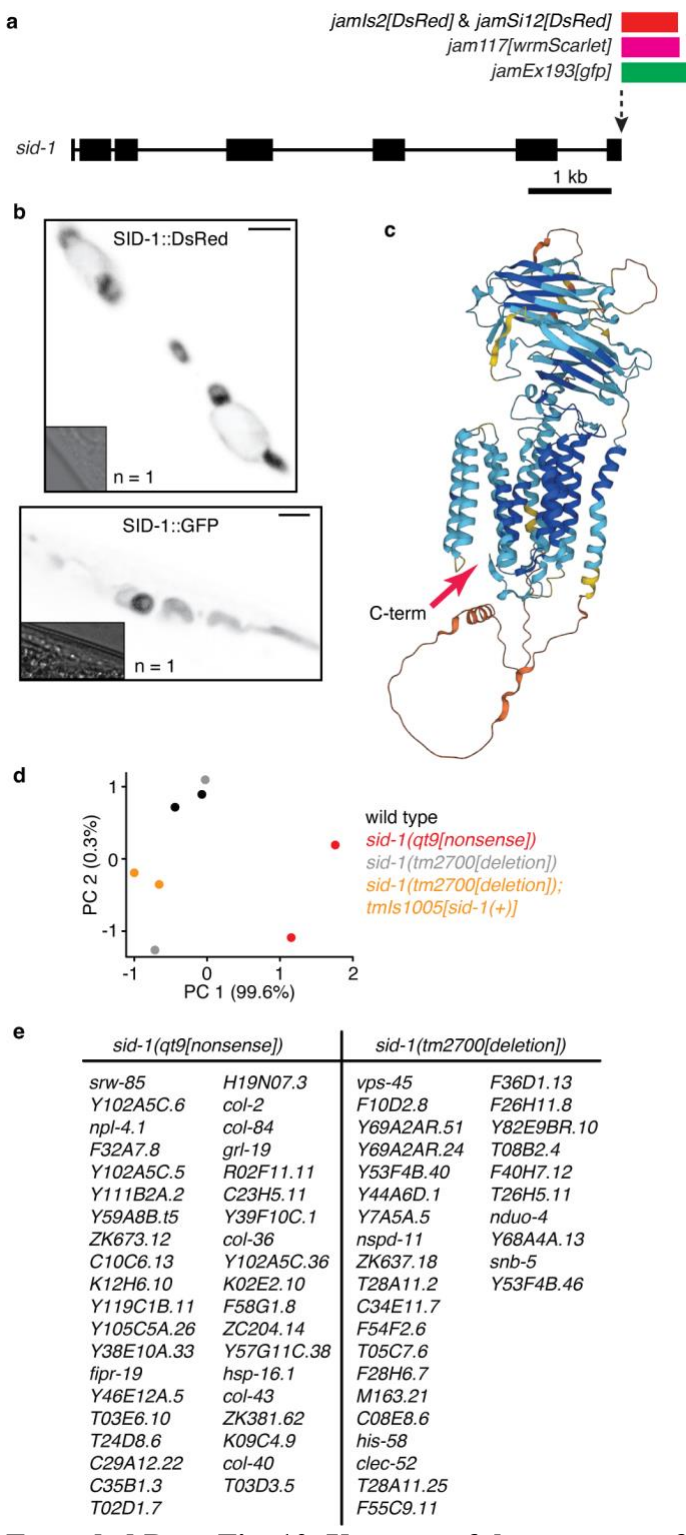
Extended Data Fig. 8. The *sid-1*-dependent gene *sdg-1* is expressed from two identical loci (*W09B7.2/F07B7.2*) and loss of its expression in *sid-1(nonsense)* animals fails to recover in *sid-1(revertant)* animals. a, Schematic adapted from UCSC Genome Browser depicting *W09B7.2/F07B7.2* (red) located within a repeated ~40-kb locus on chromosome V (8813207-8854700 depicted; duplicate locus at 8855302-8896495) that includes many histone genes (dark blue; duplicate genes also depicted). *W09B7.2/F07B7.2* are located within full-length *Cer9* retrotransposons with repeated regions in grey (darker color indicates fewer repeat element-associated mismatches/insertions/deletions). Loci encoding *gag* and *pol* elements (PR: protease, RT: reverse transcriptase, RH: RNaseH, IN: integrase) within *Cer9* are depicted. b, Alignment of the SDG-1 protein sequence encoded by *W09B7.2/F07B7.2* to the paralogs ZK262.8 and C03A7.2 with conserved residues between two (grey) or three (black) proteins highlighted. c, Schematic depicting insertion of *mCherry* sequence that lacks piRNA binding sites<sup>42,43</sup> at the 3' end of *sdg-1(jam137[mCherryΔpi]*), as well as deletion of the *sdg-1* coding sequence (*jam232*, *jam241*, *jam244*, *jam245*, and *jam246*). d, Genotyping gels showing insertion of *mCherryΔpi* sequences (1095 bp) (*left*) or deletion of *sdg-1* coding sequences (425 bp) (*right*) at

both loci of sdg-1. Absence of wild-type bands in either case confirm genome editing of both copies. **e**, Levels of spliced sid-1 (left) and sdg-1 (right) transcripts in wild-type animals and sdg-1 ( $jam137[mCherry\Delta pi]$ ) animals with a wild-type (+), sid-1(jam150[nonsense]) or sid-1(jam169[revertant]) background measured using RT-qPCR. The median of three technical replicates is plotted for each of three biological replicates (bar indicates median). Asterisks indicate P < 0.05 with Bonferroni correction using two-tailed Student's t-test.



Extended Data Fig. 9. Mating but not genome editing can initiate distinct heritable changes in sdg-1 expression. a, (P0 to F10, top) Quantification of SDG-1::mCherry fluorescence intensity (a.u.) in adult gonad arms (anterior arm, dark grey; posterior arm, light grey) across generations after mating hermaphrodite and male  $sdg-1(jam137[mCherry\Delta pi])$  animals with

male and hermaphrodite wild-type animals, respectively. The generations assayed and numbers of gonad arms quantified (n) are indicated. In F1 and F2, fluorescence intensity values of animals with lineages that were not propagated to F10 but were heterozygous or homozygous sdg- $1(jam137/mCherry\Delta pi)$ , respectively, were pooled with values of animals with lineages that were propagated to F10. In F3 to F10, top, animals from four different F1 lineages were scored. Fluorescence intensity of animals descending from the self-progeny of P0 sdg- $1(jam137[mCherry\Delta pi])$  animals was measured in each generation and is depicted, with the same data plotted for each mating direction for comparison. Asterisk indicates P < 0.05 with Bonferroni correction using Mann-Whitney U test for two-sided comparisons. (F10, bottom) Levels of spliced sdg-1 mRNA transcripts in wild-type animals,  $sdg-1(jam137[mCherry\Delta pi])$ animals and two lineages of wild-type F10 progeny from each cross direction, measured using RT-qPCR. The median of three technical replicates is plotted for each of three biological replicates (bar indicates median). Asterisks indicate P < 0.05 with Bonferroni correction using two-tailed Student's t-test. b, (P0 and F1) Schematic illustrating mutation of dpy-10 in three P0 lineages of  $sdg-1(jam137/mCherry\Delta pi)$  animals and subsequent segregation of the dpy-10mutation. (F2 and F3) Both dpy-10(-) and dpy-10(+) F2 and F3 animals from each of the three P0 lineages were imaged and SDG-1::mCherry intensity was quantified (a.u.) in adult gonad arms (anterior arm, dark grey; posterior arm, light grey). Minor differences in SDG-1::mCherry expression were observed between mutants and nonmutants in some cases, as well as between lineages. The numbers of gonad arms quantified (n) are depicted. Asterisks indicates P < 0.05with Bonferroni correction using Mann-Whitney U test for two-sided comparisons.



Extended Data Fig. 10. Unsuccessful attempts to functionally tag SID-1 and to determine SID-1-dependent genes. a, Schematic illustrating the tagging of *sid-1* (box, exon; line, intron) at the 3' end to generate fusion proteins with fluorophores (GFP, DsRed, or wrmScarlet) tagged at the C-terminus. b, Images showing subcellularly localized fluorescence (black) from SID-1::DsRed (top) and SID-1::GFP (bottom) within muscle cells when expressed from multicopy

transgenes. Scale bar = 10 µm and insets show brightfield images. **c**, Structure of SID-1 predicted by AlphaFold shaded based on pLDDT scores (blue/cyan, high; yellow/orange, low). Red arrow indicates the C-terminus. **d**, Principal component analysis of RNA-seq experiment comparing transcriptomes from wild-type, sid-1(qt9[nonsense]), sid-1(tm2700[deletion]), and sid-1(tm2700[deletion]); tmIs1005[sid-1(+)] animals. **e**, List of sid-1-dependent genes identified by comparing polyA+ RNA from sid-1(qt9[nonsense]) animals with wild-type animals (left) and by comparing sid-1(tm2700[deletion]) animals with sid-1(tm2700[deletion]); tmIs1005[sid-1(+)] animals (right).

### **Extended Data Movie Legends**

**Extended Data Movie 1.** Animals expressing SDG-1::mCherry (black) showing nuclear localization in -1 oocytes, but cytoplasmic localization in other oocytes and in the distal germline.

**Extended Data Movie 2.** Animals expressing SDG-1::mCherry (black) showing dynamic entry of SDG-1::mCherry into the nucleus in a zygote *in utero* after the maternal and paternal pronuclei meet.

**Extended Data Movie 3.** Animals expressing SDG-1::mCherry (black) showing nuclear localization in -1 oocytes and in an early-staged embryo *in utero* during cell divisions.

**Extended Data Movie 4.** Animals expressing SDG-1::mCherry (black) showing nuclear localization in oocytes during fertilization and in embryos *in utero* during cell divisions.

# Extended Data Table 1. Summary of constraints on intergenerational transport of extracellular dsRNA.

Stage of exposure	dsRNA type	Genetic requirement for germline entry	Heritability
L1 to L3	mixed, ingested	none tested	not heritable
early L4	mixed, ingested	rme-2 required	no persistent silencing in P0 adults, heritable to F1
	mixed, injected	rme-2 not required	heritable to F1
early adult	mixed, ingested	rme-2 required	partial silencing in P0 adults, heritable to F1
	mixed, injected	rme-2 not required	heritable to F1
late adult	mixed, ingested	rme-2 not required	persistent silencing in P0 adults, heritable to F1
	mixed, injected	sid-1 or rme-2 required	heritable to F1
	synthesized 50-bp, injected	sid-1 and rme-2 required	heritable to F1 with partial silencing
	Synthesized 50-bp with 5'-phosphate, injected	rme-2 is partially required	heritable to F1

Extended Data Table 2. List of genes changed in sid-1(jam80[nonsense)] animals or in sid-

1(jam113[deletion] animals compared with wild-type animals.

Genes	Change compared with wild type
sid-1	Down in sid-1(jam80) and sid-1(jam113)
sdg-1 (W09B7.2/F07B7.2)	Up in <i>sid-1(jam80)</i> and <i>sid-1(jam113)</i>
sdg-2 (Y102A5C.36)	Up in <i>sid-1(jam80)</i> and <i>sid-1(jam113)</i>
cls-3	Down in sid-1(jam80) and Up in sid-1(jam113)
sax-2	Down in sid-1(jam80)
Y46G5A.23	Up in <i>sid-1(jam80)</i>
F14F9.5	Up in <i>sid-1(jam113)</i>
T10D4.6	Up in <i>sid-1(jam113)</i>
F47D12.9	Down in sid-1(jam113)
C07G1.7	Up in <i>sid-1(jam113)</i>
Y48G1BL.5	Up in <i>sid-1(jam113)</i>
Y20F4.4	Up in <i>sid-1(jam113)</i>
ZK177.9	Up in <i>sid-1(jam113)</i>

C27C7.1	Up in <i>sid-1(jam113)</i>
Y38H6C.4	Up in <i>sid-1(jam113)</i>
C40A11.8	Up in <i>sid-1(jam113)</i>
C24H11.2	Up in <i>sid-1(jam113)</i>
C18D4.6	Up in <i>sid-1(jam113)</i>
F15B9.10	Up in <i>sid-1(jam113)</i>
F07B7.1	Up in <i>sid-1(jam113)</i>
ZC204.14	Down in sid-1(jam113)
Y47D7A.19	Up in <i>sid-1(jam113)</i>
Y26G10.5	Down in sid-1(jam113)
B0554.1	Down in sid-1(jam113)
F13A2.1	Down in sid-1(jam113)
C10C6.13	Down in sid-1(jam113)
H25K10.141	Down in sid-1(jam113)
Y43D4A.1	Up in <i>sid-1(jam113)</i>

### **Extended Data Table 3. Strains.**

Strains	Genotype
AMJ3	sid-1(qt9) V; jamIs2[myo-3p::sid-1::gfp]
AMJ308	ccIs4251[myo-3p::gfp::lacZ::nls & myo-3p::mito-gfp & dpy-20(+)] I; sid-1(qt9)
	V
AMJ327	ccIs4251[myo-3p::gfp::lacZ::nls & myo-3p::mito-gfp & dpy-20(+)] I; sid-1(qt9)
	V; jamIs2[myo-3p::sid-1 cDNA::DsRed]
AMJ471	jamEx140[rgef-1p::gfp-dsRNA & myo-2p::DsRed]
AMJ477	qtEx136[rgef-1p::unc-22-dsRNA & rgef-1p::DsRed]
AMJ576	jamSi12[mex-5p::sid-1::DsRed::sid-1 3'UTR]; unc-119(ed3) III; sid-1(qt9) V
AMJ577	hrde-1(tm1200[4X outcrossed]) III
AMJ581	oxSi487[mex-5p::mCherry::h2b::gfp::h2b & Cbr-unc-119(+)] dpy-2(e8) II; unc-
	119(ed3) III
AMJ592	hrde-1(tm1200) III; jamEx140[rgef-1p::gfp-dsRNA & myo-2p::DsRed]
AMJ602	oxSi487[mex-5p::mCherry::h2b::gfp::h2b & Cbr-unc-119(+)] dpy-2(e8) II; unc-
	119(ed3) hrde-1(tm1200) III
AMJ706	sid-1(qt9) V; jamEx193[myo-3p::sid-1::gfp]
AMJ819	eri-1(mg366) gtbp-1(ax2053[gtbp-1::gfp]) IV
AMJ837	jamEx209[rgef-1p::PH::miniSOG & myo-2p::DsRed]
AMJ936	jamEx210[rgef-1p::PH::miniSOG & rgef-1p::DsRed]
AMJ1007	eri-1(mg366) IV; jamEx213[rgef-1p::PH::miniSOG & rgef-1p::bli-1-dsRNA &
	myo-2p::DsRed]
AMJ1009	eri-1(mg366) gtbp-1(ax2053[gtbp-1::gfp]) IV; jamEx214[rgef-1p::PH::miniSOG
	& rgef-1p::gfp-dsRNA & myo-2p::DsRed]
AMJ1019	jamSi36[rgef-1p::PH::miniSOG & Cbr-unc-119(+)] II; unc-119(ed3) III
AMJ1108	eri-1(mg366) IV; sid-1(qt9) V; jamEx213[rgef-1p::PH::miniSOG & rgef-1p::bli-
	1-dsRNA & myo-2p::DsRed]

```
sid-1(qt9) V; jamEx213[rgef-1p::PH::miniSOG & rgef-1p::bli-1-dsRNA & myo-
AMJ1114
           2p::DsRed]
           rme-2(jam71[deletion]) IV; sid-1(qt9) V
AMJ1120
AMJ1123
           jamEx213[rgef-1p::PH::miniSOG & rgef-1p::bli-1-dsRNA & myo-2p::DsRed]
AMJ1131
           rme-2(jam71[deletion]) IV
           jamEx214[rgef-1p::PH::miniSOG & rgef-1p::gfp-dsRNA & myo-2p::DsRed]
AMJ1134
           oxSi487[Pmex-5::mCherry::h2b::gfp::h2b]; unc-119(ed9) III;
AMJ1146
           rme- 2(jam71[deletion]) IV
           rme-2(jam71[del]) IV; jamEx140[Prgef-1::gfp-dsRNA & Pmyo- 2::DsRed]
AMJ1204
           sid-1(tm2700) V; jamEx213[rgef-1p::PH::miniSOG & rgef-1p::bli-1-dsRNA &
AMJ1151
           myo-2p::DsRed]
AMJ1153
           sid-1(tm2700)[3X outcrossed] V
           sid-1(jam80[nonsense]) V
AMJ1159
AMJ1173
           eri-1(mg366) IV; sid-1(tm2700) V; jamEx213[rgef-1p::PH::miniSOG & rgef-
           1p::bli-1-dsRNA & myo-2p::DsRed]
AMJ1217
           sid-1(jam86[revertant]) V
AMJ1220
           hrde-1(tm1200) III; gtbp-1(ax2053[gtbp-1::gfp]) IV
           sid-1(jam115[sid-1::wrmScarlet13]) V
AMJ1280
AMJ1281
           rme-2(jam116[rme-2::wrmScarlet13]) IV
AMJ1282
           sid-1(jam117[sid-1::wrmScarlet]) V
AMJ1284
           rme-2(jam119[rme-2::wrmScarlet]) IV
           sid-1(jam80[nonsense]) V; jamEx214[rgef-1p::PH::miniSOG & rgef-1p::gfp-
AMJ1312
           dsRNA & myo-2p::DsRed]
AMJ1323
           sid-1(jam112[sid-1::tetracycline-K4-aptazyme::3'UTR]) V
AMJ1324
           sid-1(jam113[deletion]) V
AMJ1330
           sid-1(jam112[sid-1::tetracycline-K4-aptazyme::3'UTR]) V; qtEx136[rgef-
           1p::unc-22-dsRNA & rgef-1p::DsRed]
AMJ1332
           sid-5(jam122[deletion]) X
AMJ1350
           sid-1(jam112[sid-1::tetracycline-K4-aptazyme::3'UTR]) V; jamEx140[rgef-
           1p::gfp-dsRNA & mvo-2p::DsRed]
           gtbp-1(ax2053[gtbp-1::gfp]) IV; sid-1(jam112[sid-1::tetracycline-K4-
AMJ1355
           aptazyme::3'UTR]) V
AMJ1365
           hrde-1(tm1200) III; sid-1(jam117[sid-1::wrmScarlet]) V
AMJ1366
           rme-2(jam71[deletion]) IV; sid-1(jam113[deletion]) V
           sid-1(jam113[deletion]) V; sid-5(jam122[deletion]) X
AMJ1367
AMJ1368
           sid-2(jam134[deletion]) III
AMJ1372
           W09B7.2/F07B7.2(jam137[W09B7.2/F07B7.2::mCherry\Delta pi]) V
AMJ1380
           sid-2(jam134[deletion]) III; sid-1(jam113[deletion]) V
AMJ1383
           gtbp-1(ax2053[gtbp-1::gfp]) IV; nrde-3(tm1116) X
AMJ1389
           sid-1(jam150[nonsense])
           W09B7.2/F07B7.2(jam137[W09B7.2/F07B7.2::mCherry\Delta pi]) V
AMJ1399
           sid-1(jam157[nonsense]) V
AMJ1405
           sid-1(jam163[revertant]) V
           sid-1(jam164[revertant]) V
AMJ1406
AMJ1407
           sid-1(jam165[revertant]) V
           sid-1(jam166[revertant]) V
AMJ1408
```

```
sid-1(jam167[revertant]) V
AMJ1409
AMJ1410
           sid-1(jam168[revertant]) V
AMJ1412
           sid-1(jam170[revertant])
            W09B7.2/F07B7.2(jam137[W09B7.2/F07B7.2::mCherry\Delta pi]) V
AMJ1413
           sid-1(jam171[revertant])
            W09B7.2/F07B7.2(jam137[W09B7.2/F07B7.2::mCherry\Delta pi]) V
           sid-1(jam172[sid-1\ N-term::mCherry\Delta pi::sid-1\ C-term])\ V
AMJ1438
AMJ1442
           sid-1(jam173[nonsense])
            W09B7.2/F07B7.2(jam137[W09B7.2/F07B7.2::mCherry\Delta pi]) V
AMJ1443
           sid-1(jam174[nonsense])
            W09B7.2/F07B7.2(jam137[W09B7.2/F07B7.2::mCherry\Delta pi]) V
AMJ1444
           sid-1(jam175[nonsense])
            W09B7.2/F07B7.2(jam137[W09B7.2/F07B7.2::mCherry\Delta pi]) V
AMJ1445
           sid-1(jam176[nonsense])
            W09B7.2/F07B7.2(jam137[W09B7.2/F07B7.2::mCherry\Delta pi]) V
AMJ1446
           sid-1(jam177[nonsense])
            W09B7.2/F07B7.2(jam137[W09B7.2/F07B7.2::mCherry\Delta pi]) V
AMJ1447
            W09B7.2/F07B7.2(jam137[W09B7.2/F07B7.2::mCherryΔpi]) rde-
            1(jam178[nonsense]) V
AMJ1448
            W09B7.2/F07B7.2(jam137[W09B7.2/F07B7.2::mCherry\Delta pi]) rde-
            1(jam179[nonsense]) V
AMJ1449
            W09B7.2/F07B7.2(jam137[W09B7.2/F07B7.2::mCherrv\Delta pi]) V: sid-
            3(jam180[nonsense]) X
AMJ1450
            W09B7.2/F07B7.2(jam137[W09B7.2/F07B7.2::mCherry\Delta pi]) V; sid-
            3(jam181[nonsense]) X
AMJ1451
           deps-1(jam182[nonsense]) I;
            W09B7.2/F07B7.2(jam137[W09B7.2/F07B7.2::mCherry\Delta pi]) V
AMJ1452
           deps-1(jam183[nonsense]) I;
            W09B7.2/F07B7.2(jam137[W09B7.2/F07B7.2::mCherry\Delta pi]) V
AMJ1479
           sid-1(iam189[deletion])
            W09B7.2/F07B7.2(jam137[W09B7.2/F07B7.2::mCherry\Delta pi]) V
           sid-1(jam190[deletion])
AMJ1480
            W09B7.2/F07B7.2(jam137[W09B7.2/F07B7.2::mCherry\Delta pi]) V
AMJ1481
           sid-1(jam191[deletion])
            W09B7.2/F07B7.2(jam137[W09B7.2/F07B7.2::mCherry\Delta pi]) V
AMJ1482
           sid-1(jam192[deletion])
            W09B7.2/F07B7.2(jam137[W09B7.2/F07B7.2::mCherry\Delta pi]) V
AMJ1485
           sid-1(jam195[sid-1 N-term::linker::mCherry\Delta pi::sid-1 C-term]) V
AMJ1504
           oxSi487[mex-5p::mCherry::h2b::gfp::h2b & Cbr-unc-119(+)] dpy-2(e8) II; unc-
            119(ed3) III; sid-1(jam80[nonsense]) V
AMJ1542
           gtbp-1(jam210[gtbp-1::gfp::tetracycline-K4-aptazyme::3'UTR]) IV
AMJ1574
           deps-1(jam229[nonsense]) I; sid-1(jam170[revertant])
            W09B7.2/F07B7.2(jam137[W09B7.2/F07B7.2::mCherry\Delta pi]) V
           deps-1(jam230[nonsense]) I; sid-1(jam170[revertant])
AMJ1575
            W09B7.2/F07B7.2(jam137[W09B7.2/F07B7.2::mCherry\Delta pi]) V
            W09B7.2/F07B7.2(jam232[deletion]) V
AMJ1577
```

```
W09B7.2/F07B7.2(jam241[deletion]) V
AMJ1612
AMJ1613
            W09B7.2/F07B7.2(jam242[deletion]) V
            W09B7.2/F07B7.2(jam244[sdg-1 ORF deleted from jam137]) V
AMJ1615
AMJ1616
            W09B7.2/F07B7.2(jam245[sdg-1 ORF deleted from jam137]) V
            W09B7.2/F07B7.2(jam246[sdg-1 ORF deleted from jam137]) V
AMJ1617
AMJ1662
           znfx-1(gg544[3xflag::gfp::znfx-1]) II;
            W09B7.2/F07B7.2(jam137[W09B7.2/F07B7.2::mCherry\Delta pi]) V
AMJ1766
           rde-4(ne301) III; W09B7.2/F07B7.2(jam244[sdg-1 ORF deleted from jam137]) V
           rde-4(ne301) III; W09B7.2/F07B7.2(jam244[sdg-1 ORF deleted from jam137]) V
AMJ1767
            W09B7.2/F07B7.2(jam244[sdg-1 ORF deleted from jam137 1X outcrossed]) V
AMJ1770
DH1390
           rme-2(b1008) IV
EG4322
           ttTi5605 II; unc-119(ed9) III
EG6787
           oxSi487[mex-5p::mCherry::h2b::gfp::h2b & Cbr-unc-119(+)] II; unc-119(ed3)
           III
FX02700
           sid-1(tm2700) V
FX15992
           sid-1(tm2700) V; tmIs1005[sid-1(+) & vps-45 mini]
GR1373
           eri-1(mg366) IV
           sid-1(qt9) V
HC196
           eri-1(mg366) IV; sid-1(qt9) V
HC731
JH3197
           gtbp-1(ax2053[gtbp-1::gfp]) IV
N2
           wild type
           rde-4(ne301) III
WM49
```

znfx-1(gg544[3xflag::gfp::znfx-1]) II

YY916

## **Extended Data Table 4. Oligonucleotides.**

Name	Sequence
P1	caccttegecaattateacete
P2	cgtcagettctgattcgacaac
P3	ataaggagttccacgcccag
P4	ctagtgagtcgtattataagtg
P5	tgaagacgagccacttg
P6	ggaacatatggggcattcg
P7	cagacctcacgatatgtggaaa
P8	getteacetgtettateactge
P9	cgcggcgactttggttaaatc
P10	ggcttgacaaacgtcagcttc
P11	teateteggtacetgtegttg
P12	agaggcggatacggaagaag
P13	cataaccgtcgcttggcac
P14	aatgggtgagatgggcttaag
P15	gcacttcgatatttcgcgccaa
P16	gaaccaatgtggcacgaaac
P17	gcaaaacttcgattaacattttcatggcctcctccgagaacg
P18	cgttctcggaggaggccatgaaaatgttaatcgaagttttgc
P19	ggtaccetetagteaaggeetatagaaaagttgaaatateagtttttaaaaa
P20	cacgaatcattctctgtctgaaacattcaattg
P21	cagacagagaatgattcgtgtttatttgataattttaatg
P22	cggaggaggccatgaaaatgttaatcgaagttttgc
P23	taacattttcatggcctcctccgagaac
P24	aattactctactacaggaacaggtggtgg
P25	gttcctgtagtagagtaattttgttttccctatc
P26	ggctacgtaatacgactcacagtggctgaaaatttatgc
P27	gagcagcagaatacgagctc
P28	gaaaagttetteteetttaeteatgaaaatgttaategaagttttge
P29	gcaaaacttcgattaacattttcatgagtaaaggagaagaacttttc
P30	ctctcagtacaatctgctctg
P31	gaatacgagctcagaactcg
P32	atgccgcatagttaagccag
P33	atcgacgacgacgatcagcagtaaagaagcttgcatgcctgcag
P34	atgttgaagagtaattggacgtcatccatccagcagcac
P35	gtccaattactcttcaacatcccta
P36	ctttactgctgatcgtcg
P37	tetetecetaggeacaacgatggatacgetaac
P38	gagagacctaggcacgatgagcatgatttgacg
P39	atttaggtgacactatagctaccataggcaccacgaggttttagagctagaaatagcaag
P40	gcaccgactcggtgcca
P41	caettgaaetteagacaagatgagaatgaetggaaaccgtaccgcatgcggtgcctatggtagcggaget
P42	tcacatggettcagaccaacagceta
F42	atttaggtgacactatagcaaggcgcatggttctcagttttagagctagaaatagcaag

P43	attta gatan an atata gana attta atgana tanga taga atattta gang ata gana ta gana a
P44	atttaggtgacactatagcaactttcatgcaataaatgttttagagctagaaatagcaag
	ttettteattetttteataateteaeteaetagatattgeatgaaagttgataatgtetaetagtaetg
P45	aaacaccaacaacgcaatcc
P46	tgacctcatcatctcctccag
P47	tccgaatctgaaccacgaatg
P48	atttaggtgacactatagcattcaatcgagactgcagttttagagctagaaatagcaag
P49	agcetataatetatateageatteaateaaggetaeaeggttaegateaggttttgatggaaatgagggt
P50	atttaggtgacactatagcattcaatcaaggctacagttttagagctagaaatagcaag
P51	aagcctataatctatatcagcattcaatcgagactgcacggttacgatcaggttttgatggaaatgaggg
P52	tgaaatatgaaaaaccggat
P53	t catta a tacac g caa a a ctt c g atta a catt t t cat g g t cag caa g g g a g g c a g t t a t caa g g a g t t cat g g t cat g cat g ca g g a g g cag t t a t caa g g a g t cat g c
	tt caa ggt ccaa cgag gg tt ccgag ggac gt cact cca ccg gag gaat ggac gag ctcta caa gt ag a gt aat tt caa ggag gag ta can gag gag gag gag gag gag gag gag gag g
	ttgttttccctattcgtttcttcatatttcaactttttctcctgcctta
P54	acteggettetteggttee
P55	aacaccagatcactgcgtagag
P56	aaggtccaacgagcgttccg
P57	atggtcagcaagggagagg
P58	cttgtagagctcgtccattcct
P59	attgtgaacctggaaaaatg
P60	tttcactatcagtggcttcacctgtcttatcactgcttcttgtatactgaacgacgttaaacacatctcactttaacattt
100	agaattaaaactcctcatcggtttttcatatttcaactttttctcctgccttaatacgtagcccatctctcatttcttcatg
	tttaagaactttctgaatctatgtaattagttgg
P61	tttttggcacagtttttgct
P62	
P63	ggaattagagactagagctt
103	cgtgtctctcacaacagccgtttctctaacagaaaaaccttctttgttgatgtttgtctaaaatcgatttttcagcaag
	aaatcgagaactggaacgagctttggtaagtttttgttcctcgaagtgtaaataattgagtaaaagctttcttattga
DC4	aaaaaaaacgaatgttcaaattatgaagattgaaaaatg
P64	tttccgcgtactcctctc
P65	ctaagaccaacatccaageteg
P66	tcacatttggcgaggagcca
P67	aatcgaatgactccagcgaa
P68	cagacgtttggctatacgcc
P69	caactggtttcgtcagatcggcttccgcaccatttgccggtgtgatccgtttcgaaaatgatagtttattaatggtca
	gcaagggaggaggtattatcaaggagttcatgcgtttcaagttccgagggacgtcactccaccggaggaatgg
	acgagetetacaagtgaattetactacaaaattactaaatcagatgtet
P70	ctgctttgatggccgaatactg
P71	aaacaaaatatacaaatcg
P72	ccttcgctacattggaaagc
P73	catatgaa atttttaaa taaagttgttttctaactgttcccaatattcttaaatcccattgaacagaatttcattttcaaaac
	cct gat at ttt cag ga at ttt at tcca at aat at gat ttt ga aa aac tat ta at ctt acct g t g cat ca at aa a gat ctt g ta accept a consideration of the consid
	gagtatatcatcgatcacagtctccgatttgtctg
P74	ggtcttacccattccaacatcg
P75	ttcgctacattggaaagctgg
P76	caegectatgtteeettgte
P77	ttcatgcgtttcaagttccg

P78	tcgattaacattttctagagtaattttgttttcccaaacaaa
- , -	atttcgatctggagaggtgaagaatacgaccacctgtacatccagctgatgagtcccaaataggacgaaacgcg
	ctcaaacaaactatccggtttttcatatttcaactttttctcct
P79	teteceaettgaatecetetg
P80	ccaaatgttgagccagtcac
P81	ttgaggaaatgcagacgctcgttatcgacctccagatggtctccaagggagagga
P82	tgttattttgagggagccaaatgttgagccagtcagccactacctgatcccttgt
P83	gctgaaggtggatagtgtctc
P84	gagttcggaagtaaaccgtgg
P85	tcaccatctgggaggtgttcacatttggcgaggagccataggtcggctgtcgagccatcgatgtgctcaa
P86	agacgaaagggtgagaactttg
P87	cgcgaggatatgcagttcac
P88	agcattcaatcgagactgca
P89	acaagaaggaaaaaggagaa
P90	aatgcgggacaaaattagaagctttccgttctcccaaacaaa
	cagatttcgatctggagaggtgaagaatacgaccacctgtacatccagctgatgagtcccaaataggacgaaac
	gcgctcaaacaaaatttttccttcttgtaagaattgcacatccattag
P91	cacatggtccttcttgagtttg
P92	acggtgaggaaggaaggag
P93	agcattcaatcaaggctaca
P94	cgaagtaaaacaattcatgt
P95	gcttcgatctttaaaaagcgaagtaaaataatttatgtcagaacgggatggagaagatccagagccgaag
P96	tggctcatggacgggaaag
P97	ggaacaggcaacgagatgg
P98	cgtggcacatactttccgttgttg
P99	gtcatctccgacgagcac
P100	ttccgttgttggcttcgttg
P101	tgcacggcgtatcaaactg
P102	ggccattgggagaacttcg
P103	tgacggcctcttctacatatcg
P104	ccgcaagtctctcctgtatg
P105	gctgaaggtggatagtgtctc
P106	attgctccgcaaatgtagtgg
P107	gctgctcaagcaaatcgaatg
P108	ttatcacggtggagaacagc
P109	ttggtagggaatcggctgg
P110	tcaaattgttgaagagatca
P111	cagcagaaaatcaaattgttgaagagatcacagctatggtctccaagggagagga
P112	eggttteeetettetaegetegtttettgattttegeeaetaeetgateeettgt
P113	caacgggacatggatttgag
P114	ttgaatttcccggtttccctc
P115	tgttgaagagatcacagcta
P116	cag caga aa aat caa at t g t t g aa gag at cacag c t g g t g g t g g t g g a g g a g g g g
	gaggcagtatggtctccaagggaggaagataacatggctat
P117	taatacgactcactatagg
P118	cccacactaccatcggcgctac

P119	cactcttactgctaccaacgcttctggaagcgacaaacat
P120	atgtttgtcgcttccagaagcgttggtagcagtaagagtg
P121	tcgttgttccaggagatcagaaaacagcaactgttccaaa
P122	tttggaacagttgctgttttctgatctcctggaacaacga
P123	acceactteacagtegatteacteaacaagggagateatt
P124	aatgatctcccttgttgagtgaatcgactgtgaagtgggt
P125	tagaaaaaatgagtaaaggagaagaacttttcactggagt
P126	actccagtgaaaagttcttctcctttactcattttttcta
P127	agtttgaaggtgatacccttgttaatagaatcgagttaaa
P128	tttaactcgattctattaacaagggtatcaccttcaaact
P129	ggattacacatggcatggatgaactatacaaatgcccggg
P130	cccgggcatttgtatagttcatccatgccatgtgtaatcc
P131	acauuccagucaguggugaaccaacuccaacaauuacuuggacuuucgaa
P132	uucgaaaguccaaguaauuguuggaguugguucaccacugacug
P133	ugguccuucuugaguuuguaacagcugcugggauuacacauggcauggau
P134	auccaugccauguguaaucccagcagcuguuacaaacucaagaaggacca
P135	5'Atto 565-auccaugecauguguaaucccagcagcuguuacaaacucaagaaggacca
P136	5'Atto 488-ugguccuucuugaguuuguaacagcugcugggauuacacauggcauggau
P137	aggcgacccgtgcggagccagacgtttggctatacgcctgaattcgattcgaaactaccatgaagagtgg
P138	cgtttggctatacgccggg
P139	tccgttgacagaggttacatgc
P140	agegtetteeageagaaatg
P141	cttcatggtagtttcgaatcgactt
P142	gctaccataggcaccgcatg
P143	ctggttgagcttctcattct
P144	ccaaatgttgagccagtcac
P145	tccgtttttttcgaaacttttcgtaatattttttgtttcttcaattgatctcttgaatattcatcgtgaatta
P146	gagttcggaagtaaaccgtgg
P147	gctgaaggtggatagtgtctc
P148	cgcagtacgcagagtgaac
P149	gatggtctccaagggagagg
P150	ttacagtaaaacagccggatcccaccgagaatggtctccaagggaggaagataacatg
P151	teteceaettgaateeetetg
P152	atcgtcttgatcgacggaacac
P153	ttgaggtggtttatctctggac
P154	cttgtagttcccgtcatctttg
P155	atttcgttctgattccgtgagg
P156	tteetgeaacttteegaee
P157	gaactteetgaaggetteg
P158	atcgtcttgatcgacggaacac
P159	acccaggattcctccgtaag
P160	gagttcggaagtaaaccgtgg